

Technical Report

PERFORMANCE OF AN EVACUATED TUBE SOLAR COLLECTOR

by

David Murray Frick

and

Susumu Karaki

Solar Energy Applications Laboratory
Colorado State University
Fort Collins, Colorado

July 1976

217⁴³²⁸⁰⁵ XL 559
11/00 38-000-00 GBC

U18400 5059363

N

FOLIO

TA7

C6

CER-76/77-9

CER76-77DMF-SK9

LIBRARIES
COLORADO STATE UNIVERSITY
Fort Collins, Colorado 80529

ABSTRACT OF THESIS

PERFORMANCE OF AN EVACUATED TUBE SOLAR COLLECTOR

Analysis of the performance characteristics of an evacuated tube solar collector is presented. Although the analysis is general enough to apply to other evacuated tube solar collectors, the work primarily concerns a prototype test module of a collector furnished by Corning Glass Works Company.

A detailed theoretical analysis is presented along with the predicted performance of the test module. The theoretical analysis of the collector is given in two parts; the analysis of the optical characteristics of the glass tubes and the predictions of the thermal performance of the collector.

Tests were made to compare the predicted with actual performance. Some test results are compared to the performance of a "conventional" flat-plate collector to show that the evacuated tube collector operates at greater collection efficiency. Analysis also shows that the performance of the collector can be increased by increasing the spacing between the tubes to allow for reflections onto the back sides of the absorber.

ACKNOWLEDGMENTS

The authors wish to acknowledge the assistance of George O. G. Löf, Paul Wilbur, Charles C. Smith and Dan S. Ward for their suggestions and comments during the conduct of this study.

Financial support for the study was provided by the Colorado Energy Research Institute and Colorado State University. The test collector module was provide by the Corning Glass Works Company.

TABLE OF CONTENTS

| <u>Chapter</u> | | <u>Page</u> |
|----------------|--|-------------|
| | ABSTRACT | iii |
| | ACKNOWLEDGMENTS | iv |
| | LIST OF TABLES | vii |
| | LIST OF FIGURES | viii |
| I | INTRODUCTION | 1 |
| | 1.0 General Comments | 1 |
| | 1.1 Background | 1 |
| | 1.2 Review of Previous Research | 3 |
| | 1.3 Collector Studied | 4 |
| II | OPTICAL ANALYSIS | 9 |
| | 2.0 General Comments | 9 |
| | 2.1 Angle of the Sun | 9 |
| | 2.2 Transmittance of Incoming Beam Radiation | 12 |
| | 2.3 Shading Effects of Adjacent Tubes | 16 |
| | 2.4 Reflections from Adjacent Tubes | 19 |
| | 2.5 Diffuse Reflections from Back Surfaces | 22 |
| | 2.6 Internal Reflection | 27 |
| | 2.7 Effective $\tau\alpha$ Product | 29 |
| | 2.8 Tube Orientation | 32 |
| III | THERMAL ANALYSIS | 34 |
| | 3.0 General Comments | 34 |
| | 3.1 Heat Loss Coefficient | 34 |
| | 3.2 Heat Removal Efficiency Factor | 40 |
| IV | COLLECTOR TESTING | 45 |
| | 4.0 General Comments | 45 |
| | 4.1 Test Facility | 45 |
| | 4.2 Test Parameters and Accuracies of Measurement | 49 |
| | 4.3 Testing Procedures | 51 |
| | 4.4 Results of the Theoretical Analysis | 57 |
| | 4.5 Test Results | 59 |
| | 4.6 Total Daily Performance | 64 |
| V | SUMMARY AND CONCLUSIONS | 67 |
| | REFERENCES | 70 |

| <u>Chapter</u> | <u>Page</u> |
|--|-------------|
| APPENDIX I OPTICAL CALCULATIONS. | 71 |
| APPENDIX II THERMAL CALCULATIONS | 76 |
| APPENDIX III TEST DATA | 79 |

LIST OF TABLES

| <u>Table</u> | | <u>Page</u> |
|--------------|--|-------------|
| 2-1 | Average Energy Flux Increases Due to Reflections from Back Surfaces | 26 |
| 2-2 | Effective Transmittance of the Test Module | 31 |
| 2-3 | Calculated Energy Absorbed for Corning Collector with Change in Tube Axis Orientation | 33 |
| 3-1 | Calculated Loss Coefficients and Heat Removal Efficiency Factors for the Test Module | 41 |
| 4-1 | Summary of Test Data for June 26, 1975 | 53 |
| 4-2 | Results of Theoretical Analysis | 60 |
| A-I-1 | Transmission Calculations for the Test Module | 72 |
| A-I-2 | Shading Calculations for the Test Module | 73 |
| A-I-3 | Reflection Calculations from Adjacent Tubes for the Test Module | 74 |
| A-I-4 | Internal Reflection Calculations | 75 |
| A-II-1 | U_L Calculations for the Test Module | 77 |
| A-II-2 | F_r Calculations for the Test Module | 78 |
| A-III-1 | Summary of Test Data for June 19, 1975 | 80 |
| A-III-2 | Summary of Test Data for June 20, 1975 | 83 |
| A-III-3 | Summary of Test Data for June 23, 1975 | 87 |
| A-III-4 | Summary of Test Data for June 25, 1975 | 91 |
| A-III-5 | Summary of Test Data for June 27, 1975 | 94 |
| A-III-6 | Summary of Test Data for July 8, 1975 | 97 |
| A-III-7 | Summary of Test Data for July 14, 1975 | 101 |
| A-III-8 | Summary of Test Data for July 16, 1975 | 104 |
| A-III-9 | Summary of Test Data for July 25, 1975 | 107 |
| A-III-10 | Summary of Test Data for August 4, 1975 | 111 |

LIST OF FIGURES

| <u>Figure</u> | | <u>Page</u> |
|---------------|--|-------------|
| 1-1 | Test Module Furnished by Corning Glass Work Company | 5 |
| 1-2 | Test Module Details | 7 |
| 2-1 | Tube Orientation Angles | 10 |
| 2-2 | Transmissivity of Glass Tube | 13 |
| 2-3 | Transmittance Glass (from Duffie and Beckman, 1974) | 15 |
| 2-4 | Shading Effects of Adjacent Tubes | 17 |
| 2-5 | Reflections from Adjacent Tubes | 20 |
| 2-6 | Reflectance of Glass with Index of Refraction of 1.526 (from Duffie and Beckman, 1974) | 21 |
| 2-7 | Reflection off Back Surfaces | 23 |
| 2-8 | Optimum Tube Spacing | 25 |
| 2-9 | Internal Reflection | 28 |
| 3-1 | Effective Emissivity of Test Module Absorber Surface | 37 |
| 4-1 | Solar Collector Test Stand | 46 |
| 4-2 | Schematic of Solar Collector Test Facility | 47 |
| 4-3 | Solar Radiation and Useful Heat Collected | 55 |
| 4-4 | Wind Speed and Operating Temperatures | 56 |
| 4-5 | Manufacturing Variations in Absorber Surface Coating | 58 |
| 4-6 | Performance Curve for the Corning Solar Collector ± 1 Hour from Solar Noon | 61 |
| 4-7 | Performance Curve for the Corning Solar Collector for $\pm(1$ to 3) Hours from Solar Noon | 62 |
| 4-8 | Total Daily Performance of Test Module | 65 |
| A-III-1 | Test Data Plot | 81 |

| <u>Figure</u> | | <u>Page</u> |
|---------------|--------------------------|-------------|
| A-III-2 | Test Data Plot | 82 |
| A-III-3 | Test Data Plot | 85 |
| A-III-4 | Test Data Plot | 86 |
| A-III-5 | Test Data Plot | 89 |
| A-III-6 | Test Data Plot | 90 |
| A-III-7 | Test Data Plot | 92 |
| A-III-8 | Test Data Plot | 93 |
| A-III-9 | Test Data Plot | 95 |
| A-III-10 | Test Data Plot | 96 |
| A-III-11 | Test Data Plot | 99 |
| A-III-12 | Test Data Plot | 100 |
| A-III-13 | Test Data Plot | 102 |
| A-III-14 | Test Data Plot | 103 |
| A-III-15 | Test Data Plot | 105 |
| A-III-16 | Test Data Plot | 106 |
| A-III-17 | Test Data Plot | 109 |
| A-III-18 | Test Data Plot | 110 |
| A-III-19 | Test Data Plot | 113 |
| A-III-20 | Test Data Plot | 114 |

Chapter I

INTRODUCTION

1.0 General Comments

The concept of an evacuated tube solar collector was first introduced by Speyer in 1964. Since then, few attempts have been made to improve and develop this concept. There have been some recent achievements of production models of evacuated tube collectors but little analysis on the performance characteristics of these collectors is available in the literature. This work, on the analysis of the performance characteristics of an evacuated tube solar collector is oriented toward a unit manufactured by the Corning Glass Works Company, but is adaptable to other evacuated tube designs with minor modifications in the analysis. A collector module was provided by Corning Glass Works Company and the performance of the module was tested against the theoretical analysis.

1.1 Background

The performance of any flat-plate solar collector is dependent upon the rate of solar energy absorbed by the collector surface and the thermal loss rate from the collector. The thermal loss from a conventional flat-plate collector occurs through all the heat transfer mechanisms, radiation, conduction and convection, through the cover plates. There are additional thermal losses by conduction through the edges and the back of the collector. The rates are dependent upon the temperature difference between the absorber plate and ambient air. Thus, the higher the desired operating temperature of a collector, the greater is the heat loss and the poorer is the performance. This characteristic of a

conventional flat-plate collector has deterred use of solar energy for higher temperature applications such as for absorption air conditioners for space cooling and generation of process heat.

The evacuated tube solar collector consists of an absorber plate surrounded by a glass envelope. The space between the absorber and the envelope is evacuated to a partial vacuum of 10^{-4} to 10^{-6} torr. The absorber is suspended in the envelope with minimal contact with the glass. The effect of the vacuum is to virtually eliminate the conduction and convection losses from the absorber. To reduce radiation losses an absorber plate may be coated with a selective surface coating. If this can be done without sacrifice of transmittance and absorptance, the effect of these improvements is to increase the performance of the collector at higher plate and hence fluid temperatures. An evacuated tube solar collector with a selective surface makes it possible to obtain working temperatures greater than 200° C, which provides some advantages to a solar cooling system.

The evacuated tube collector has an optical advantage in that a single glass cover increases the transmissivity as compared to conventional two glass cover system on a flat-plate collector. Also, the circular shape of the tubes enhances the transmissivity at lower sun angles due to both the lower angle of incidence and the reflection from adjacent tubes. These effects increase the collection of useful energy over a greater period of each day as compared to conventional flat-plate collectors.

The design of the collector is relatively simple, and less quantity of material is used for its construction than for conventional solar collectors, thus the cost of the materials for an evacuated tube

collector would be less. The disadvantage to the evacuated tube collector is that production costs are high at the present time, being several times that of conventional collector designs. It is expected, however, that mass production techniques can lower these costs significantly.

1.2 Review of Previous Research

A review of the literature has indicated that the only published research to date concerning evacuated tube collectors is by Speyer in 1964 [1]. He analyzed the effects of evacuation on the performance of a flat-plate solar collector enclosed in a glass tube. Several absorber geometries were tried. He also proposed silvering the interior of the bottom half of the tube to reflect the light not intercepted by the absorber. The results of his experiments showed that an evacuated tube collector had superior performance to conventional collector designs and could be produced at less cost.

Since Speyer's original work, two other papers have been recently published regarding the performance of evacuated tube solar collectors. Beekley and Mather [2] analyze the performance of an evacuated tube collector which is currently manufactured by Owens-Illinois, Inc. This collector consists of three concentric glass tubes. The middle tube is the absorber, which is coated with a selective surface. A vacuum is maintained between the middle and outer tubes. Fluid is circulated from one end, entering the inner tube and exiting from the same end through the middle tube. The outer tube is 5.1 cm in diameter and the tubes are manifolded together in arrays to form the desired collector size. Their work included the development of an analytical model to predict the performance characteristics of this collector. They contend

in their analysis that the Owens-Illinois collector has greater efficiency at sun angles of about 30 degrees from normal to the collector than at sun angles near normal to the collector because of the circular absorber. The performance is also improved because the tubes are spaced 5.1 cm apart, and the radiation passing between the collector tubes is reflected from the surface behind the collector, and is absorbed by the collector. The cost effectiveness of spacing tubes was analyzed to determine that the best tube spacing was one tube diameter.

Ortabasi and Buel [3], present a semi-empirical analysis of an evacuated tube collector developed by Corning Glass Works Company. Their analysis is verified with test data. They also simulated the performance of the collector in solar heating and cooling systems. Their calculations and measurements indicate that it is possible to obtain better than 55 percent efficiency with a fluid temperature 120° C above ambient at a solar flux of $800 \text{ W hr}^{-1} \text{ m}^{-2}$ with the Corning collector.

Beach [4] analyzed the performance of evacuated tube collectors. His work was concerned mainly with the thermal performance of the collector, and little detail was provided on the optical analysis of radiation reaching the absorber tube. No experimental data was provided in his work to verify the analysis.

1.3 Collector Studied

The evacuated tube solar collector studied was a prototype test module assembled by the Corning Glass Works Company. The module consisted of six 10.2 cm diameter glass tubes that were held together at each end by molded plastic, (see Figure 1-1). Inside each tube is a flat copper absorber plate supported along the sides by spring clips

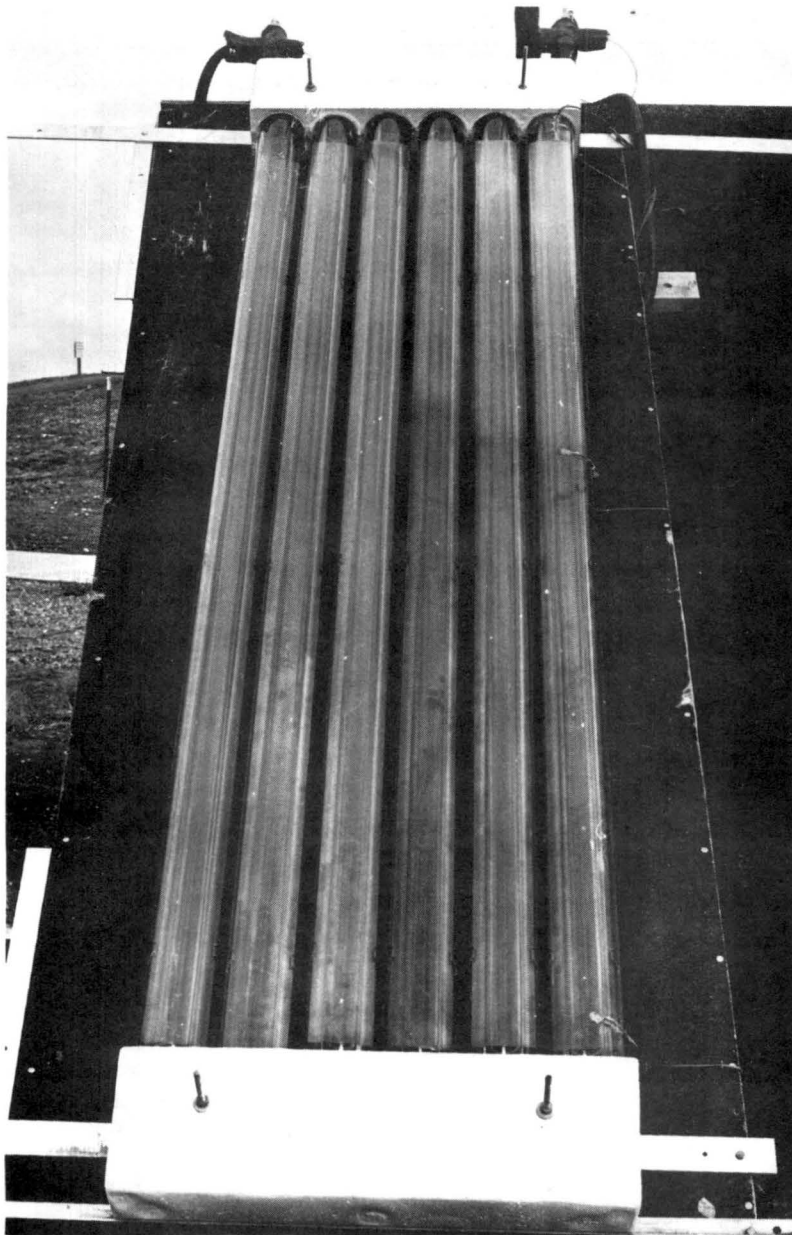


Figure 1-1. Test Module Furnished by Corning Glass Work Company.

between the absorber plate and the glass tube. A 6.35 mm diameter copper 'U' tube was soldered to the absorber plate. The U tube allows for fluid circulation in and out from the same end of the glass tube and for differential expansion between the absorber plate and the glass tube. Details and dimensions of an absorber tube are shown in Figure 1-2. The copper absorber plate is coated with a selective surface on both sides.

The performance of flat-plate solar collectors is analyzed by the general collector equation which assumes steady-state operation. The useful heat gained, Q_{out} , is the difference between the solar radiation absorbed and the thermal losses. This can be expressed by:

$$Q_{out} = F_R A_c [HR(\tau\alpha)_e - U_L(T_{in} - T_a)] \quad (1)$$

where: HR is the solar radiation measured parallel to the collector surface,

$(\tau\alpha)_e$ is the effective transmittance-absorptance product of the cover absorber system,

U_L is the thermal loss rate from the collector

T_{in} is the heat transfer fluid inlet temperature,

T_a is the ambient temperature,

A_c is the area of the collector, and

F_R is the heat removal efficiency factor to relate the thermal loss from the mean plate temperature to the inlet fluid temperature.

These terms can be determined by both analytical and empirical means for any flat-plate solar collector. This work analyzes the collector performance based on this equation. First a theoretical analysis is

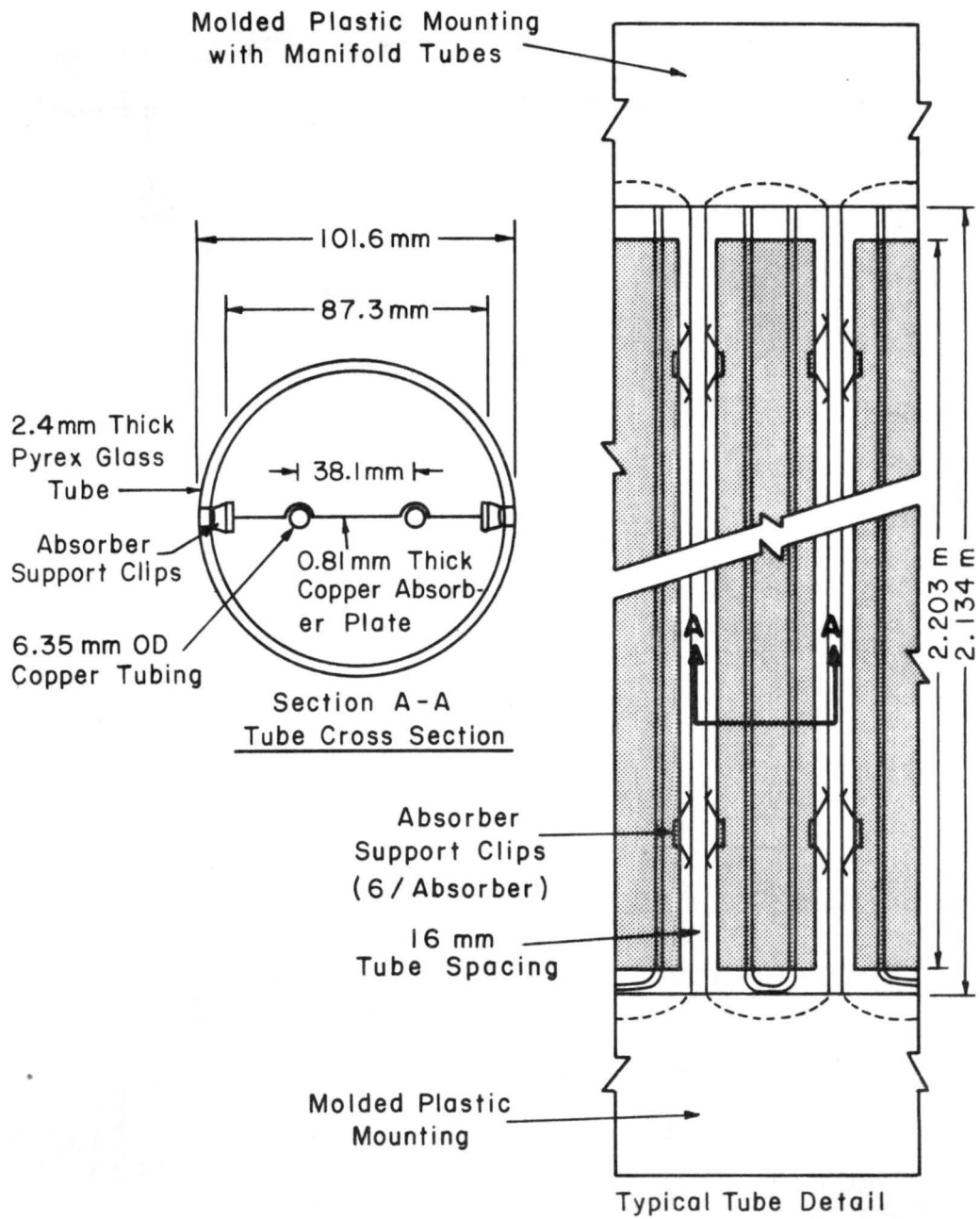


Figure 1-2. Test Module Details.

completed to estimate the performance. The optical performance is calculated to determine the effective $\tau\alpha$ product and the thermal performance is then analyzed to calculate the U_L and F_R terms. The performance of the collector is then measured by testing, and these results are then compared with the results of the theoretical analysis.

Chapter II

OPTICAL ANALYSIS

2.0 General Comments

In order to evaluate the solar transmittance characteristics of the cylindrical glass tubes several considerations must be made. The total amount of solar radiation actually transmitted to the absorber plate is affected by transmittance characteristics of the glass, the effect of the tube curvature, the shading effects of adjacent tubes, the reflections from adjacent tubes and the diffuse reflection from surfaces behind the collector. These effects must be considered for both diffuse and beam components of solar radiation. Knowing the effective transmittance through the glass, the absorptivity of the absorber, and the internal reflections between the tube and the absorber, the effective transmittance-absorptance product can be calculated.

Computations are made assuming the angle of the beam component can be expressed by the angles shown in Figure 2-1. The angle of the sun along a plate perpendicular to the tube axis is given by ψ with positive angles measured left and negative angles measured right. The angle of the sun measured from the tube axis is θ .

2.1 Angle of the Sun

The angle of the sun with respect to the collector axis, measured in terms of ψ and θ can be determined for any sun position. The position of the sun can be described in terms of several angles. These angles are defined below and are consistent with the notations and definitions given by Duffie and Beckman [6]:

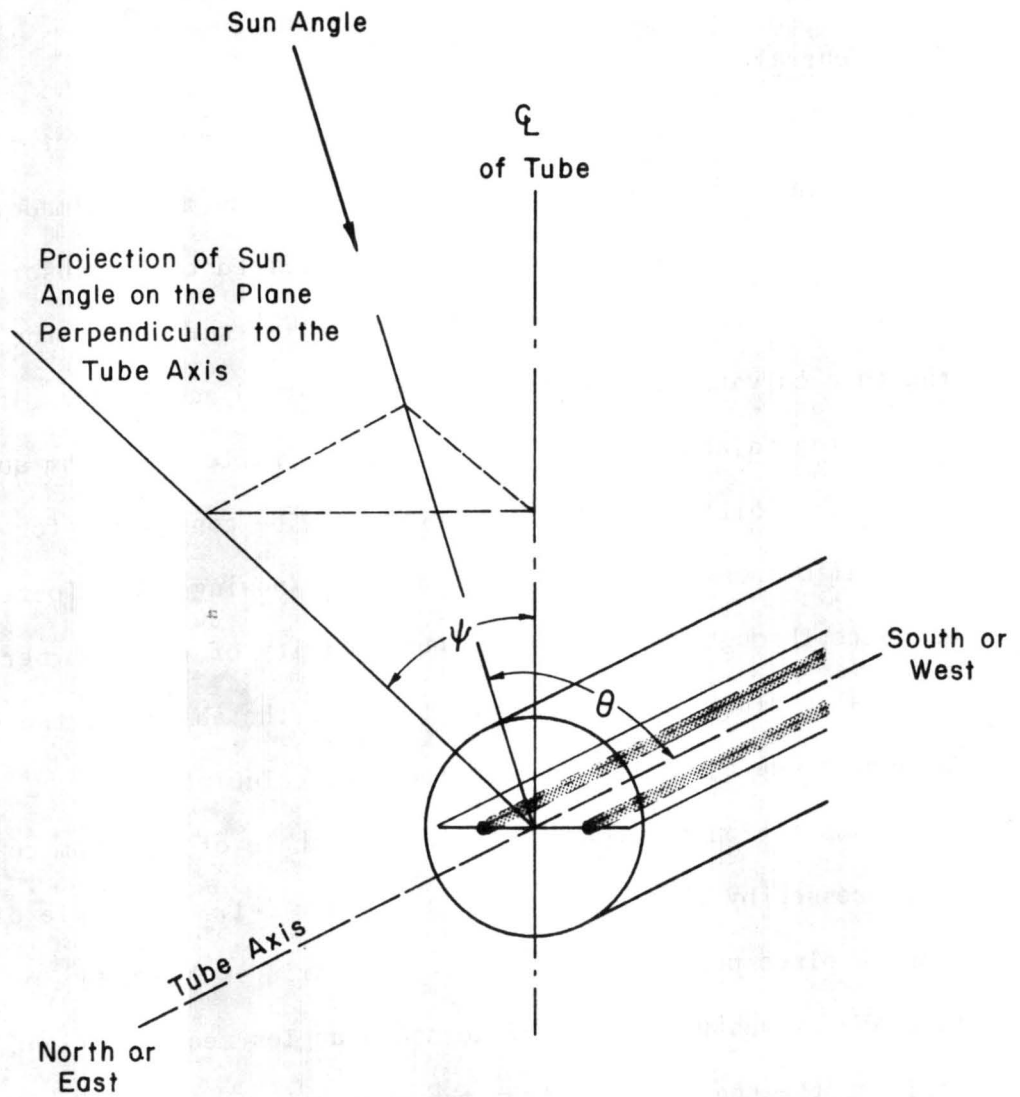


Figure 2-1. Tube Orientation Angles.

- ϕ is the latitude (north positive);
- δ is the declination (the angular position of the sun at solar noon with respect to the plane of the equator);
- γ is the surface azimuth angle, that is, the deviation of the normal to the surface from the local meridian, zero point being due south, east positive, west negative;
- ω is the hour angle, solar noon being zero, and each hour equaling 15 degrees of longitude with mornings positive and afternoons negative;
- s is the angle between the horizontal and the plane (i.e., the slope).

The relationship between these angles and ψ and θ is a function of collector orientation. The tubes can be oriented with the axis sloped north-south or the tube axis can be horizontal with an east-west alignment and the absorber sloped southward.

For the first case of the inclined tube axis, ψ can be determined from an equation given by Threlkeld [7] which is rewritten in Equation 2-1.

$$\tan \psi_{N-S} = \frac{\cos \delta \sin \omega}{\sin \delta \sin \phi' + \cos \delta \cos \phi' \cos \omega} \quad (2-1)$$

where ϕ' (the artificial latitude) is determined by:

$$\phi' = \phi - s - 90^\circ . \quad (2-2)$$

The angle θ can be calculated from Equation (2-3):

$$\cos \theta_{N-S} = \cos \delta \cos \phi' \cos \omega + \sin \phi' \sin \delta . \quad (2-3)$$

The above equations apply to a collector with the tube axis oriented north-south and for $\gamma = 0$. If the tube axis is oriented in an east-west direction then ψ becomes the profile angle given by:

$$\tan \psi_{E-W} = \frac{\tan (90 - \beta)}{\cos \alpha} \quad (2-4)$$

where,

$$\tan \alpha = \frac{-\cos \delta \sin \omega}{\cos \beta} \quad (2-5)$$

and,

$$\cos \beta = \cos \delta \cos \phi' \cos \omega + \sin \phi' \sin \delta. \quad (2-6)$$

The angle θ is then given by:

$$\cos \theta_{E-W} = \sin \psi_{E-W} \sin \alpha. \quad (2-7)$$

2.2 Transmittance of Incoming Beam Radiation

The transmission of incoming beam radiation through the glass tube is affected by angular variation in two ways. The first is the effect of increasing angle of incidence on the glass with decreasing θ , which reduces transmittance. The second is the effect of smaller aperture at larger angles of ψ due to the cosine of the sun angle which increases effective transmittance as a result of smaller angles of incidence on the glass tube.

In order to simplify the analysis several assumptions are made:

1. Light displacement due to refraction and glass curvature is assumed negligible;
2. Variations in transmissivity of the glass due to manufacturing defects are ignored;

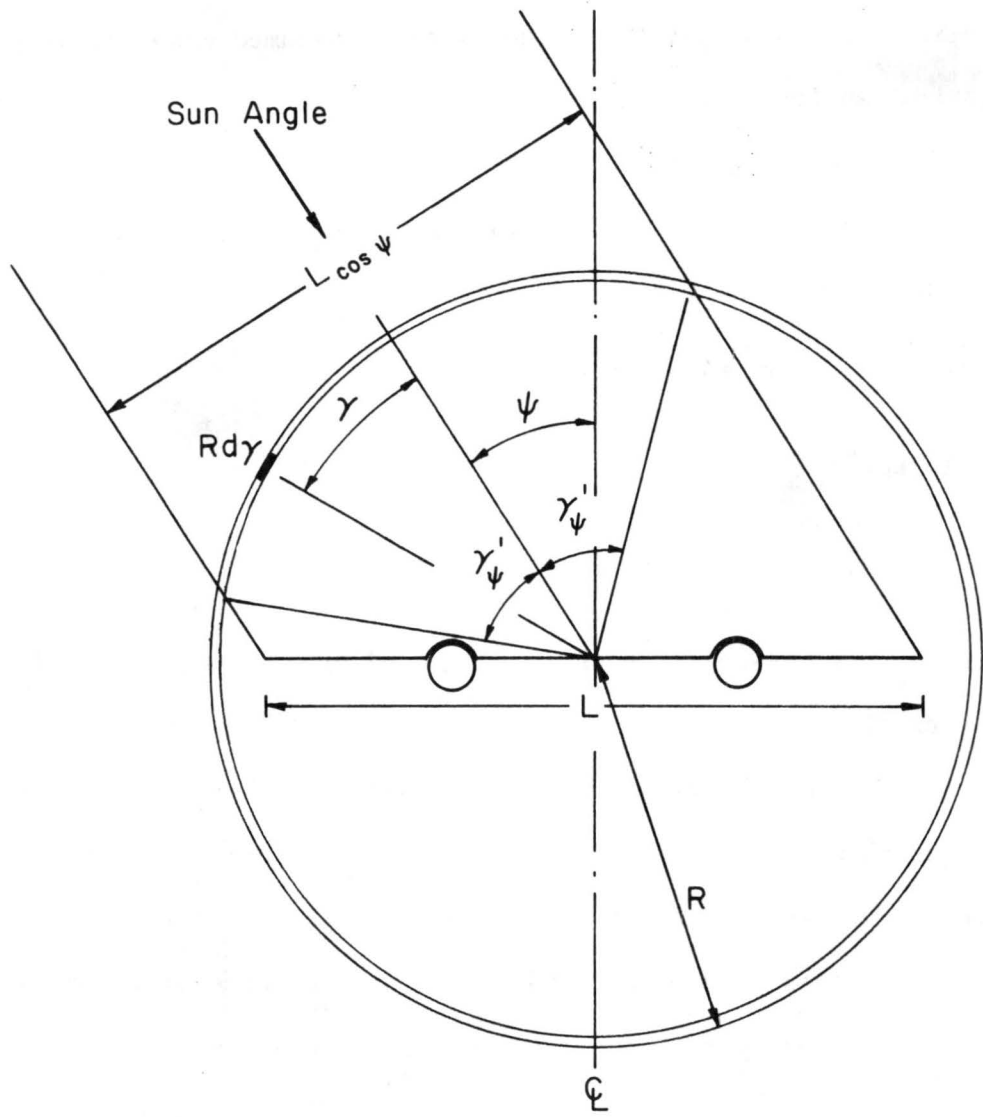


Figure 2-2. Transmissivity of Glass Tube.

3. The absorptivity of the plate is assumed constant at all angles of incidence.

The general problem considered for the transmittance calculations is shown in Figure 2-2. From this figure, γ_ψ can be determined by the relationship:

$$R \sin \gamma_\psi = \frac{L}{2} \cos \psi,$$

or solving for γ_ψ ,

$$\gamma_\psi = \sin^{-1} \left(\frac{L}{2R} \cos \psi \right), \quad (2-8)$$

where γ_ψ is one-half the angle subtended by the projection of the absorber plate on the glass tube for a sun angle ψ .

The transmissivity of glass is a function of the angle of incidence as shown in Figure 2-3. This curve is a function of Fresnel reflection losses and absorption within the glass. For one small section of glass tube, $Rd\gamma$, the angle of incidence of light on the section is given by the spherical geometric relationship:

$$\cos \lambda = \cos \gamma \sin \theta, \quad (2-9)$$

where λ is the angle of incidence measured from the normal to $Rd\gamma$.

The effective transmittance is determined for each angle ψ and θ by integrating the transmittance through each section $Rd\gamma$ for γ from 0 to γ_ψ , and dividing by the projected width of the absorber on the glass tube. Thus,

$$\tau_{\text{eff}} = \frac{\int_0^{\gamma_\psi} \tau_\lambda R \cos \gamma d\gamma}{\frac{L}{2} \cos \psi}, \quad (2-10)$$

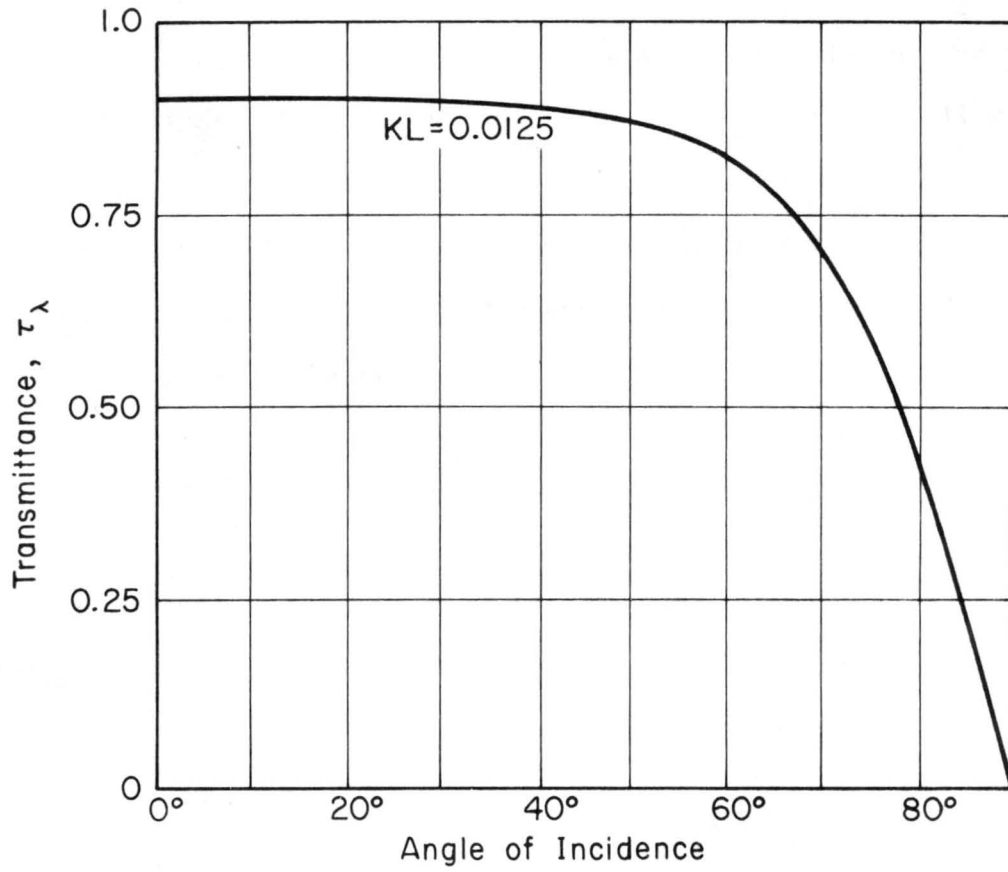


Figure 2-3. Transmittance Glass (from Duffie and Beckman, 1974).

in which τ_λ is a function of reflection and absorption of the glass. Because a closed-form analytical solution of Equation (2-10) is not readily apparent, a numerical integration was performed, dividing γ_ψ into several segments $\Delta\gamma$, with τ_λ determined for the midpoints of each segment using Figure 2-3. For the analysis of the test module this approximation is satisfactory because the variation of τ_λ is small over the ranges of γ_ψ . The results of the calculations for the test module are presented in Appendix I.

The calculations show that there is a slight variation of transmissivity with ψ , increasing with ψ . This is due to the decreasing aperture on the glass at increasing values of ψ .

2.3 Shading Effects of Adjacent Tubes

The shading by adjacent tubes becomes significant at large values of ψ , particularly when the tubes are closely spaced as in the test module. The effects of shading are shown in Figure 2-4. The minimum angle ψ' , at which these effects occur is given by:

$$\psi' = \sin^{-1} \left(\frac{1}{2 + \frac{d}{R} - \frac{L}{2R}} \right) \quad (2-11)$$

In considering the effects of shading, the effective transmissivity was analyzed assuming:

1. The transmission through the glass layers of the adjacent tube over the distance ℓ is averaged over $L \cos \theta$ because the transmissivity of the tube at large angles of ψ is nearly uniform over the distance $L \cos \theta$;

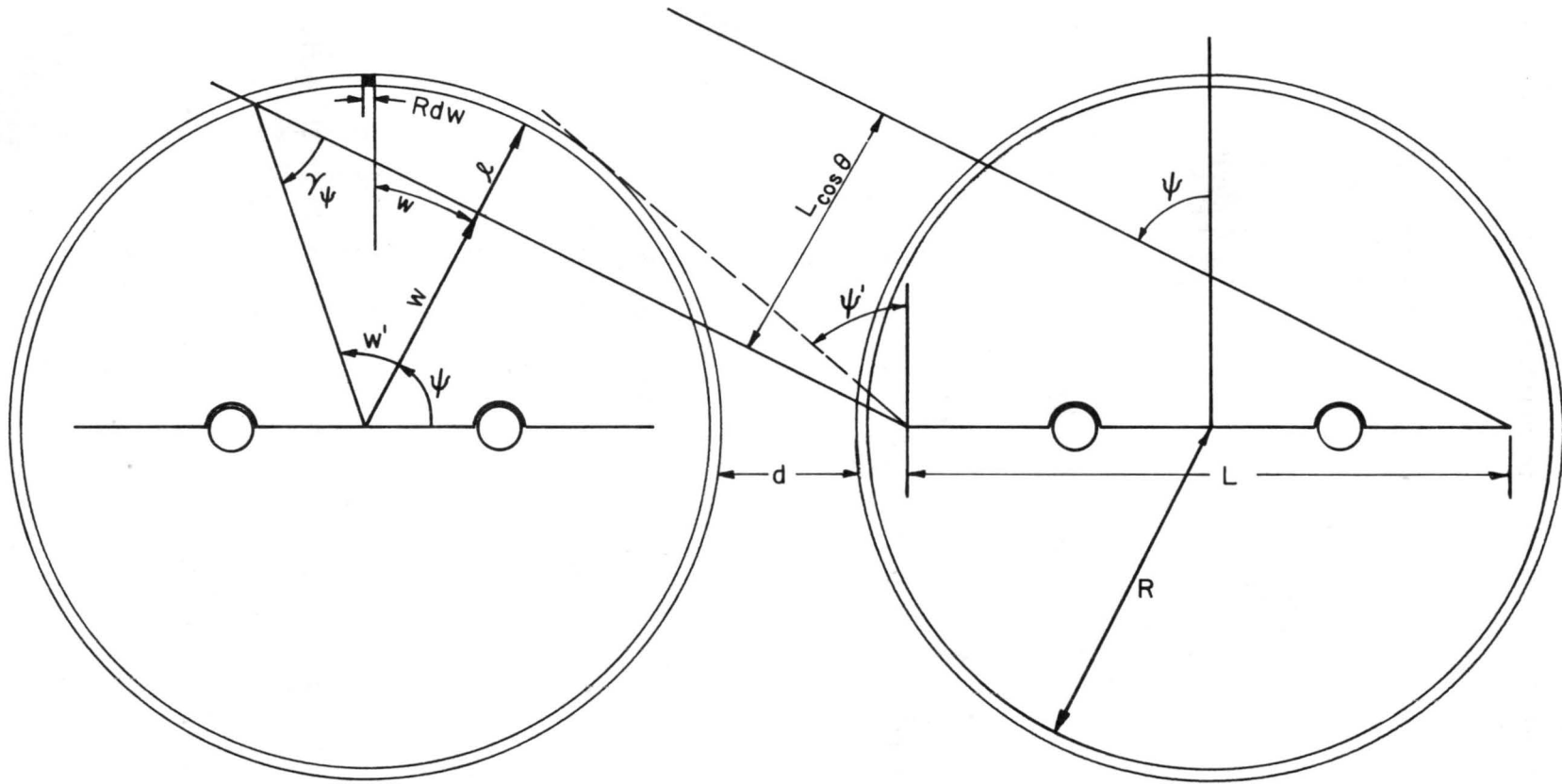


Figure 2-4. Shading Effects of Adjacent Tubes.

2. The shading effects of more than one tube was not considered because the solar energy available at very large angles ψ is not significant.

From Figure 2-4, the following distances and angles can be derived:

$$W = [R + d + (R - \frac{L}{2})] \cos \psi \quad (2-12)$$

$$\cos w' = \frac{1}{R} [R + d + (R - \frac{L}{2})] \cos \psi \quad (2-13)$$

$$\gamma_{\psi} = 90 - w' \quad (2-14)$$

$$\gamma_{\psi} = \sin^{-1} \left\{ \frac{1}{R} [R + d + (R - \frac{L}{2})] \cos \psi \right\} \quad (2-15)$$

$$\ell = R - W \quad (2-16)$$

The light transmitted through the glass surface Rdw , is again determined by the relationship:

$$\cos \lambda = \sin w \sin \theta \quad (2-17)$$

and τ_{λ} can be determined for any λ . Knowing the transmissivity at any angle, w , the following integral can be obtained:

$$\tau_s = \left\{ \frac{\int_0^W \tau_{\lambda} R \sin w \, dw}{\ell} \right\}^2 \quad (2-18)$$

where τ_s is the effective transmittance through the section of tube with width ℓ . The entire term is squared to account for the effects of the two glass layers through which the light must pass. Again, the complexity of the expression for τ_{λ} makes it necessary to integrate numerically. The results of the computations for shading effects for the test module are shown in Appendix I. Generally, the effects of

shading are substantial only for diffuse radiation calculations because of large angles of ψ .

2.4 Reflections from Adjacent Tubes

Previous testing by the Corning Glass Works Company indicates that groups of tubes perform better than individual tubes. This can be partially explained by the reflection from adjacent tubes which provides a slight concentrating effect which increases the amount of incident energy onto an absorber. Figure 2-5 shows the reflection from a segment of the adjacent glass tube. From Figure 2-5 it can be seen that the gains from reflection can be expressed by the product, $h\rho_\lambda\tau_\theta$, where:

$$h = R (\sin \beta_1 - \sin \beta_2) \quad (2-19)$$

and

$$\beta_1 = 90 - \frac{\psi}{2} - \frac{1}{2} \tan^{-1} \left(\frac{2R + d - \frac{L}{2} - R \sin \beta_1}{R \cos \beta_1} \right) \quad (2-20)$$

$$\beta_2 = 90 - \frac{\psi}{2} - \frac{1}{2} \tan^{-1} \left(\frac{2R + d + \frac{L}{2} - R \sin \beta_2}{R \cos \beta_2} \right) \quad (2-21)$$

These formulas are based on the assumption that the angle of incidence is equal to the angle of reflection. To solve Equations (2-20) and (2-21) β_1 and β_2 must be iterated. Knowing β_1 and β_2 the Fresnel reflections ρ_λ were determined from Figure 2-6 and the average angle of incidence is determined from the relationship,

$$\cos \lambda = \cos \delta \sin \theta, \quad (2-22)$$

where $\delta = \psi + \beta$. The calculations must be done for positive and negative values of ψ in order to account for tubes on each side. For any

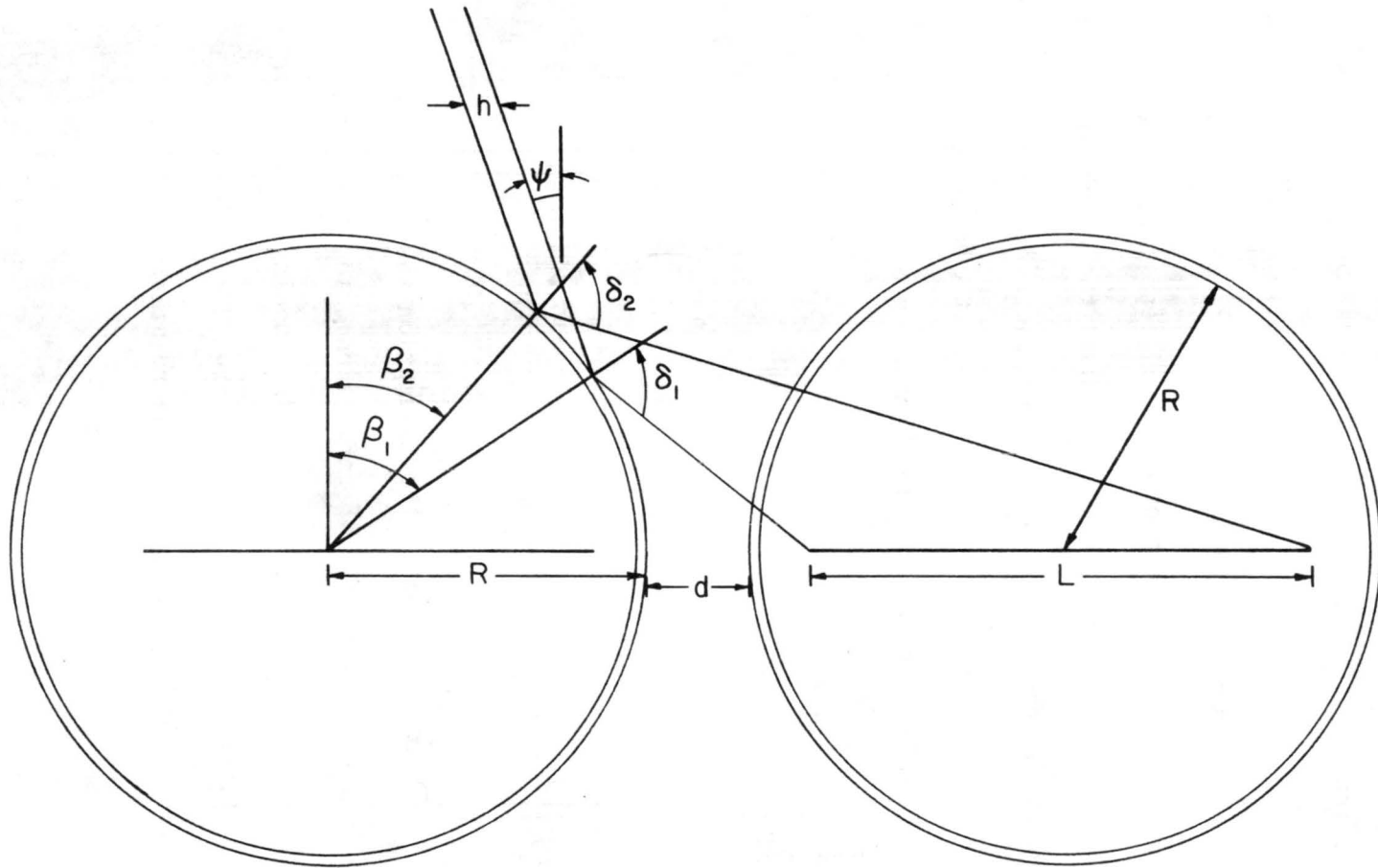


Figure 2-5. Reflections from Adjacent Tubes.

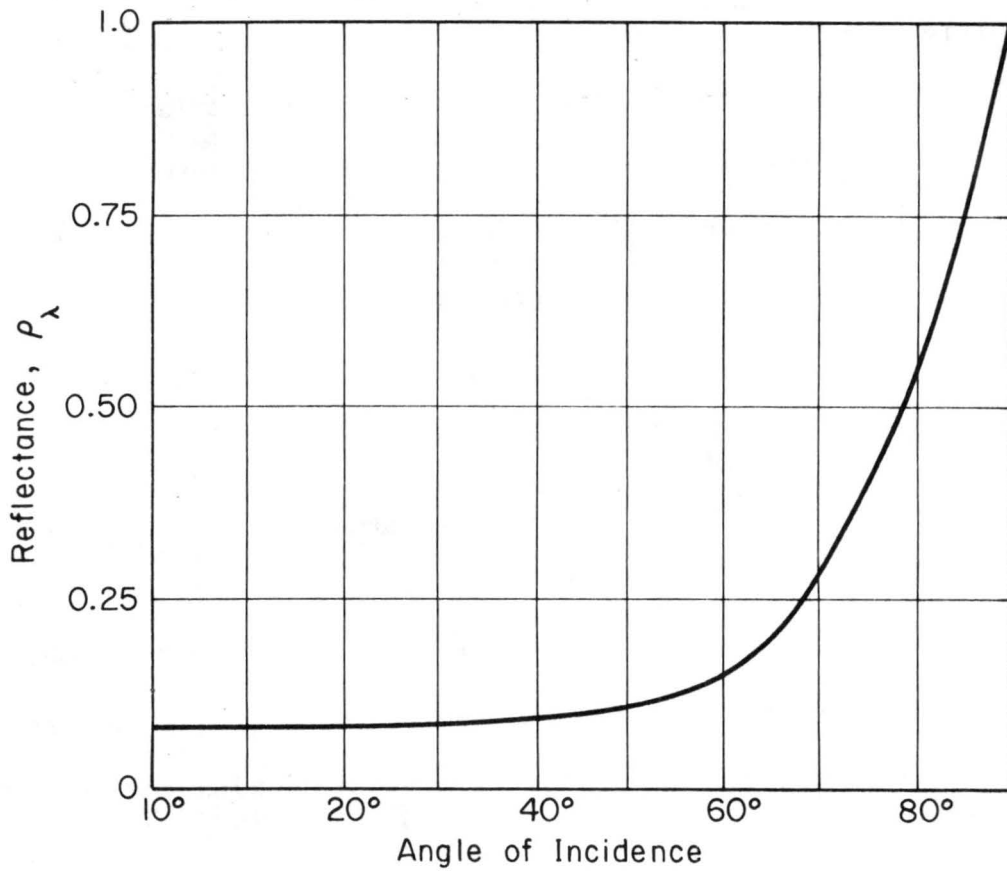


Figure 2-6. Reflectance of Glass with Index of Refraction of 1.526 (from Duffie and Beckman, 1974).

given ψ and θ , h and ρ_λ can be determined for ψ and the reflection gains can be calculated by assuming a transmissivity, τ_θ , for the angle ψ because the reflected rays are nearly normal to the tube surface. This analysis neglects second order reflections. The results of the calculations for the test module are presented in Appendix I. There is a limited range of ψ for which reflections will be intercepted by an absorber plate but these angles are a function of the absorber width, glass tube diameter, and spacing between the glass tubes. The calculation for the test module shows that maximum reflection gains occur when ψ is about 40 degrees.

2.5 Diffuse Reflections from Back Surfaces

The tubular construction of the collector necessitates spaces between the tubes, and spaces between adjacent absorber plates which will not intercept solar radiation. If collectors are to be mounted over roofs or other surfaces, these surfaces will reflect radiation onto the back of the absorber plates. Because the cost of the collectors is dependent on the area of the absorber and almost independent of the tube spacing, the tubes should be spaced to provide the greatest amount of absorbed radiation per net area of the collector.

This analysis for the amount of back reflection absorbed by the collector assumes that the reflections are totally diffuse and the tubes are uniformly spaced. The definition sketch used for the development which follows is shown in Figure 2-7. From this figure, the following can be shown:

$$\Delta\gamma_n = \arctan \frac{H + R}{(n(ZR+d) - L/2+a)} - \arctan \frac{H + R}{(n(ZR+d) - L/2+a)} \quad (2-23)$$

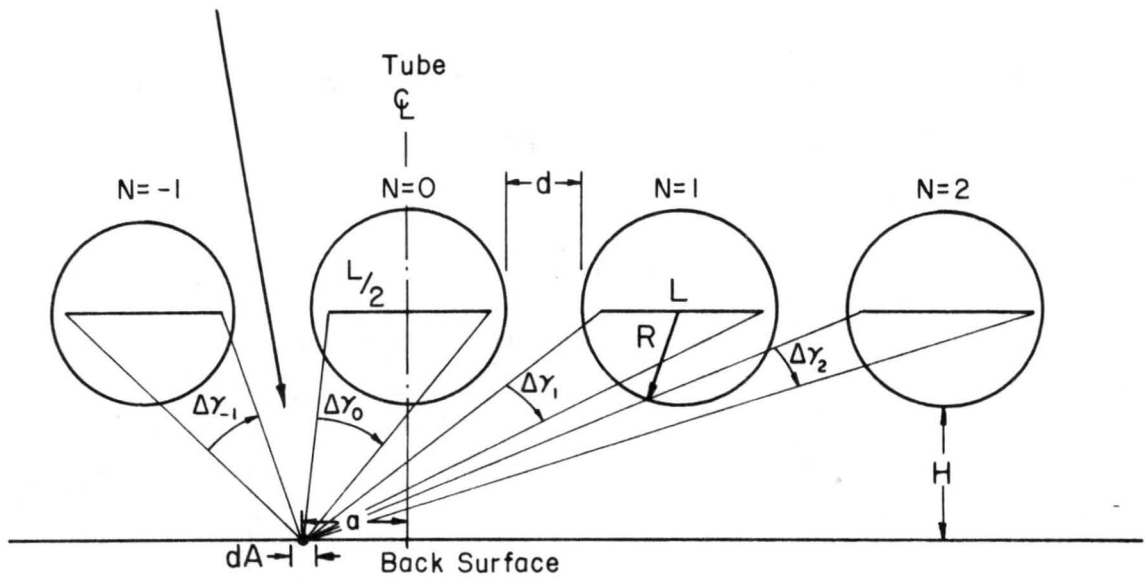


Figure 2-7. Reflection off Back Surfaces.

where H is the distance from the back reflecting surface to the tubes and n is the tube number in the bank of $2N+1$ tubes. The distance from a small area, dA , to the centerline of the tube in question is designated by a . Assuming infinite tube lengths, the fraction of reflected radiation that is intercepted by the absorber is given by I_{ρ} , where:

$$I_{\rho} = \sum_{n=-N}^N \frac{\Delta\gamma_n}{\pi} \quad (2-24)$$

Clearly, the fraction of reflected light intercepted by the absorber is dependent upon H , N , R , L , d , and a . For a given collector design, the only variables are H , d , and a . The amount of radiation reflected onto the absorber is proportional to the product $I_{\rho} d$. Therefore, the optimum spacing would be the spacing which produces the greatest product, $I_{\rho} d$.

The test module has a tube spacing of 16 mm and was mounted over a black surface which increased the total collection of radiation by less than 0.5 percent. Therefore, these effects were ignored for the test module.

To account for the changes in intercepted reflection at the edge of tube bank the back reflections must be analyzed for each space and averaged to determine the reflections for each absorber tube. The average reflection intercepted by a tube can be expressed by:

$$\bar{I}_{\rho} = \frac{\sum_{n=-N}^{-N} I_{\rho n}}{2N+1} \quad (2-25)$$

Consideration was given to optimum spacing of adjacent tubes. For collectors, with dimensions equal to the test module, and spacing ratio

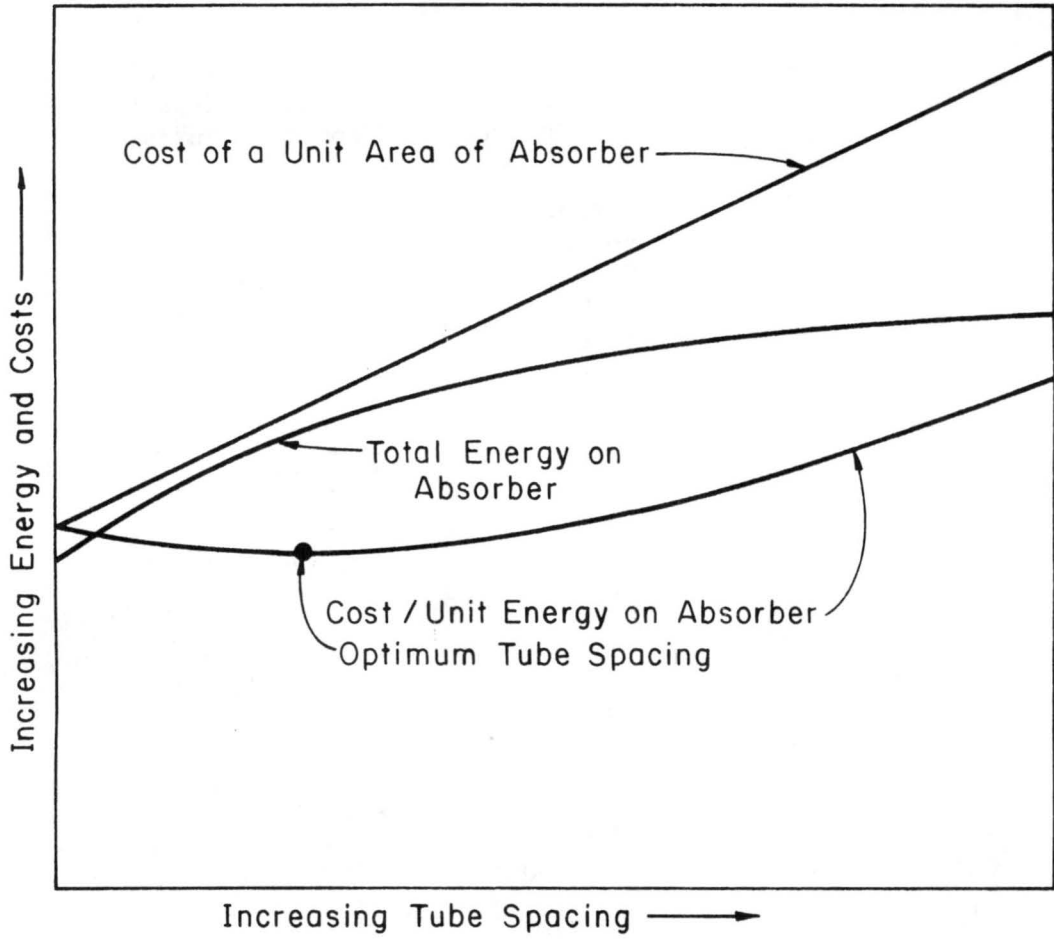


Figure 2-8. Optimum Tube Spacing.

H/d greater than 0.75, I_{ρ} is nearly independent of a . There is no maximum for the product $I_{\rho} d$ with increase in d ; $I_{\rho} d$ increases monotonically. Therefore, an optimum in terms of intercepted radium does not exist. Table 2-1 shows calculations for the test module.

TABLE 2-1 Average Energy Flux Increases Due to Reflections from Back Surfaces

| Tube Spacing d diameters* | Distance to Back Surface H diameters | Average Reflection \bar{I}_{ρ} | Increase in Energy Flux Per Unit Area of Collector $I_{\rho} d/L$ |
|-----------------------------------|--|---|---|
| 0.5 | 0.5 | 0.563 | 0.33 |
| 0.5 | 1 | 0.559 | 0.32 |
| 0.5 | 2 | 0.549 | 0.32 |
| 1.0 | 0.5 | 0.425 | 0.49 |
| 1.0 | 1.0 | 0.422 | 0.49 |
| 1.0 | 2.0 | 0.416 | 0.48 |
| 2.0 | 0.5 | 0.289 | 0.67 |
| 2.0 | 1.0 | 0.283 | 0.66 |
| 2.0 | 2.0 | 0.281 | 0.65 |

*Calculations done for test module tubes (diameter 10.2 cm).

An optimum spacing can, however, be determined on the basis of collector and reflector costs. An illustration of optimum spacing as shown in Figure 2-8 is seen to depend on $I_{\rho} d$ (total energy absorbed) and cost of a unit area of the absorber. A linear cost function is

assumed for purposes of illustration, based on increase of mounting surface area and attendant structural costs.

The optimum tube spacing can be different for each system because of differing costs of construction. With increased spacing, the effects of reflections from adjacent tubes become negligible. However, the reduction of absorbed radiation because of reduced reflection is less than the gain from reflections from the back surface.

2.6 Internal Reflection

The reduced absorptivity of the absorber surface, compared to a flat-black surface (characteristic of selective coatings), means that the reflected portion of the solar radiation can be significant. It is necessary, therefore, to consider the reflection from the inside surface of the glass tube back to the absorber. The curved surface of the tube complicates the analysis of these internal reflections. In this analysis, a large L/R and total diffuse reflection from the absorber are assumed.

The internal reflections from the tube that is intercepted by the absorber is a function of the position of the source of these reflections as shown in Figure 2-9. For any small area on the absorber at distance x from the centerline, and angle ψ_r , β can be expressed from the cosine law as follows:

$$\cos \beta = \frac{R - x \sin \psi_r}{(x^2 + R^2 - 2Rx \sin \psi_r)^{1/2}} \quad (2-26)$$

and x' can be determined from the relation:

$$x' = R(\sin \beta) / \cos (\psi_r + \beta) \quad (2-27)$$

where the angle of incidence is equal to the angle of reflection.

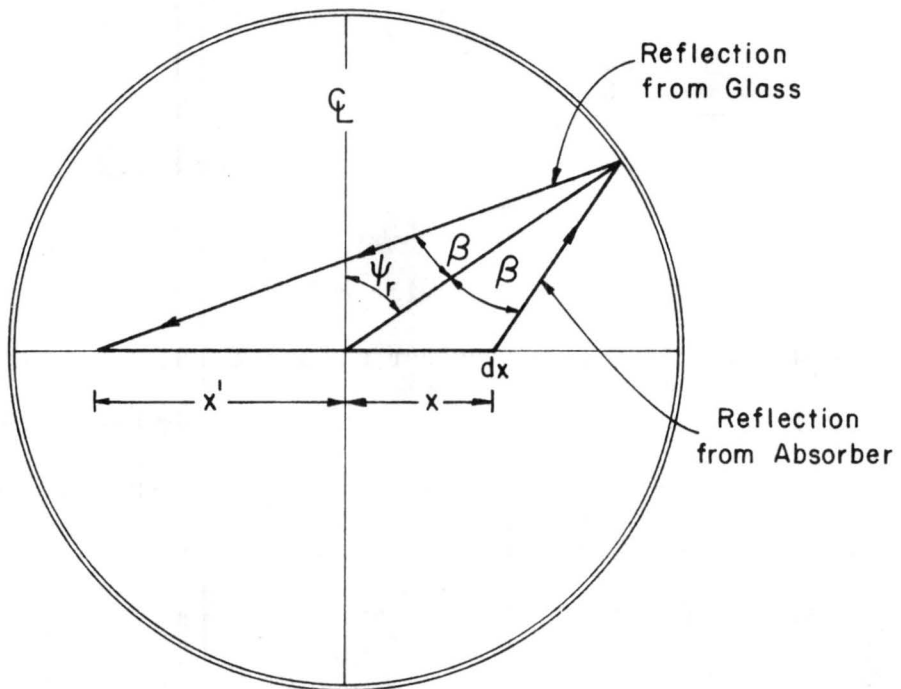


Figure 2-9. Internal Reflection.

The internal reflection effects for a cross section of absorber can be determined by calculating the reflectance from each increment of area at x on the absorber for ψ_r from -90 to 90 degrees and for θ_r from 0 to 90 degrees. The angles, ψ_r and θ_r , are reflection angles measured from the center of the absorber in the same orientation of ψ and θ . Then the amount of reflected radiation absorbed is determined by:

$$\rho = \frac{\int_0^{L/2} \int_0^{90} \int_{-90}^{90} \rho_{\gamma\theta} d\gamma d\theta dx}{\int_0^{L/2} \int_0^{90} \int_{-90}^{90} d\gamma d\theta dx} \quad (2-28)$$

where $\rho_{\gamma\theta}$ is a function of λ and θ given in Figure 2-6 and ρ is 0 when x' is greater than $L/2$. The solution is most quickly determined by numerical integration by dividing the absorber into sections and determining the reflections for the midpoint of each section. When $x = 0$, x' is 0 for all angles, and for $x = L/2$, $x' > L/2$ for γ from 0 to an angle equal to the arc tan $(2R/L)$. The results of the computations for the test module are tabulated in Appendix I. The total internal reflectivity, ρ , back to the absorber from the tube is 0.0843, which is the fraction of reflected radiation from the absorber that is re-reflected to the absorber. Duffie and Beckman [6] show that the infinite sum of internal reflections for flat-plate collectors is given by:

$$\rho_{\text{eff}} = \frac{1}{1 - (1-\alpha)\rho} - 1 \quad (2-29)$$

2.7 Effective $\tau\alpha$ Product

The effective transmissivity absorptivity product is the combination of the effects discussed previously. These effects can be

combined into what is called the effective transmissivity absorptivity product:

$$(\tau\alpha)_e = [I_b \tau_b + (I_d + \bar{I}_d/L) \tau_d] (1 + \rho_{eff}) \alpha \quad (2-30)$$

where:

$$\tau_b = \tau_{\theta\psi} = \tau_{eff} + h/L \rho_\lambda \tau_\theta \quad (2-31)$$

$$\tau_d = \frac{\int_0^{90} \int_0^{90} \tau_{\theta\psi} d\psi d\theta}{\int_0^{90} \int_0^{90} d\psi d\theta} \quad (2-32)$$

and τ_{eff} includes the effects of shading if $\psi > \psi'$.

The transmissivity of the beam component, τ_b , for various angles of θ and ψ are computed for the test module and tabulated in Table 2-2. The diffuse radiation transmissivity, τ_d , was computed to be 0.774, assuming uniform distribution of diffuse radiation. If the distribution of the diffuse component is known, the limits of integration of Equation (2-32) can be altered and Equation (2-30) will have additional terms of $I_d \tau_d$ for each value of I_d . The values I_d and I_b are the diffuse and beam components of total radiation, respectively, measured at the orientation of the collector absorber. The reflection and shading effects are multiplied by $N-1/N$ to account for the end tubes in a collector array, where N is the number of tubes in the array. There is some effect of the absorptivity of radiation in the glass which can affect the performance of the collector. Duffie and Beckman [6] include this in the $\tau\alpha$ product in the general collector equation, however, this is a thermal consideration that is dependent

TABLE 2-2 Effective Transmittance of the Test Module

| $\psi \backslash \theta$ | 90° | 80° 100° | 70° 110° | 60° 120° | 50° 130° | 40° 140° | 30° 150° | 20° 160° |
|--------------------------|-------|-------------|-------------|-------------|-------------|-------------|-------------|-------------|
| 0° | 0.911 | 0.906 | 0.906 | 0.909 | 0.894 | 0.871 | 0.811 | 0.675 |
| 10° | 0.919 | 0.919 | 0.912 | 0.913 | 0.909 | 0.874 | 0.821 | 0.688 |
| 20° | 0.925 | 0.916 | 0.917 | 0.919 | 0.914 | 0.881 | 0.826 | 0.692 |
| 30° | 0.957 | 0.936 | 0.939 | 0.945 | 0.934 | 0.901 | 0.848 | 0.722 |
| 40° | 0.956 | 0.958 | 0.958 | 0.963 | 0.950 | 0.918 | 0.866 | 0.735 |
| 50° | 0.823 | 0.823 | 0.821 | 0.814 | 0.807 | 0.773 | 0.718 | 0.661 |
| 60° | 0.802 | 0.802 | 0.744 | 0.726 | 0.712 | 0.661 | 0.584 | 0.478 |
| 70° | 0.616 | 0.616 | 0.607 | 0.582 | 0.589 | 0.466 | 0.355 | 0.193 |

on both optical effects and thermal losses and will be discussed in Chapter III.

There are several interesting aspects to the optical analysis of the evacuated tube collector. Non-normal incidence of solar radiation on the absorber plate can increase the performance of the collector. The maximum increase of these effects, which are mainly due to reflections from adjacent tubes occur at angles, ψ , of about 40° . It is also noted that because of the reflections onto the back of the tubes, there is an optimum spacing for the tubes for a cost-effective use of a fixed absorber area. This optimum spacing is a function of the variation of collector and surface cost with spacing and must be determined for a particular collector and cost of the back surface.

2.8 Tube Orientation

The effect of orientation of the tube axes is considered for a typical day. The values for $(\tau\alpha)_e$ were calculated for both north-south and east-west orientations of the tube axes for the test module configuration. Table 2-3 shows the hourly energy absorbed, $(HR(\tau\alpha)_e)$, for a typical day of solar radiation that was measured during the test period.

The table shows that with the tubes axes oriented in an east-west direction there is 10 percent increase in average hourly energy absorbed over a 10-hr day, as compared to a north-south orientation. This means that for best performance the tubes should be oriented in an east-west direction. The increase in performance is due to nonshading by adjacent tubes for the east-west orientation. The experimental data were obtained only for the north-south tube orientation.

TABLE 2-3 Calculated Energy Absorbed for Corning Collector with Change in Tube Axis Orientation. For July 25, 1975*

| Time (hr) | Hour Angle w degrees | Solar Radiation HR^{**} W_M^{-2} | North-South Tube Orientation 45° Slope | | | | East-West Tube Orientation 45° Slope | | | |
|---------------------|------------------------|--------------------------------------|--|------------------------|-------------------------|---|--------------------------------------|------------------------|-------------------------|---|
| | | | ψ_{N-S} degrees | θ_{N-S} degrees | Transmissivity τ_b | Energy Absorbed $HR(\tau\alpha)_e$ W_M^{-2} | ψ_{E-W} degrees | θ_{E-W} degrees | Transmissivity τ_b | Energy Absorbed $HR(\tau\alpha)_e$ W_M^{-2} |
| 7 | 67.5 | 280 | 67.4 | 111.2 | 0.641 | 149 | -45.3 | 131.0 | 0.871 | 196 |
| 8 | 52.5 | 506 | 63.1 | 112.2 | 0.738 | 305 | -42.1 | 126.7 | 0.923 | 374 |
| 9 | 37.5 | 675 | 55.7 | 113.1 | 0.773 | 425 | -37.1 | 119.1 | 0.954 | 514 |
| 10 | 22.5 | 808 | 41.9 | 113.7 | 0.933 | 603 | -30.5 | 109.8 | 0.939 | 607 |
| 11 | 7.5 | 874 | 16.9 | 114.0 | 0.916 | 641 | -24.0 | 96.8 | 0.929 | 650 |
| 12 | -7.5 | 887 | -16.9 | 114.0 | 0.916 | 651 | -24.0 | 83.2 | 0.929 | 659 |
| 13 | -22.5 | 841 | -41.9 | 113.7 | 0.933 | 628 | -30.5 | 70.2 | 0.939 | 631 |
| 14 | -37.5 | 729 | -55.7 | 113.1 | 0.773 | 459 | -37.1 | 60.1 | 0.954 | 555 |
| 15 | -52.5 | 568 | -63.1 | 112.2 | 0.738 | 343 | -42.1 | 53.3 | 0.923 | 420 |
| 16 | -67.7 | 280 | -67.4 | 111.2 | 0.641 | 149 | -45.3 | 49.0 | 0.871 | 196 |
| 17 | | | | | | | | | | |
| Average over 10 hrs | | 648 | | | | 435 | | | | 480 |

* $\delta = 19.6^\circ$ $\phi = 40.6^\circ$ $s = 45^\circ$

**Measured solar radiation for this day.

Chapter III

THERMAL ANALYSIS

3.0 General Comments

The thermal analysis of a solar collector consists of determining the thermal loss from the collector as well as the efficiency of heat removal by the working fluid. The losses for an evacuated tube collector can be evaluated by determining the heat transfer from the absorber to the glass tube and the heat transfer from the glass tube to the surroundings. The heat removal efficiency factor is a function of the thermal loss rate, and heat transfer from the absorber to the working fluid.

3.1 Heat Loss Coefficient

The heat loss coefficient U_L for the collector was determined by analyzing each source of loss and equating the heat transfer from the absorber to the glass tube with the heat losses from the glass tube. The temperature of the glass tube can thus be determined, and U_L can be calculated. The heat transfer from the absorber to the tube occurs by radiation from the absorber, conduction through the supporting springs, and from conduction and convection that occurs in the partially evacuated space. The losses from the outside surface of the glass tube occur through radiation and convection.

The heat transfer per unit area of absorber by radiation from the absorber to the tube is given by the Stefan-Boltzman equation:

$$h_{pg} = 2 \epsilon_{pg} \sigma (T_p^4 - T_g^4) / (T_p - T_g) \quad (3-1)$$

where: T_p is the absorber plate temperature in degrees Kelvin
 T_g is the tube temperature in degrees Kelvin
 ϵ_{pg} is the effective emissivity of the absorber plate to the glass
 σ is the Stefan-Boltzman constant
 and h_{pg} is the radiative heat transfer coefficient for radiation from the absorber to the glass. The effective emissivity, ϵ_{pg} , is determined from the relationship:

$$\epsilon_{pg} = \frac{1}{\epsilon_p + A_p/A_g (1/\epsilon_g - 1)}$$

where: ϵ_p is effective emissivity of the absorber
 A_p is absorber plate area
 A_g is half the glass surface area
 ϵ_g is emissivity of the glass

The factor is to account for losses from both sides of the absorber plate. The view factor, which is a function of the geometry of the two surfaces was determined to be one for the case of a flat-absorber plate.

The plate emissivity is dependent on temperature especially for a selective surface. The effective emissivity of the absorber is determined from:

$$\epsilon_p = \frac{\int_0^{\infty} \epsilon_{\lambda} E_{b\lambda} d\lambda}{\sigma T_p^4} \quad (3-2)$$

where: $E_{b\lambda}$ is determined from Plank's Equation:

$$E_{b\lambda} = \frac{C_1 \lambda^{-5}}{\exp(C_2/\pi T_p)}^{-1} \quad (3-3)$$

which is the black body emissive power per unit wave length, λ ; C_1 and C_2 are Planck's first and second radiation constants. The effective emissivity was computed for the test module for several different temperatures, as shown in Figure 3-1, with the emissivity of the plate varying from 0.036 to 0.045 over the range of normal operating temperatures.

The heat transfer for both conduction and convection in the partially evacuated space with pressures of 10^{-4} torr is less than one percent of the thermal conductivity of air at one atmosphere pressure. The effective conductivity is $2.6 \times 10^{-4} \text{ W/m}^\circ\text{C}$, and is a function of spacing. The heat loss coefficient is nearly constant at about $0.013 \text{ W/m}^2\text{C}$. An error of about one percent in the heat loss coefficient results if it is assumed that convection and conduction losses are negligible.

The support clips holding the absorber plate in the glass tube conducts heat. The heat loss coefficient through these clips is given by:

$$h_s = \frac{m A_s}{A_p} \frac{K_s}{L_c} \quad (3-4)$$

where: A_p is the area of absorber per tube
 m is the number supports per tube
 A_s is the average cross-sectional area of the support
 K_s is the thermal conductivity of the support
 L_c is the length of support from the absorber to the glass.

In Equation (3-4), it is assumed that the absorber plate is of uniform temperature which is a reasonable approximation because of the high

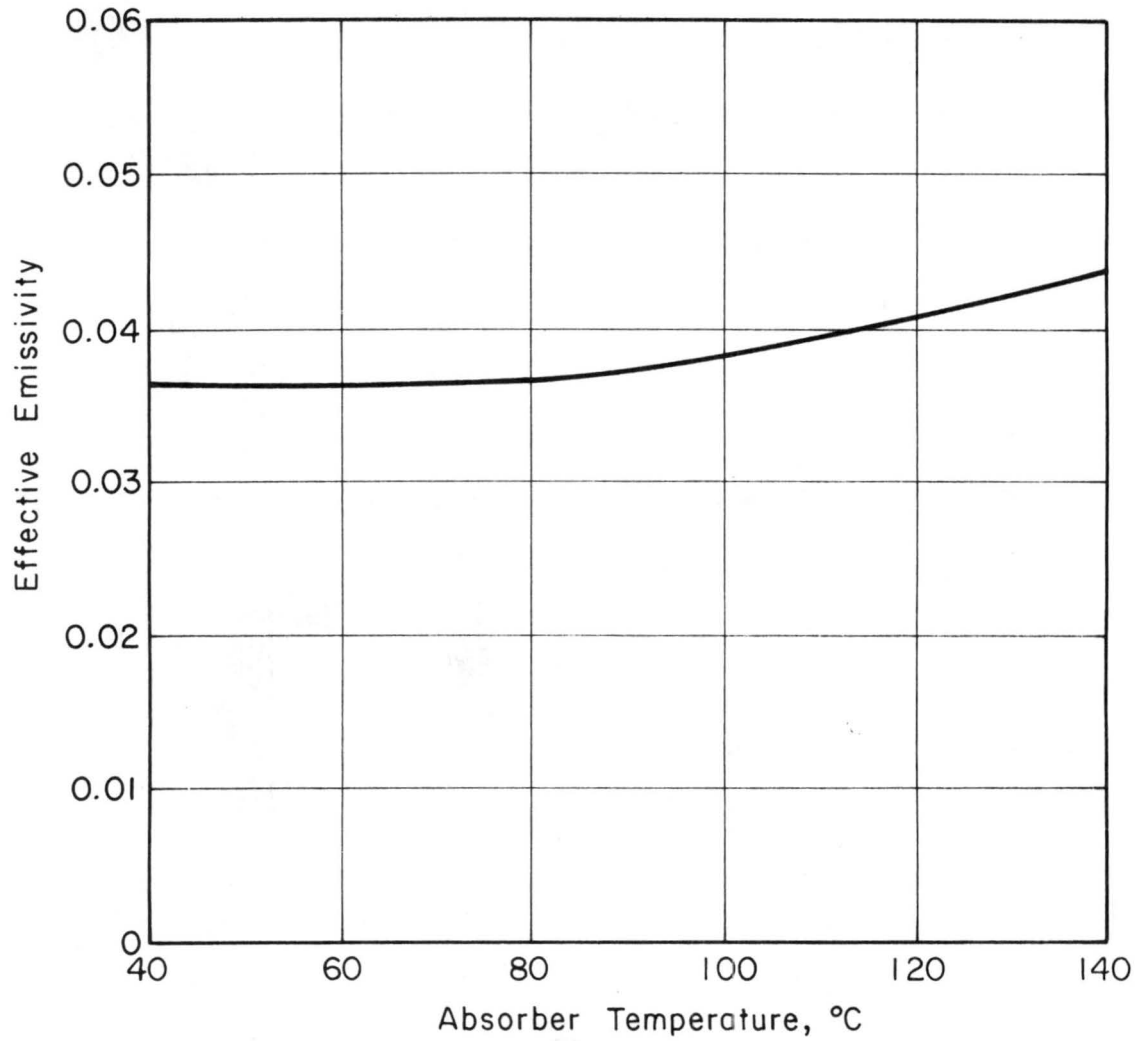


Figure 3-1. Effective Emissivity of Test Module Absorber Surface.

thermal conductivity of the copper absorber with respect to the conductivity of the support. It is also assumed that the glass temperature is uniform, although this is less valid because of the low conductivity of glass. This assumption will result in somewhat higher calculated heat loss rates than if variable temperature is used. The contact resistance is not considered in this analysis and the test results appear to support these assumptions.

The convection coefficient at the outer surface of the glass tube was determined for forced convection at a tube surface in a cross flow. Although the wind direction may cause the air flow to be in almost any direction on the tube the actual heat transfer coefficient will be very nearly the same. For this situation Holman [8], recommends the following relationship:

$$\frac{h_w 2R}{k_f} = c \left(\frac{u_\infty 2R}{v_f} \right)^n Pr^{1/3} \quad (3-5)$$

where:

- h_w is the surface convection coefficient
- u_∞ is the freestream velocity
- k_f is the thermal conductivity of air
- P_r is the Prandtl number
- v_f is the kinematic viscosity of the air

and C and n are functions of the Reynolds number. For the case of several tubes in the collector mounted on a roof or other surface, Beach [4], recommends reducing the convection coefficient to 60 percent of the value calculated in Equation (3-5) to account for this effect. The surface convection coefficient is multiplied by the ratio of tube surface to absorber surface area or:

$$h'_w = 0.6 \frac{A_T}{A_p} h_w \quad (3-6)$$

The surface convection coefficients are calculated for the test module and are shown in Appendix II.

In order to determine the radiation losses from the tube, the sky radiation temperature must be determined. Duffie and Beckman [6] give the following relation between sky radiation temperature and ambient temperature:

$$T_s = 0.0552 T_a^{1.5} \quad (3-7)$$

where the temperatures are in degrees Kelvin. The radiation losses from the tube can be determined by assuming that the adjacent tubes and the back surface are at equal temperatures so that the only area of tube radiating is the portion open the sky, i.e., the angle $\psi = 2 \arcsin \left(\frac{R}{2R+d} \right)$. The adjacent tubes at the same temperatures cause a smaller effective surface area for radiation. For an array of $2N+1$ tubes the radiation heat transfer coefficient is given by:

$$h_r = \frac{2N\pi R \arccos \left(\frac{R}{2R+d} \right) + 90 R\pi}{90A_p (2N+1) (T_g - T_a)} \epsilon_g \sigma (T_g^4 - T_s^4) \quad (3-8)$$

where ϵ_g is the emissivity of the glass, and is assumed to be 0.90 for the test module.

To determine the overall loss coefficient for the general collector Equation (1-1), the tube temperature must be determined. Equating the losses from the absorber to the glass tube to the losses from the glass tube to the surrounding, for a steady-state situation, the following expression can be derived:

$$T_g = h'_w [h_{pg} (T_p - T_g) + h_s (T_p - T_g) - h_r (T_g - T_a)] + T_a \quad (3-9)$$

From Equation (3-9) the tube temperature can be determined by iteration, first by assuming the glass temperature is equal to ambient then solving the right hand side of Equation (3-9) for T_g and substituting back into the equation until equality is achieved. This usually converges to a solution in two or three iterations. The overall heat loss coefficient, U_L , can be calculated by:

$$U_L = \frac{1}{\frac{1}{h_{pg} + h_s} + \frac{1}{h'_w + h_r}} \quad (3-10)$$

Table 3-1 shows the U_L calculations for the test module for a range of plate temperatures from 40 to 100°C.

Another factor affecting the thermal losses is the absorption of solar radiation into the glass. Duffie and Beckman [6] give the following expression to account for this effect:

$$(\tau\alpha) = (\tau\alpha) + (1-\tau\alpha) \frac{U_L}{U_2} \quad (3-11)$$

where U_2 is loss coefficient from the glass and $\tau\alpha$ is the transmissivity considering only the absorptance of the glass. Computations for the test module show that the maximum increase in $(\tau\alpha)$ would only be 0.0014 which is insignificant and was neglected.

3.2 Heat Removal Efficiency Factor

The thermal loss rate is proportional to the absorber plate temperature. In most types of flat-plate solar collectors the fluid temperature is the important parameter and the plate temperature is generally unknown. The plate temperature is somewhat higher than the fluid

TABLE 3-1 Calculated Loss Coefficients and Heat Removal Efficiency Factors for the Test Module

| Plate Temperature | Ambient Temperature | Loss Coefficient | Heat Removal Efficiency (F_R) (Flow Rates/m ² Collector Area) | | |
|-------------------|---------------------|--------------------------------|---|---------------------------------|----------------------------------|
| T_p (°C) | T_a (°C) | U_L (W/m ² °C) | 0.028* ℓ/sec m ² | 0.056** ℓ/sec m ² | 0.084*** ℓ/sec m ² |
| 40 | 0 | 1.07 | 0.988 | 0.993 | 0.994 |
| 40 | 20 | 1.15 | 0.987 | 0.993 | 0.994 |
| 60 | 0 | 1.11 | 0.987 | 0.992 | 0.994 |
| 60 | 20 | 1.16 | 0.987 | 0.992 | 0.994 |
| 60 | 40 | 1.21 | 0.986 | 0.992 | 0.993 |
| 80 | 0 | 1.16 | 0.987 | 0.992 | 0.994 |
| 80 | 20 | 1.21 | 0.986 | 0.992 | 0.994 |
| 80 | 40 | 1.26 | 0.986 | 0.991 | 0.993 |
| 100 | 0 | 1.23 | 0.986 | 0.992 | 0.993 |
| 100 | 20 | 1.28 | 0.986 | 0.991 | 0.993 |
| 100 | 40 | 1.33 | 0.984 | 0.991 | 0.993 |

* 0.5 gpm total flow in test module

** 1.0 gpm total flow in test module

*** 1.5 gpm total flow in test module

temperature for collection of useful heat. In most cases it is necessary to relate the thermal loss rate to a known or measurable quantity such as inlet fluid temperature. The use of fluid temperature requires the introduction of a heat removal efficiency factor F_R to relate the thermal loss rates to the inlet fluid temperature rather than plate temperature.

Generally the heat removal efficiency factor is the product of two factors, F' and F'' . The fin efficiency factor, F' , is a factor relating the absorber plate temperature to the mean fluid temperature, and is a function of heat transfer through the absorber plate to the fluid. The collector flow factor, F'' , is the factor which relates the mean fluid temperature to the inlet fluid temperature.

The heat removal factor can be solved analytically for a normal flat-plate with bonded tubes. The solution requires an assumption that the temperature in each tube is the same at any cross-section of the absorber plate. For the case of a U-tube in the absorber plate this assumption is not valid. A recent paper by Abdel-Khalik [10] gives the analytical solution for F_R for the case of serpentine tubes in an absorber plate, including the case of a U-tube bonded to a plate. The variables needed for the solution are: W , the fluid tube spacing, D , the diameter of these tubes, k , the thermal conductivity of the absorber plate, δ , the thickness of the absorber plate, r , the sum of the tube to absorber plate bonding resistance and the tube wall to fluid thermal resistance, and L , the length of the absorber plate. The fluid to wall thermal resistance, r_{fw} , can be determined from the relationship given by Holman [8]:

$$r_{fw} = \frac{D}{k_f} \frac{1}{1.86(\text{Re}_D \text{Pr})^{1/3} (D/2L)^{1/3} (\mu_f/\mu_{f_w})^{0.14}} \quad (3-11)$$

where: μ_f is the fluid viscosity evaluated at the mean fluid temperature

μ_{f_w} is the fluid viscosity evaluated at the tube wall temperature

k_f is the thermal conductivity of the fluid.

Given the above variables and knowing the loss coefficient, U_L , F_R can be calculated by the following equations:

$$n^2 = U_L (W-D)^2 / k\delta \quad (3-12)$$

$$\kappa = k\delta n / (W-D) \sinh n \quad (3-13)$$

$$\gamma = 2 \cosh n - DU_L / \kappa \quad (3-14)$$

$$\beta_1 = \frac{L \kappa [\kappa r (1+\gamma)^2 - 1] - \gamma - \kappa r}{\dot{m} C_p [\kappa r (1+\gamma) - 1]^2 - (\kappa r)^2} \quad (3-15)$$

$$\beta_2 = \frac{L\kappa}{\dot{m}C_p} \frac{1}{[\kappa r (1+\gamma) - 1]^2 - (\kappa r)^2} \quad (3-16)$$

$$\lambda_1 = + (\beta_1^2 - \beta_2^2)^{0.5} \quad (3-17)$$

$$\lambda_2 = \frac{(\beta_1 + \lambda_1 - \beta_2)}{(\beta_2 - \beta_1 + \lambda_1) e^{-2\lambda_1} + (\beta_1 + \lambda_1 - \beta_2)} \quad (3-18)$$

$$F_R = \frac{\dot{m}C_p}{U_L A_c} [1 + (2\lambda_2 \lambda_1 - \beta_1 - \lambda_1) / \beta_2] \quad (3-19)$$

The results of the calculations of F_R for the test module are given in Table 3-2. The values of F_R are for three different flow rates that were used in the tests, and are nearly 0.99 for every case considered. The intermediate calculations for F_R are shown in Appendix II. The optical and thermal analyses in Chapters II and III were used to predict the performance of an evacuated tube collector. The test results are compared with the predictions in Chapter IV.

Chapter IV

COLLECTOR TESTING

4.0 General Comments

Extensive testing of the test module was conducted over a three-month period at the Solar Energy Applications Laboratory at CSU. This testing was conducted primarily to verify the results of the theoretical analysis of the collector. The testing was also helpful in determining the relative performance of the Corning collector with other collectors operating simultaneously under the same solar and weather conditions.

4.1 Test Facility

The basic test facility consisted of a support structure for two collector test panels, the hardware for fluid circulation and temperature control, and a data acquisition system. The test stand was located next to Solar House I, which is situated 40.6 N and 105.1 W, at an altitude of 5200 feet (1585 meters) above sea level.

The test stand supports the collectors and houses the mechanical equipment. A photo of the test stand with the Corning collector and a module of the collector used on Solar House I mounted on the stand is shown in Figure 4-1. A schematic flow diagram is presented in Figure 4-2. The working fluid used was a 50 percent ethylene-glycol and water mixture. The fluid was circulated by means of one of two pumps into a 40 gallon hot water heater, equipped with a resistance heater. The hot water heater provided a reservoir to maintain a relatively constant temperature fluid to the inlet side of the collectors. The fluid circulates into a manifold which directs the flow to the collector being tested. The flow rate is measured by means of positive



Figure 4-1. Solar Collector Test Stand.

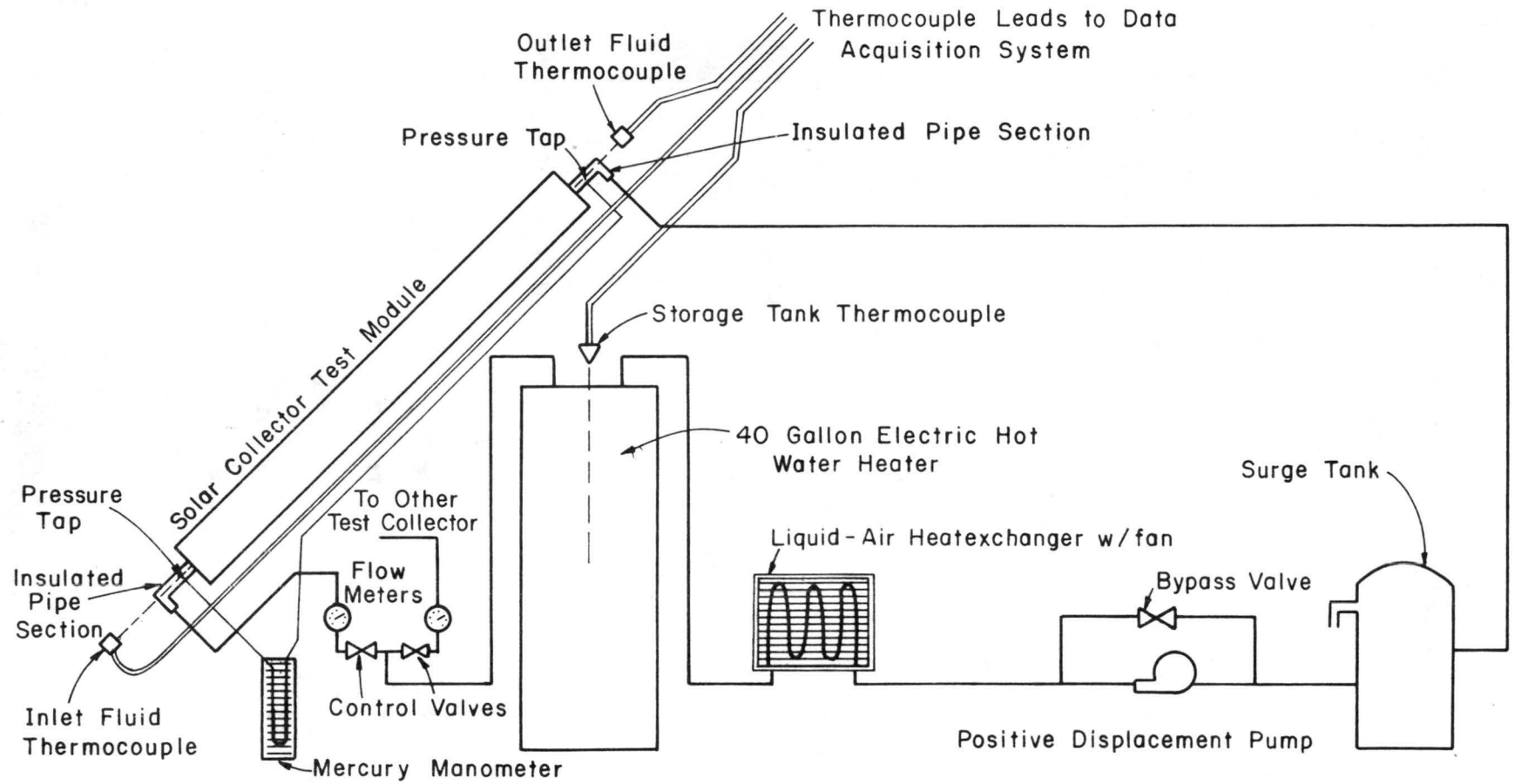


Figure 4-2. Schematic of Solar Collector Test Facility.

displacement flow meters. Although the system allows for testing two collectors simultaneously, there is difficulty in controlling the flow to maintain constant flow rates through each collector. From the collector, the fluid is released into a surge tank to maintain a reasonably constant pressure in the system. The surge tank is connected into the inlet side of the pumps.

For tests with fluid temperatures close to the ambient temperature, heat had to be rejected, as thermal losses from the system were not large enough to maintain a constant inlet fluid temperature. Heat was rejected through an air heat exchanger mounted in the line between the pumps and the water heater.

There are two positive displacement pumps mounted in the system, each pump has a different operating range. This allows constant flows to be maintained over a range from 0.015 to 0.30 liters/sec. A bypass valve was initially used to regulate the flow rate, but was abandoned because of flow instability. Flow was regulated by a variable speed motor drive on the pumps.

The flow meters in the system are high temperature water meters which measure total displacement. The flow rate was determined over timed intervals during testing, usually over one-half hour periods.

A manometer was used to measure the pressure drop through the collector. Copper constantine thermocouples were installed in insulated sections of the inlet and outlet pipes from the collector and also in the hot water tank. Thermocouples were also installed on the glass tubes in three locations to determine the outer surface temperatures along the tube.

The data acquisition system is an analog to digital converter with a magnetic tape recorder which is used to collect data for Solar House I.

This system includes a 100-channel data scanner, which samples all of the channels every two minutes. A magnetic tape is used to store the data for computer processing. The system routinely records climatological data including solar radiation, on a horizontal and 45-degree inclined angle, ambient temperatures, and wind speed. These data were used in conjunction with the collector data obtained at the test stand. All data obtained from the tests, except for flow rates, were recorded by the data acquisition system.

4.2 Test Parameters and Accuracies of Measurement

All the variables needed for determining the useful heat collected by the test collector were measured. The useful heat collected can be determined by

$$Q_{\text{out}} = \dot{m} C_p (T_{\text{out}} - T_{\text{in}}) \quad (4-1)$$

where: Q_{out} is the useful heat collected per unit area of collector
 \dot{m} is the mass flow rate of the heat transfer fluid through the collector per unit of collector area
 C_p is the specific heat of the working fluid
 T_{in} is the inlet fluid temperature, and
 T_{out} is the outlet fluid temperature from the collector.

The efficiency of the collector can be determined by knowing the solar radiation and can be expressed by rearranging the general collector equation in the following form:

$$\eta = \frac{Q_{\text{out}}}{HR} = F_R(\tau\alpha) - F_R U_L \left(\frac{T_{\text{in}} - T_a}{HR} \right) \quad (4-2)$$

where η is the efficiency. If F_R , U_L and $\tau\alpha$ are constants, then efficiency is a linear function of $\frac{T_{in}-T_a}{HR}$. In the limit, when T_{in} is equal to T_a , $F_R(\tau\alpha)$ is the maximum efficiency, η_0 , obtainable. The product, $F_R U_L$, is then the slope of the linear function. However, F_R and U_L are generally functions of plate and fluid temperatures and for high temperatures (or large $T_{in}-T_a$), nonlinearities can be expected.

The temperature rise of the fluid flowing through the collector was measured by thermocouples installed at the inlet and outlet to the collector. The temperature difference was determined from the difference of these two measurements. A more suitable technique is to determine the temperature difference by using both thermocouples in a single bridge. However, there were difficulties with grounding loops and circuits, and individual measurements were made. The thermocouples were calibrated to $\pm 0.1^\circ\text{C}$.

The flow meters were calibrated volumetrically to one percent accuracy. The pumps maintained flow rates to ± 0.05 gpm. The specific heat of the ethylene-glycol-water mixture was determined from frequent samples to determine the concentration of ethylene glycol and the mean fluid temperatures. Tables of ethylene glycol properties were used to determine the specific heat rather than measuring the specific heat by direct means.

The solar radiation was measured with an Eppley pyranometer mounted at the same tilt angle as the collector (45 degrees). The calibration on the pyranometer is checked regularly and the resolution of the instrument is ± 1 percent.

Measurement of ambient temperature and wind speed were routinely taken but were not used in determining collector performance. The

greatest uncertainty in the measurements is the determination of fluid temperature rise through the collector. An error of up to five percent can result in determining the amount of heat collected and also the efficiency.

4.3 Testing Procedures

The actual testing procedure was based on a method outlined by Hill and Kusuda [5]. They recommend that instantaneous efficiencies be measured by maintaining constant inlet temperatures, and flow rates during a 15 minute period with clear sky solar radiation. In the tests during this study, the fluid was heated to the desired operating temperature with the hot water heater before starting the circulation pumps. The flow rate was adjusted to a predetermined discharge and the manometer was then checked to assure there was no air in the system. The system was operated for at least 15 minutes for warm-up time to reach operating temperature and steady-state conditions. The flow meter was read and the system was then monitored continuously throughout the day recording flow measurements every half hour.

The steady-state implications are that the variation of any factor measured during a 15-minute test period is not significant enough to alter the performance of the collector. The amount of allowable variation in the measured parameters is a function mainly of the heat capacity of the collector. The thermal capacity of the collector produces a time delay and affects the magnitude of the test variable. Thermal capacity causes the greatest amount of experimental error and to eliminate these effects data were taken only when the variables in the test were constant for at least 15 minutes before the test period.

The effects of non-steady-state operation is illustrated in Table 4-1 with some typical computer output of processed test data. This is the summary for one day of testing showing 15-minute averages of all the measurements taken during the test period. The recording of data in two-minute time intervals necessitated averaging for an integral multiple of 2-minute intervals. Seven intervals were chosen, resulting in 14-minute test periods. From the data summary in Table 4-1, it is not readily apparent which data segment is acceptable for steady-state conditions. It was necessary to prepare a graphical output of solar radiation, useful heat collected, the temperature differences between the inlet fluid temperature and ambient temperature, and the wind velocity. Examples are shown in Figure 4-3, and 4-4.

The solar radiation (Figure 4-3) throughout the day shows no clouds were present, therefore, the entire day could be used for testing. The curve of useful heat collected is not as smooth, therefore some conditions other than fluctuations in solar radiation must have caused the variation in the curve. The temperature difference between inlet fluid and ambient ($T_{in} - T_a$) shown in Figure 4-4 can account for fluctuations in useful heat collected. For example, at 11:15 the temperature drops suddenly and the useful heat collected rises suddenly. This can be explained in terms of the heat capacity of the collector in which heat is drawn from the hot collector while it is cooling down, thus, giving an artificially high efficiency just after the temperature drops. Usable data is obtained during periods of nearly constant temperature as shown in Figure 4-4. These periods are taken at least 15 minutes after any sudden change in operating temperatures.

TABLE 4-1 Summary of Test Data for June 26, 1975

| Test Period Ending Hr.-Min. | Average Inlet Fluid Temperature °C | Average Outlet Fluid Temperature °C | Fluid Flow Rate GPM | Average Ambient Temperature °C | Average Wind Speed KPH | Average Solar Radiation KJ Hr ⁻¹ m ⁻² | Average Energy Collected KJ Hr ⁻¹ m ⁻² | Test Period Efficiency | $\frac{T_{IN}-T_a}{(HR)}$ °Cm ² -MJ ⁻¹ |
|--------------------------------------|--|---|------------------------------|---|---------------------------------|--|---|------------------------------|---|
| 10 15 | 66.4 | 68.8 | 1.19 | 19.6 | 18.6 | 2830.1 | 1955.7 | 69.1 | 16.54 |
| 10 29 | 69.4 | 71.9 | 1.19 | 20.4 | 18.8 | 2921.4 | 2027.4 | 69.4 | 16.77 |
| 10 45 | 72.8 | 75.3 | 1.17 | 21.0 | 19.3 | 3008.0 | 2063.8 | 68.6 | 17.21 |
| 10 59 | 75.4 | 78.0 | 1.17 | 21.6 | 29.0 | 3063.3 | 2114.2 | 69.0 | 17.56 |
| 11 15 | 75.5 | 78.4 | 1.12 | 22.1 | 22.1 | 3138.9 | 2264.7 | 72.1 | 17.01 |
| 11 29 | 75.1 | 77.9 | 1.12 | 22.1 | 26.1 | 3184.6 | 2168.4 | 68.1 | 16.64 |
| 11 45 | 78.3 | 81.0 | 1.09 | 22.8 | 25.6 | 3215.5 | 2063.4 | 64.2 | 17.25 |
| 11 59 | 79.8 | 82.6 | 1.09 | 23.7 | 21.9 | 3224.2 | 2110.3 | 65.5 | 17.40 |
| 12 15 | 79.4 | 82.2 | 1.09 | 23.5 | 22.8 | 3224.7 | 2091.5 | 64.9 | 17.33 |
| 12 29 | 76.9 | 79.8 | 1.09 | 23.9 | 29.2 | 3211.3 | 2204.1 | 68.6 | 16.49 |
| 12 45 | 76.3 | 79.1 | 1.11 | 24.2 | 22.1 | 3203.9 | 2120.4 | 66.2 | 16.25 |
| 12 59 | 75.2 | 78.0 | 1.11 | 24.0 | 23.9 | 3169.8 | 2120.4 | 66.9 | 16.16 |
| 13 15 | 75.8 | 78.3 | 1.13 | 25.2 | 23.1 | 3121.4 | 1983.5 | 63.5 | 16.21 |
| 13 29 | 78.6 | 81.1 | 1.13 | 25.9 | 18.8 | 3051.8 | 1925.2 | 63.1 | 17.28 |
| 13 45 | 79.8 | 82.3 | 1.13 | 25.7 | 27.8 | 2967.5 | 1905.8 | 64.2 | 18.23 |
| 13 59 | 79.2 | 81.7 | 1.13 | 26.3 | 27.8 | 2890.5 | 1905.8 | 65.9 | 18.32 |
| 14 15 | 76.7 | 79.1 | 1.14 | 26.0 | 30.9 | 2778.9 | 1873.6 | 67.4 | 18.25 |
| 14 29 | 76.4 | 78.6 | 1.14 | 26.9 | 23.5 | 2688.1 | 1795.1 | 66.8 | 18.41 |

TABLE 4-1 (Continued)

| Test Period Ending Hr.-Min. | Average Inlet Fluid Temperature °C | Average Outlet Fluid Temperature °C | Fluid Flow Rate GPM | Average Ambient Temperature °C | Average Wind Speed KPH | Average Solar Radiation KJ Hr ⁻¹ m ⁻² | Average Energy Collected KJ Hr ⁻¹ m ⁻² | Test Period Efficiency | $\frac{T_{IN}-T_a}{(HR)}$ °Cm ² -MJ ⁻¹ |
|--------------------------------------|--|---|------------------------------|---|---------------------------------|--|---|------------------------------|---|
| 14 45 | 75.1 | 77.2 | 1.14 | 26.3 | 25.2 | 2556.2 | 1628.3 | 63.7 | 19.09 |
| 14 59 | 76.4 | 78.2 | 1.14 | 26.6 | 18.9 | 2421.6 | 1422.3 | 58.7 | 20.55 |
| 15 15 | 79.3 | 80.9 | 1.15 | 27.2 | 17.9 | 2271.8 | 1296.3 | 57.1 | 22.91 |
| 15 29 | 79.8 | 81.3 | 1.15 | 27.5 | 21.3 | 2121.5 | 1177.5 | 55.5 | 24.62 |
| 15 45 | 78.3 | 79.6 | 1.14 | 26.9 | 34.5 | 1948.2 | 1079.0 | 55.4 | 26.34 |
| 15 59 | 75.9 | 76.5 | 1.14 | 26.3 | 25.0 | 1788.2 | 431.6 | 24.1 | 27.76 |

CORNING COLLECTOR JUNE 26, 1975

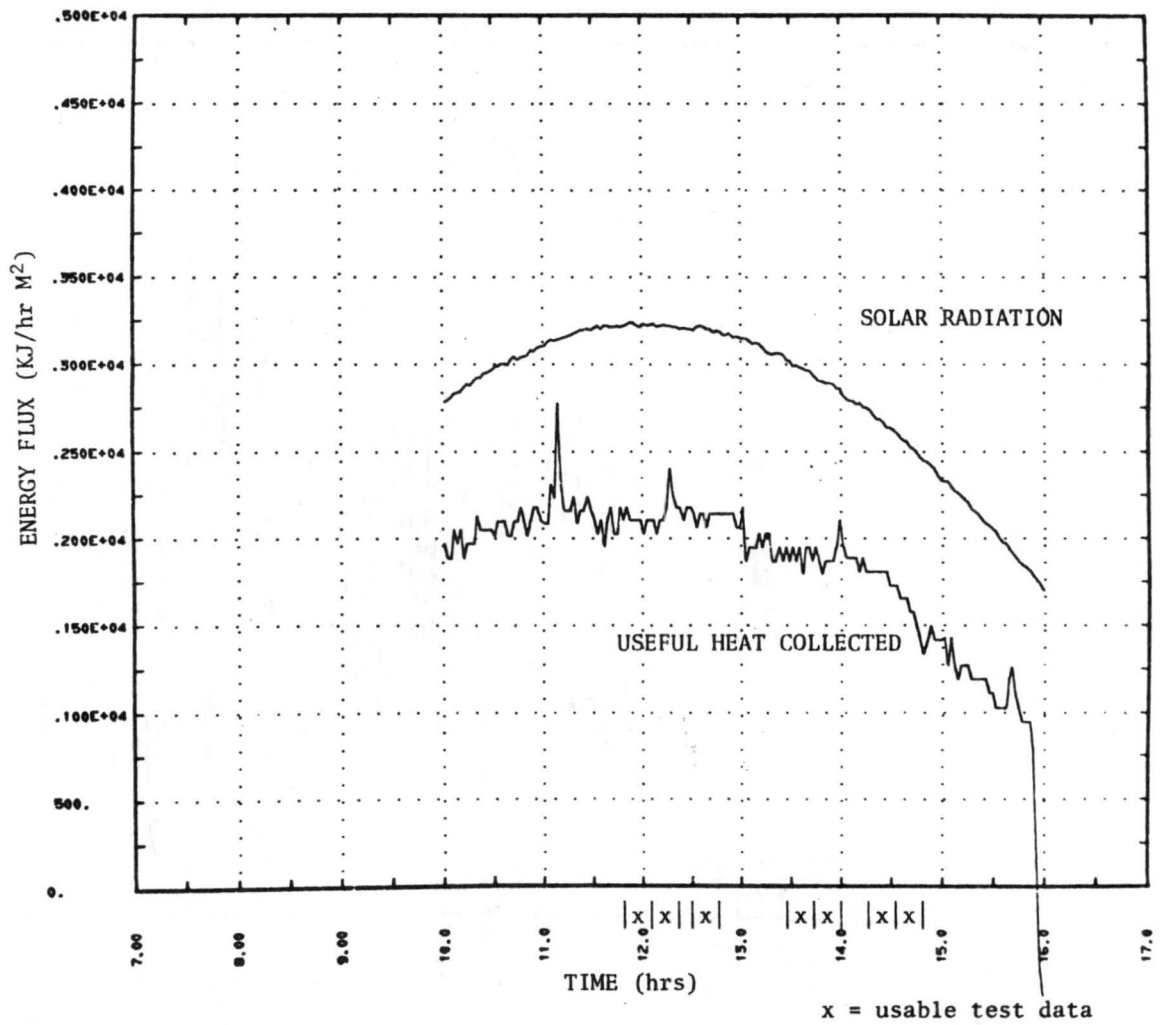


Figure 4-3. Solar Radiation and Useful Heat Collected.

CORNING COLLECTOR JUNE 26, 1975

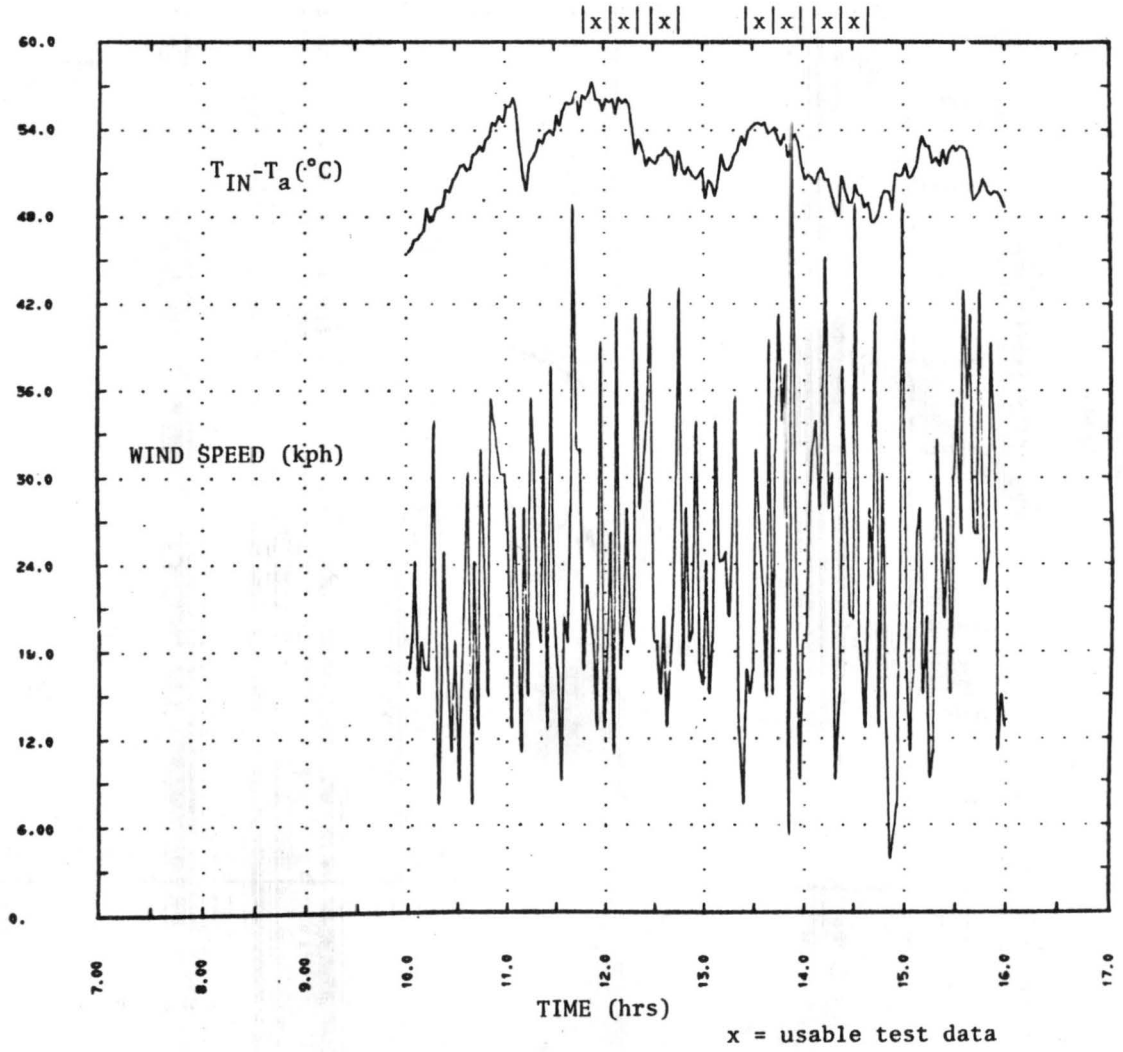


Figure 4-4. Wind Speed and Operating Temperatures.

The variability of the operating conditions causes large amounts of unusable data for short-term performance analysis and therefore, out of 18 days of testing only 11 provided usable data. Within the 11 days there were only about 70, 4-minute periods that were usable for determining the short-term performance of the collector. These data represent about 25 percent of the test period that provided useful data. The data summaries for the Corning collector tests are given in Appendix III.

4.4 Results of the Theoretical Analysis

The optical and thermal analysis for the evacuated tube collector was performed in accordance with the developments in Chapters II and III, using the geometry of the Corning test collector module. The calculations were made for the same range of operating conditions as the experiments.

The transmittance-absorptance product, was calculated for two conditions, one for ψ ranging from 0 to ± 15 degrees and one for ψ ranging from ± 15 degrees to ± 40 degrees; in both cases, θ ranged from 90 degrees to 60 degrees. The collector had several areas on the absorber where the selective surface coating was not applied properly. Some of these areas of defective coating are shown at the upper right hand portion of Figure 4-5. The coating absorptivity was 0.86 but the absorptivity of the uncoated areas was estimated to be 0.35, therefore the area averaged effective absorptivity was calculated to be 0.80. The diffuse component of radiation was estimated to be 10 percent of the total and from Equation (2-30) the $\tau\alpha$ products were determined to be .729 for the case of ψ ranging from 0 degrees to ± 15 degrees, and

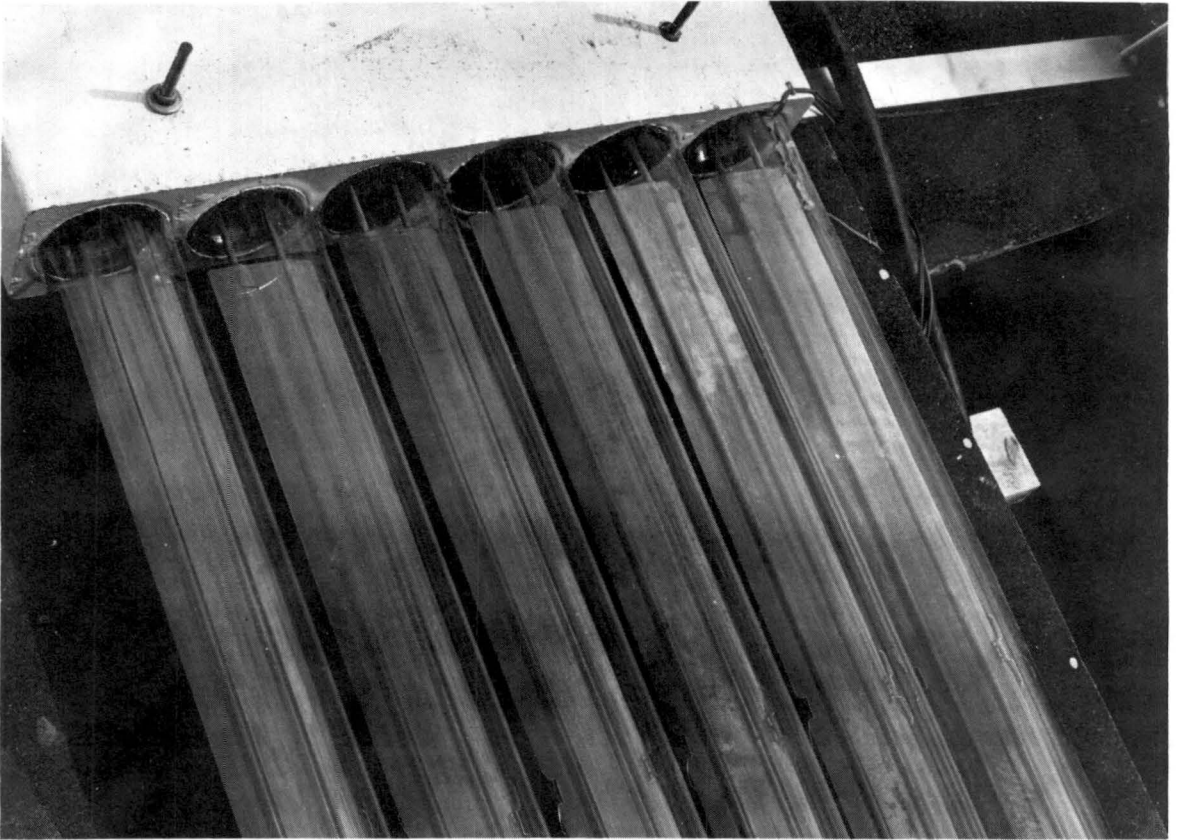


Figure 4-5. Manufacturing Variations in Absorber Surface Coating.

.759 for the case of ψ ranging from ± 15 degrees to ± 40 degrees. The reason the product is greater for the angles of ψ close to 30 degrees is due to reflections from adjacent tubes.

For fluid temperatures ranging from 20°C to 100°C and ambient temperatures ranging from 0°C to 40°C, U_L was calculated, and are presented in Table 4-2. Because U_L increases with temperature the plot of η vs. $\frac{T_{in} - T_a}{HR}$ will be a curve with a decreasing slope. Assuming F_R is constant at .99, the efficiencies were calculated for average values of solar radiation measured during testing and the results are shown in Table 4-2. These efficiencies are based on a net absorber area of the test module which is 1.12 m².

4.5 Test Results

The test data taken were processed and usable data were divided into two groups. The first group includes all the data within one hour of solar noon which corresponds with the first curve developed from the theoretical analysis. The second group includes data taken from hour angles between one and three hours from solar noon and corresponds with the second curve developed in the theoretical analysis. The data were divided into these groups to account for the changes in the effective transmissivity that was calculated in the theoretical analysis. The comparisons of test data with predicted results are shown in Figures 4-6 and 4-7 respectively.

Overall there is excellent agreement between the test data and predicted results. The least squares fit of the test data produced the lines shown which seem to match the predicted curves. The width of predicted curves represents the variation in U_L over ambient

TABLE 4-2 Results of Theoretical Analysis

| Inlet Fluid Temp. T_{in} (°C) | Ambient Fluid Temp. T_a (°C) | Thermal Loss Rate U_L (W/m ² °C) | HR=722 W/m ² $\tau\alpha=0.759$ | | HR=890 W/m ² $\tau\alpha=0.729$ | |
|---------------------------------------|--------------------------------------|--|--|---|--|---|
| | | | Efficiency η | $T_{in}-T_a$ /HR °C W/m ² | Efficiency η | $T_{in}-T_a$ /HR °C W/m ² |
| 40 | 0 | 1.07 | 0.692 | 0.055 | 0.674 | 0.045 |
| 60 | 0 | 1.11 | 0.660 | 0.083 | 0.648 | 0.067 |
| 80 | 0 | 1.16 | 0.623 | 0.111 | 0.618 | 0.090 |
| 100 | 0 | 1.23 | 0.592 | 0.139 | 0.583 | 0.112 |
| 40 | 20 | 1.15 | 0.720 | 0.028 | 0.697 | 0.022 |
| 60 | 20 | 1.16 | 0.688 | 0.055 | 0.670 | 0.045 |
| 80 | 20 | 1.21 | 0.652 | 0.083 | 0.641 | 0.067 |
| 100 | 20 | 1.28 | 0.611 | 0.111 | 0.606 | 0.090 |
| 60 | 40 | 1.21 | 0.718 | 0.028 | 0.695 | 0.022 |
| 80 | 40 | 1.26 | 0.682 | 0.055 | 0.666 | 0.045 |
| 100 | 40 | 1.33 | 0.642 | 0.083 | 0.633 | 0.067 |

F_R is assumed constant at 0.99 (see Table 3-1)

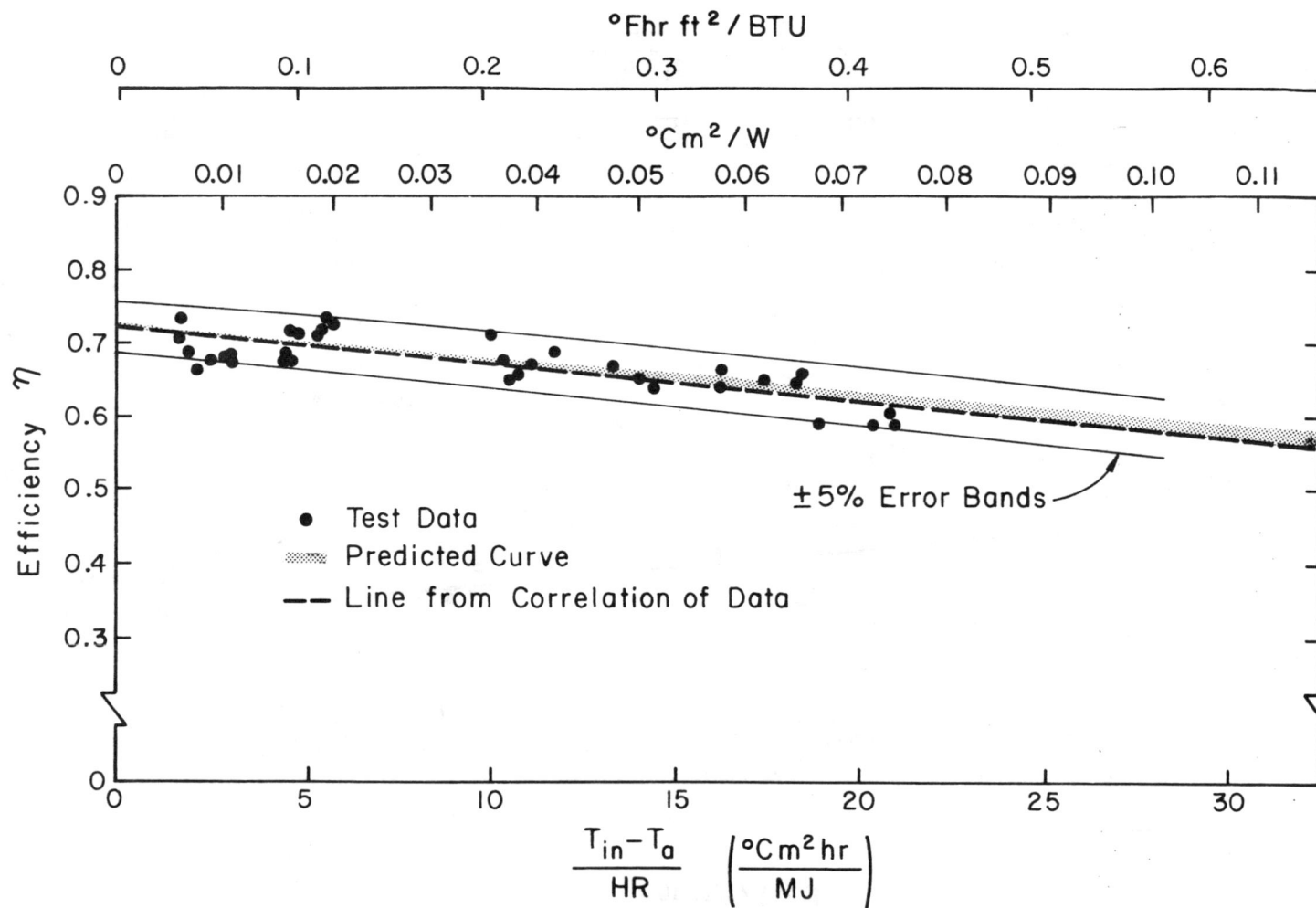


Figure 4-6. Performance Curve for the Corning Solar Collector ± 1 Hour from Solar Noon.

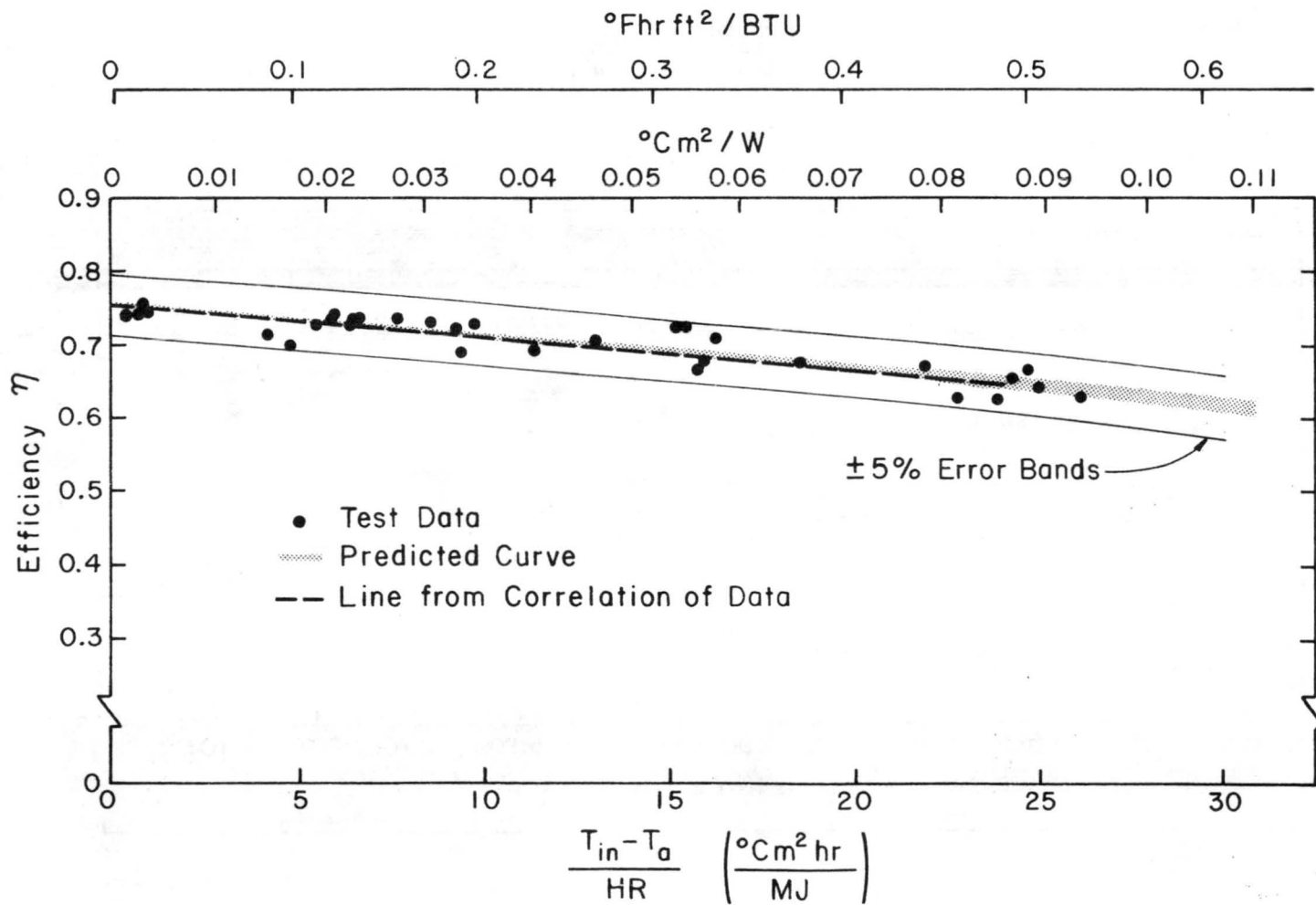


Figure 4-7. Performance Curve for the Corning Solar Collector for $\pm(1$ to $3)$ Hours from Solar Noon.

temperature variations from 0 degrees to 40°C with the lower portion being the 40°C curve. The test data were taken at ambient temperatures around 30°C, therefore the data should follow the lower portion of the curves. The data falls within the error band of five percent that was discussed in section 4.2.

The data shown on Figure 4-7 have more scatter about the predicted curve because of the greater variability in the transmissivity over the range of hour angles from which the data were taken. This curve actually lies above the curve for hour angles closer to noon (Figure 4-6) which indicate that the reflections from adjacent tubes increase the efficiency about three percent, as was indicated in the predicted curves.

The best fit curve to the data has the same trend as for the calculated curves, indicating that the theoretical loss coefficients are close to the actual thermal losses from the collector. The data also indicate that the performance of the collector did not change significantly over the three months of testing. The data from the last days of testing is not distinguishable from the first few days. A major concern was that outgassing of collector materials would degrade the vacuum and increase the thermal losses but within the period of these tests, the data do not indicate any evidence of this having occurred.

The tubes were kept free of dust as much as possible but some dust did accumulate on the glass tubes. This may account for some of the data points which lie below the predicted curve, but no conclusion can be drawn because the scatter is within the experimental error band. The predicted curve assumes a 10 percent diffuse component of solar radiation, which was not measured, but was estimated from other

measurements under similar conditions, and appears to be a realistic estimate based on the comparison with the predicted performance curve.

The performance of the test module indicates that the Corning collector is several times more efficient than conventional flat-plate collectors in the operating temperature range. This is very important when considering moderate and high temperature collector operation such as might be required for operation of an absorption air conditioning system. There is increased optical performance because of the single, tubular glass cover, and increased thermal performance because of the evacuated space between the absorber and the cover, and the selective surface on the absorber.

4.6 Total Daily Performance

The instantaneous collector efficiencies are important in comparing collector performance and in system design but another perhaps more meaningful measure is the total daily energy collected. Because of the lower sun angles during early morning and late afternoon the daily efficiency of a collector is generally less than the instantaneous efficiency. The difficulty in measuring total daily performance is that it requires a day of cloudless weather which is often difficult to obtain.

One day of clear-sky testing of the Corning collector was obtained in the period of the experiments. The curves for solar radiation and useful heat collected for this day are shown in Figure 4-8. There are two spikes in the useful heat curves which are due to changes in inlet temperature and heat capacity as previously discussed in section 4.3. The general flatness of the curve around 12:00 is caused by the effects of reflections from adjacent tubes which increases the performance in the hours before and after solar noon as discussed previously. During

CORNING COLLECTOR JULY 25, 1975

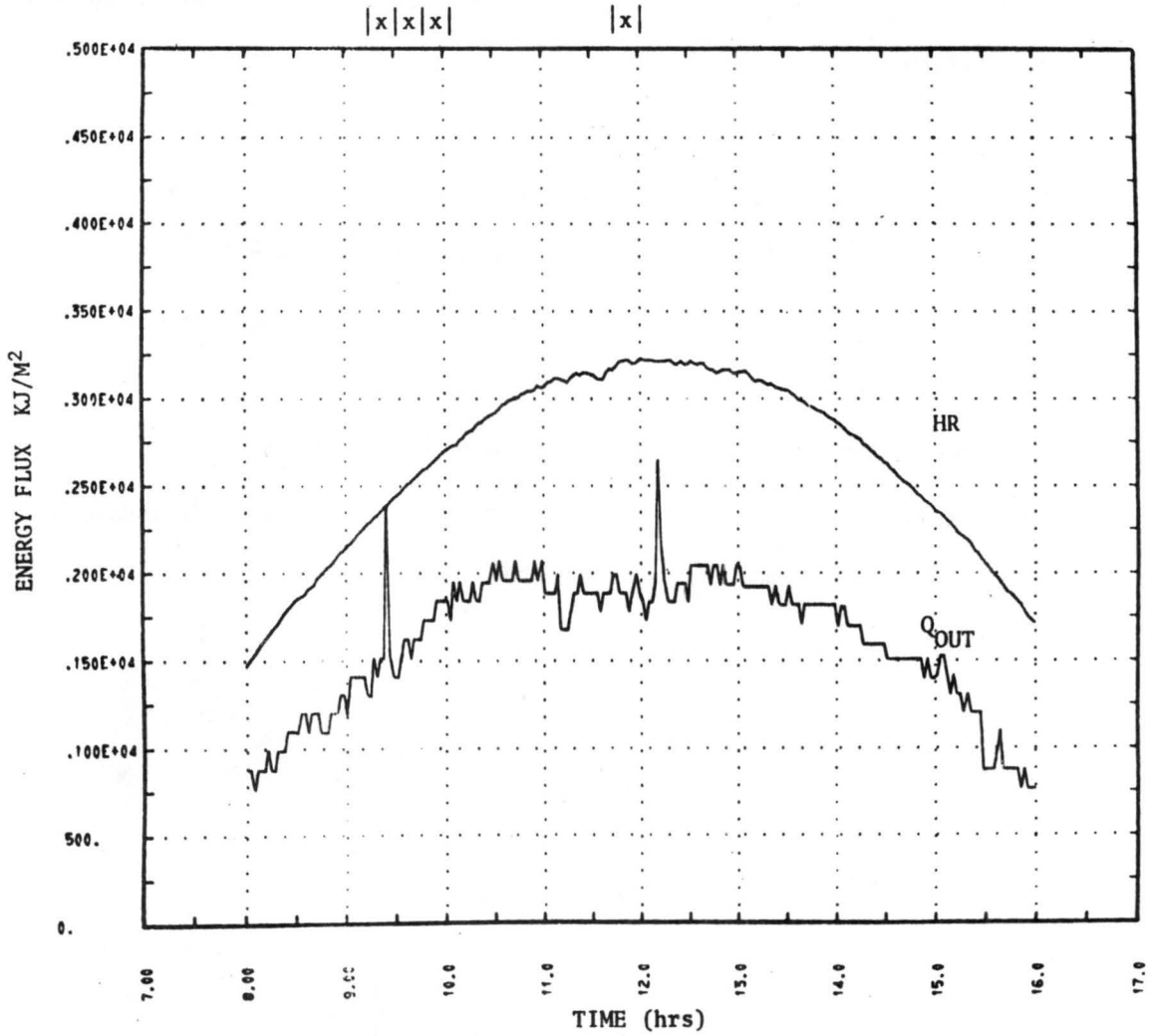


Figure 4-8. Total Daily Performance of Test Module.

the eight hours of testing, the overall efficiency was 60.8 percent. The inlet fluid temperature ranged between 70° and 92°C. Extrapolating the performance over the entire day (dotted curve), the daily efficiency was calculated to be 51.4 percent.

A good comparison of this performance was obtained from Solar House I during the same day of July 25, 1975. During this day the collectors were operating the air conditioning system with an average collector inlet temperature of 80°C. The overall daily performance of the collectors on Solar House I was 22.7 percent. This indicates that when operating with moderate temperature conditions (70 to 100°C) the Corning collector can collect better than twice as much useful energy during a day as compared to the flat-plate solar collectors on Solar House I.

Chapter V

SUMMARY AND CONCLUSIONS

The objective of this work was to analyze the performance of an evacuated tube solar collector. The Corning collector was analyzed, tested and the performance was compared to conventional flat-plate solar collectors. The theoretical analysis agreed with the test results and showed that the evacuated tube solar collector was superior in performance as compared to a conventional collector design.

The theoretical analysis of the Corning solar collector indicated several interesting features unique to the evacuated tube solar collector. The optical analysis of the collector indicated some unique advantages of the tubular cover configuration of the collector. The transmission of radiation through the glass is less dependent on sun angle because of the curvature of the glass. This effect is only for one direction of sun angle (ψ) and indicates that the tube axis should be mounted perpendicular to the greatest variation in sun angle, that is, a north-south orientation. The analysis of the shading effect of adjacent tubes showed that these effects are minimal and occur only at very low sun angles. The greatest advantage of the tubular covers is that reflections from adjacent tubes increase the performance at sun angles not normal to the collector. Another advantage of the tubes is that the diffuse reflection from surfaces behind the collector is absorbed by the back of the absorber surfaces thus increasing the total energy absorbed by a single unit. A tube spacing of one tube diameter and back surface reflectance of 0.75 will increase the amount of energy absorbed by about 35 percent. The internal reflections between the

absorber and the glass tube is about the same as for conventional flat-plate collectors. The determination of the effective transmissivity absorptivity product showed that for solar hour angles of one to three hours from noon, the effective transmissivity absorptivity product was about three percent greater than for hour angles less than one hour about noon due primarily to reflections from adjacent tubes.

The thermal analysis of the collector indicated that the heat transfer from the absorber to the glass was almost equally divided between the radiation from the absorber plate and conduction through the absorber support clips. Therefore, the performance of the collector could be improved if some design improvements are made to decrease the thermal losses through the support clips. The heat loss calculations from the glass tube showed that the glass tube temperature was very nearly the same as ambient temperature under most operating temperatures, therefore, the effects of convection losses from the glass tubes due to wind are minimal. The overall loss coefficient of the test module increased with increasing ambient temperature as well as increasing operating temperatures. The analysis of the heat removal efficiency factor showed that F_R was 0.99 and almost constant over the range of the operating conditions for which the collector was tested.

The operation of the test module produced results that were in agreement with the theoretical analysis. Some problems were encountered in performing the tests which were attributable to instrumentation and controls. The cumulative errors in instrumentation result in an uncertainty of about 5 percent for the data. The control of the testing was difficult especially in obtaining steady-state conditions. This resulted in more than half the data obtained being unusable. The thermocouples

that were installed on one of the tubes did not measure the tube surface temperature accurately because of direct heating of the thermocouples by solar radiation.

A problem that was encountered in performing the tests was that the collector had to be covered when not in operation. The solder used in bonding the U-tubes to the absorber plate vaporized at the high temperatures which the absorber would reach during stagnation conditions. This problem has been eliminated in newer prototypes of the collector by welding the absorber to the U-tube.

Generally, there was excellent agreement between the predicted and measured performance. The data fit the theoretical curve within the expected error in the measurements. The total daily performance of the Corning collector was better than twice the daily performance of a conventional collector design under moderately high operating temperatures.

The result of this analysis show that the evacuated tube solar collector can offer improved performance over conventional collector designs. This performance increase allows the use of evacuated tube collectors for both moderate and high temperature applications of solar energy. By spacing the absorber tubes and using a reflective back surface, a more cost-effective use of the collectors is possible.

REFERENCES

1. E. Speyer, (1974), Solar Energy Collection with Evacuated Tubes, Transactions of ASME, 64 WA/SOL-2.
2. D. C. Beekley and G. R. Mather, (1975), Analysis and Experimental Test of High-Performance Tubular Solar Collectors. Presented at 1975 ISES Meeting, Los Angeles, California, July.
3. U. Ortabasi and W. M. Buehl, (1975), Analysis and Performance of an Evacuated Tubular Collector. Presented at the 1975 ISES Meeting, Los Angeles, California, July.
4. Charles D. Beach, (1975), Thermal Performance Model for Collectors in Evacuated Tubes. Prepared for Dr. Paul J. Wilbur, Colorado State University, Fort Collins, Colorado, April.
5. James E. Hill and Tamami Kusuda, (1974), Method of Testing for Rating Solar Collectors Based on Thermal Performance. National Bureau of Standards Interim Report 74-635, December.
6. John A. Duffie and William A. Beckman, (1974), Solar Energy Thermal Processes, John Wiley and Sons, 385 pages.
7. James L. Threlkeld, (1970), Thermal Environmental Engineering, Second Edition, 495 pages.
8. J. P. Holman, (1972), Heat Transfer, Third Edition, McGraw-Hill Book Company, 460 pages.
9. Frank Kreith, (1973), Principles of Heat Transfer, Intext Educational.
10. Abdiel-Khalik, (1975), Heat Removal Factor for a Flat-Plate Solar Collector with a Serpentine Tube. Presented at the ISES Meeting, Los Angeles, California, July.
11. Colorado State University/Westinghouse Electric Corporation, (1974), Solar Thermal Electric Power Systems Final Report, Volume 3, "Appendices." NSF/RANN/SE/GI-37815/FR/74/3, November.
12. Design and Construction on a Residential Solar Heating and Cooling System, (1974). Semi-Annual Progress Report, Colorado State University, and University of Wisconsin, August.

APPENDIX I
OPTICAL CALCULATIONS

TABLE A-I-1 Transmission Calculations for the Test Module

| ψ | $\text{cosyR}\Delta y$ mm | $\theta=90^\circ$ | | | $\theta=80^\circ$ | | | $\theta=70^\circ$ | | | $\theta=60^\circ$ | | | $\theta=50^\circ$ | | | $\theta=40^\circ$ | | | $\theta=30^\circ$ | | | $\theta=20^\circ$ | | | |
|--------|------------------------------|---------------------|-------------------|--------|---------------------|-------------------|--------|---------------------|-------------------|--------|---------------------|-------------------|--------|---------------------|-------------------|--------|---------------------|-------------------|--------|---------------------|-------------------|--------|---------------------|-------------------|--------|---------------------|
| | | τ_{eff} | λ deg. | τ | τ_{eff} |
| 90° | | | | | | | | | | | | | | | | | | | | | | | | | | |
| 80° | 7.59 | 0.90 | 10.9 | 0.90 | 0.90 | 20.4 | 0.90 | 0.90 | 30.3 | 0.90 | 0.90 | 40.2 | 0.90 | 0.90 | 50.1 | 0.88 | 0.88 | 60.1 | 0.82 | 0.82 | 70.1 | 0.70 | 0.70 | 0.70 | | |
| 70° | 7.37 | 0.90 | 16.2 | 0.90 | 0.90 | 23.6 | 0.90 | 0.90 | 32.4 | 0.90 | 0.90 | 41.7 | 0.90 | 0.90 | 51.2 | 0.87 | 0.87 | 60.8 | 0.82 | 0.82 | 70.5 | 0.70 | 0.70 | 0.70 | | |
| 60° | 6.91 | 0.90 | 23.4 | 0.90 | 0.90 | 28.9 | 0.90 | 0.90 | 36.2 | 0.90 | 0.90 | 44.4 | 0.89 | 0.90 | 53.2 | 0.87 | 0.87 | 62.2 | 0.81 | 0.82 | 71.4 | 0.68 | 0.68 | 0.69 | | |
| 50° | 6.25 | 0.90 | 31.0 | 0.90 | 0.90 | 35.1 | 0.90 | 0.90 | 41.1 | 0.90 | 0.90 | 48.2 | 0.88 | 0.90 | 56.0 | 0.85 | 0.87 | 64.2 | 0.79 | 0.82 | 72.7 | 0.65 | 0.65 | 0.69 | | |
| 40° | 5.38 | 0.90 | 35.4 | 0.90 | 0.90 | 41.7 | 0.90 | 0.90 | 46.5 | 0.89 | 0.90 | 52.5 | 0.87 | 0.89 | 59.3 | 0.83 | 0.86 | 66.6 | 0.75 | 0.80 | 74.2 | 0.60 | 0.60 | 0.67 | | |
| 30° | 4.37 | 0.90 | 45.5 | 0.89 | 0.90 | 48.0 | 0.88 | 0.90 | 52.0 | 0.87 | 0.90 | 57.0 | 0.85 | 0.89 | 62.8 | 0.81 | 0.85 | 69.2 | 0.72 | 0.79 | 75.9 | 0.55 | 0.55 | 0.66 | | |
| 20° | 3.22 | 0.90 | 51.7 | 0.88 | 0.90 | 53.7 | 0.86 | 0.89 | 57.0 | 0.85 | 0.89 | 61.2 | 0.82 | 0.88 | 66.1 | 0.76 | 0.84 | 71.7 | 0.68 | 0.78 | 77.6 | 0.50 | 0.50 | 0.64 | | |
| 10° | 1.96 | 0.90 | 56.4 | 0.86 | 0.90 | 58.2 | 0.84 | 0.89 | 60.9 | 0.82 | 0.89 | 64.5 | 0.79 | 0.88 | 68.8 | 0.72 | 0.84 | 73.7 | 0.65 | 0.78 | 78.9 | 0.45 | 0.45 | 0.64 | | |
| 0° | 0.66 | 0.90 | 59.1 | 0.83 | 0.89 | 60.6 | 0.82 | 0.89 | 63.1 | 0.80 | 0.89 | 66.4 | 0.76 | 0.87 | 0.4 | 0.70 | 0.84 | 74.9 | 0.60 | 0.77 | 79.7 | 0.42 | 0.42 | 0.63 | | |

$$\tau_{\text{eff}} = \frac{\Sigma \tau (\text{cosy}) R \Delta y}{\frac{L}{2} \text{cosy}}$$

TABLE A-I-2 Shading Calculations for the Test Module

| ψ deg. | l mm | $\theta=90^\circ$ | | | $\theta=80^\circ$ | | | $\theta=70^\circ$ | | | $\theta=60^\circ$ | | | $\theta=50^\circ$ | | | $\theta=40^\circ$ | | | $\theta=30^\circ$ | | | $\theta=20^\circ$ | | | $\frac{l}{l \cos \alpha}$ |
|----------------|-----------|-------------------|----------------|----------|-------------------|----------------|----------|-------------------|----------------|----------|-------------------|----------------|----------|-------------------|----------------|----------|-------------------|----------------|----------|-------------------|----------------|----------|-------------------|----------------|----------|---------------------------|
| | | λ deg. | τ_λ | τ_s | |
| | | 74.1 | 0.61 | 0.37 | 74.3 | 0.61 | 0.37 | 75.1 | 0.60 | 0.36 | 76.3 | 0.55 | 0.30 | 77.9 | 0.50 | 0.25 | 79.9 | 0.42 | 0.18 | 82.1 | 0.30 | 0.09 | 84.6 | 0.20 | 0.04 | 0.136 |
| 50 | 7.62 | 49.8 | 0.88 | 0.58 | 50.5 | 0.88 | 0.58 | 52.6 | 0.87 | 0.56 | 56.0 | 0.85 | 0.51 | 60.4 | 0.83 | 0.47 | 65.5 | 0.78 | 0.39 | 71.2 | 0.70 | 0.27 | 77.2 | 0.50 | 0.13 | 0.394 |
| 60 | 17.22 | 34.1 | 0.90 | 0.71 | 35.4 | 0.90 | 0.66 | 38.9 | 0.90 | 0.65 | 44.2 | 0.90 | 0.62 | 50.6 | 0.88 | 0.58 | 57.9 | 0.84 | 0.50 | 65.6 | 0.78 | 0.39 | 73.6 | 0.64 | 0.22 | 0.932 |
| 70 | 27.84 | | | | | | | | | | | | | | | | | | | | | | | | | |

TABLE A-I-3 Reflection Calculations from Adjacent Tubes for the Test Module

| ψ | α_1 | α_2 | $\theta=90^\circ \tau=.9$ | | | $\theta=80^\circ \tau=0.9$ | | | $\theta=70^\circ \tau=0.9$ | | | $\theta=60^\circ \tau=0.9$ | | | $\theta=50^\circ \tau=0.90$ | | | $\theta=40^\circ \tau=0.88$ | | | $\theta=30^\circ \tau=0.82$ | | | $\theta=20^\circ \tau=0.70$ | | | | |
|--------|------------|------------|---------------------------|------------------|-------------------|----------------------------|-------------------|-------------------|----------------------------|-------------------|-------------------|----------------------------|-------------------|-------------------|-----------------------------|-------------------|----------------|-----------------------------|-------------------|----------------|-----------------------------|-------------------|-------------------|-----------------------------|-------------------|-------------------|--------|-------------------|
| | | | h mm | δ deg. | λ deg. | ρ | $h\rho\tau$ mm | λ deg. | ρ | $h\rho\tau$ mm | λ deg. | ρ | $h\rho\tau$ mm | λ deg. | ρ | $h\rho\tau$ mm | ψ deg. | ρ | $h\rho\tau$ mm | ψ deg. | ρ | $h\rho\tau$ mm | λ deg. | ρ | $h\rho\tau$ mm | λ deg. | ρ | $h\rho\tau$ mm |
| -90 | 90 | 90 | 0 | 0 | | | | | | | | | | | | | | | | | | | | | | | | |
| -80 | 88 | 86 | .102 | 7 | 7 | .08 | 0 | 12 | .08 | 0 | 21 | .08 | 0 | 31 | .08 | 0 | 41 | .08 | 0 | 50 | .10 | 0 | 60 | .15 | .025 | 70 | .27 | .025 |
| -70 | 86 | 82 | .381 | 14 | 14 | .08 | .025 | 17 | .08 | .025 | 24 | .08 | .025 | 33 | .08 | .025 | 42 | .08 | .025 | 51 | .12 | .051 | 61 | .15 | .051 | 71 | .29 | .076 |
| -60 | 84 | 78 | .838 | 21 | 21 | .08 | .051 | 23 | .08 | .051 | 29 | .08 | .051 | 36 | .08 | .051 | 44 | .10 | .076 | 53 | .12 | .076 | 62 | .17 | .127 | 71 | .29 | .178 |
| -50 | 82 | 74 | 1.47 | 28 | 28 | .08 | .102 | 30 | .08 | .102 | 34 | .08 | .102 | 40 | .08 | .102 | 47 | .10 | .127 | 55 | .12 | .152 | 64 | .18 | .229 | 72 | .32 | .330 |
| -40 | 79 | 68 | 2.76 | 34 | 34 | .08 | .203 | 35 | .08 | .203 | 39 | .08 | .203 | 44 | .10 | .254 | 51 | .10 | .254 | 58 | .14 | .330 | 66 | .21 | .483 | 74 | .35 | .660 |
| -30 | 77 | 65 | 3.45 | 41 | 41 | .08 | .254 | 42 | .08 | .254 | 45 | .10 | .305 | 49 | .10 | .305 | 55 | .12 | .381 | 61 | .15 | .457 | 68 | .24 | .686 | 75 | .38 | .914 |
| -20 | 74 | 61 | 4.39 | 48 | 48 | .10 | .406 | 49 | .10 | .406 | 51 | .11 | .432 | 55 | .12 | .483 | 59 | .15 | .584 | 64 | .18 | .686 | 70 | .27 | .965 | 77 | .43 | 1.32 |
| -10 | 71 | 57 | 5.44 | 54 | 54 | .12 | .584 | 54 | .12 | .584 | 56 | .13 | .635 | 59 | .15 | .737 | 63 | .17 | .838 | 68 | .24 | 1.14 | 73 | .33 | 1.47 | 78 | .46 | 1.75 |
| 0 | 67 | 53 | 6.20 | 60 | 60 | .15 | .838 | 61 | .15 | .838 | 62 | .15 | .838 | 64 | .18 | 1.02 | 67 | .23 | 1.27 | 71 | .30 | .162 | 76 | .40 | 2.03 | 80 | .54 | 2.34 |
| 10 | 63 | 48 | 7.52 | 66 | 66 | .21 | 1.42 | 66 | .21 | 1.42 | 68 | .24 | 1.63 | 69 | .26 | 1.75 | 72 | .32 | 2.16 | 75 | .37 | 2.44 | 78 | .46 | 2.84 | 82 | .62 | .325 |
| 20 | 59 | 44 | 8.26 | 72 | 72 | .30 | 2.24 | 72 | .32 | 2.39 | 73 | .33 | 2.44 | 74 | .35 | 2.59 | 76 | .40 | 2.97 | 79 | .50 | 3.63 | 81 | .58 | 3.94 | 84 | .72 | 4.17 |
| 30 | 54 | 39 | 9.12 | 77 | 77 | .42 | 3.45 | 77 | .43 | 3.53 | 78 | .46 | 3.76 | 79 | .54 | 4.42 | 80 | .54 | 4.42 | 82 | .62 | 4.95 | 84 | .72 | 5.56 | 86 | .80 | 5.61 |
| 40 | 50 | 35 | 9.78 | 83 | 83 | .65 | 5.72 | 83 | .67 | 5.89 | 83 | .67 | 5.89 | 84 | .72 | 6.32 | 85 | .76 | 6.68 | 86 | .80 | 6.88 | 86 | .80 | 6.41 | 88 | .90 | 6.16 |

TABLE A-I-4 Internal Reflection Calculations

| | ρ_θ |
|--------------------------------------|---------------|---------------|---------------|---------------|---------------|---------------|---------------|---------------|
| θ | 90° | 80° | 70° | 60° | 50° | 40° | 30° | 20° |
| x=3.49 cm | 0.042 | 0.042 | 0.042 | 0.044 | 0.049 | 0.061 | 0.098 | 0.153 |
| x=1.75 cm | 0.071 | 0.071 | 0.071 | 0.071 | 0.076 | 0.100 | 0.150 | 0.238 |
| x=0 | 0.08 | 0.08 | 0.08 | 0.08 | 0.08 | 0.10 | 0.16 | 0.26 |
| ρ_{ave} | 0.061 | 0.061 | 0.061 | 0.062 | 0.066 | 0.084 | 0.131 | 0.208 |
| $\Sigma\Delta(\sin\theta)\rho_{ave}$ | 0.0053 | 0.0158 | 0.0258 | 0.0351 | 0.0439 | 0.053 | 0.0648 | 0.0843 |

$$\rho_\theta = \int_{-90}^{90} \rho_\psi d\psi$$

$$\rho_{ave} = \frac{\sum_{n=1}^5 \rho_\theta \Delta x_n}{L}$$

APPENDIX II
THERMAL CALCULATIONS

TABLE A-II-1 U_L Calculations for the Test Module

| T_p | T_A | T_g | ϵ_p | h_N^* | h_r | h_g | h_{pg} | U_L |
|-------------|-------------|-------------|--------------|------------------|------------------|------------------|------------------|------------------|
| $^{\circ}C$ | $^{\circ}C$ | $^{\circ}C$ | | $W/M^2^{\circ}C$ | $W/M^2^{\circ}C$ | $W/M^2^{\circ}C$ | $W/M^2^{\circ}C$ | $W/M^2^{\circ}C$ |
| 40 | 0 | - .8 | .036 | 62.5 | -116.5 | 0.64 | .412 | 1.07 |
| 40 | 20 | 19.0 | .036 | 59.6 | -84.3 | 0.64 | .455 | 1.15 |
| 40 | 40 | 39.3 | .036 | 58.6 | -59.9 | 0.64 | .578 | 15.8 |
| 60 | 0 | - .4 | .036 | 62.5 | -210.6 | 0.64 | .458 | 1.11 |
| 60 | 20 | 19.4 | .036 | 59.6 | -140.0 | 0.64 | .502 | 1.16 |
| 60 | 40 | 39.6 | .036 | 58.6 | -124.2 | 0.64 | .551 | 1.21 |
| 80 | 0 | - .1 | .037 | 62.5 | -1685.5 | 0.64 | 0.523 | 1.16 |
| 80 | 20 | 19.8 | .037 | 59.6 | -425.2 | 0.64 | 0.569 | 1.21 |
| 80 | 40 | 40.03 | .037 | 58.6 | 1948.8 | 0.64 | .622 | 1.26 |
| 100 | 0 | 0.4 | .038 | 62.5 | 252.1 | 0.64 | .596 | 1.23 |
| 100 | 20 | 20.3 | .038 | 59.6 | 315.2 | 0.64 | .646 | 1.28 |
| 100 | 40 | 40.5 | .038 | 58.6 | 114.1 | 0.64 | .702 | 1.33 |
| 300 | 0 | 11.5 | .060 | 62.5 | 13.2 | 0.64 | 2.388 | 2.91 |

* Calculations are for 5 mps wind.

TABLE A-II-2 F_r Calculations* for the Test Module

| T_{IN} | T_{AMB} | $W/M^2\text{°C}$ U_L | $g/sector$ \dot{M} | $J/g\text{°C}$ C_p^{**} | $M\text{°C/W}$ R | n | K | γ | β_1 | β_2 | λ_1 | λ_2 | F_r |
|----------|-----------|---------------------------|-------------------------|------------------------------|-----------------------|-------|------|----------|-----------|-----------|-------------|-------------|-------|
| 40 | 0 | 1.07 | 11.03 | 3.51 | 0.131 | .069 | 8.38 | -2.01 | 0.143 | 0.145 | 0.027 | 0.560 | 0.993 |
| 40 | 20 | 1.15 | 11.03 | 3.51 | 0.131 | .072 | 8.38 | -2.01 | 0.143 | 0.146 | 0.028 | 0.560 | 0.992 |
| 40 | 40 | 15.8 | 11.03 | 3.51 | 0.131 | 0.265 | 8.29 | -2.08 | 0.129 | 0.163 | 0.100 | 0.715 | 0.881 |
| 60 | 0 | 1.11 | 10.83 | 3.59 | 0.129 | 0.070 | 8.38 | -2.01 | 0.144 | 0.147 | 0.028 | 0.561 | 0.992 |
| 60 | 20 | 1.16 | 10.83 | 3.59 | 0.129 | 0.072 | 8.38 | -2.01 | 0.144 | 0.147 | 0.028 | 0.563 | 0.992 |
| 60 | 40 | 1.26 | 10.83 | 3.59 | 0.129 | 0.073 | 8.38 | -2.01 | 0.144 | 0.147 | 0.029 | 0.564 | 0.992 |
| 80 | 0 | 1.16 | 10.73 | 3.66 | 0.128 | 0.072 | 8.38 | -2.01 | 0.144 | 0.146 | 0.028 | 0.562 | 0.992 |
| 80 | 20 | 1.21 | 10.73 | 3.66 | 0.128 | 0.073 | 8.38 | -2.01 | 0.143 | 0.146 | 0.029 | 0.564 | 0.992 |
| 80 | 40 | 1.26 | 10.73 | 3.66 | 0.128 | 0.075 | 8.38 | -2.01 | 0.143 | 0.146 | 0.029 | 0.565 | 0.991 |
| 100 | 0 | 1.23 | 10.62 | 3.70 | 0.126 | 0.074 | 8.38 | -2.01 | 0.145 | 0.148 | 0.029 | 0.564 | 0.992 |
| 100 | 20 | 1.28 | 10.62 | 3.70 | 0.126 | 0.075 | 8.38 | -2.01 | 0.145 | 0.148 | 0.030 | 0.565 | 0.991 |
| 100 | 40 | 1.33 | 10.62 | 3.70 | 0.126 | 0.077 | 8.38 | -2.01 | 0.145 | 0.148 | 0.030 | 0.567 | 0.991 |

* For $Q=0.056$ liters/sec M^2 (1 gpm for test module).

** For 45% ethylene glycol solution.

APPENDIX III

TEST DATA

TABLE A-III-1 Summary of Test Data for June 19, 1975

| Test Period Ending Hr.-Min. | Average Inlet Fluid Temperature °C | Average Outlet Fluid Temperature °C | Fluid Flow Rate GPM | Average Ambient Temperature °C | Average Wind Speed KPH | Average Solar Radiation KJ Hr ⁻¹ m ⁻² | Average Energy Collected KJ Hr ⁻¹ m ⁻² | Test Period Efficiency | $\frac{T_{IN}-T_a}{(HR)}$ °Cm ² -MJ ⁻¹ |
|--------------------------------------|--|---|------------------------------|---|---------------------------------|--|---|------------------------------|---|
| 9 15 | 47.6 | 49.8 | .96 | 17.0 | 23.8 | 2350.2 | 1469.8 | 62.5 | 13.00 |
| 9 29 | 51.6 | 53.9 | .96 | 17.3 | 23.7 | 2397.7 | 1526.9 | 63.7 | 14.33 |
| 9 45 | 55.9 | 58.3 | .97 | 17.2 | 27.0 | 2535.5 | 1625.4 | 64.1 | 15.23 |
| 9 59 | 59.2 | 61.7 | .97 | 17.4 | 26.4 | 2647.1 | 1699.6 | 64.2 | 15.79 |
| 10 15 | 62.8 | 65.6 | .95 | 17.9 | 23.1 | 2763.2 | 1777.7 | 64.3 | 16.24 |
| 10 29 | 65.6 | 68.6 | .95 | 18.2 | 25.2 | 2852.7 | 1939.3 | 68.0 | 16.62 |
| 10 45 | 62.6 | 65.8 | .96 | 19.0 | 23.1 | 2934.7 | 2049.5 | 69.8 | 14.87 |
| 10 59 | 65.4 | 68.5 | .96 | 19.1 | 21.6 | 3027.8 | 1976.1 | 65.3 | 15.29 |
| 11 15 | 68.3 | 71.4 | .93 | 19.3 | 21.7 | 3013.6 | 1969.7 | 65.4 | 16.26 |
| 11 29 | 68.6 | 72.2 | .93 | 20.1 | 22.9 | 3247.7 | 2270.3 | 69.9 | 14.94 |
| 11 45 | 68.0 | 70.0 | .94 | 20.2 | 25.7 | 2038.1 | 1263.3 | 62.0 | 23.48 |
| 11 59 | 66.2 | 68.8 | .94 | 20.5 | 25.2 | 2233.5 | 1663.0 | 74.5 | 20.45 |

CORNING COLLECTOR JUNE 19, 1975

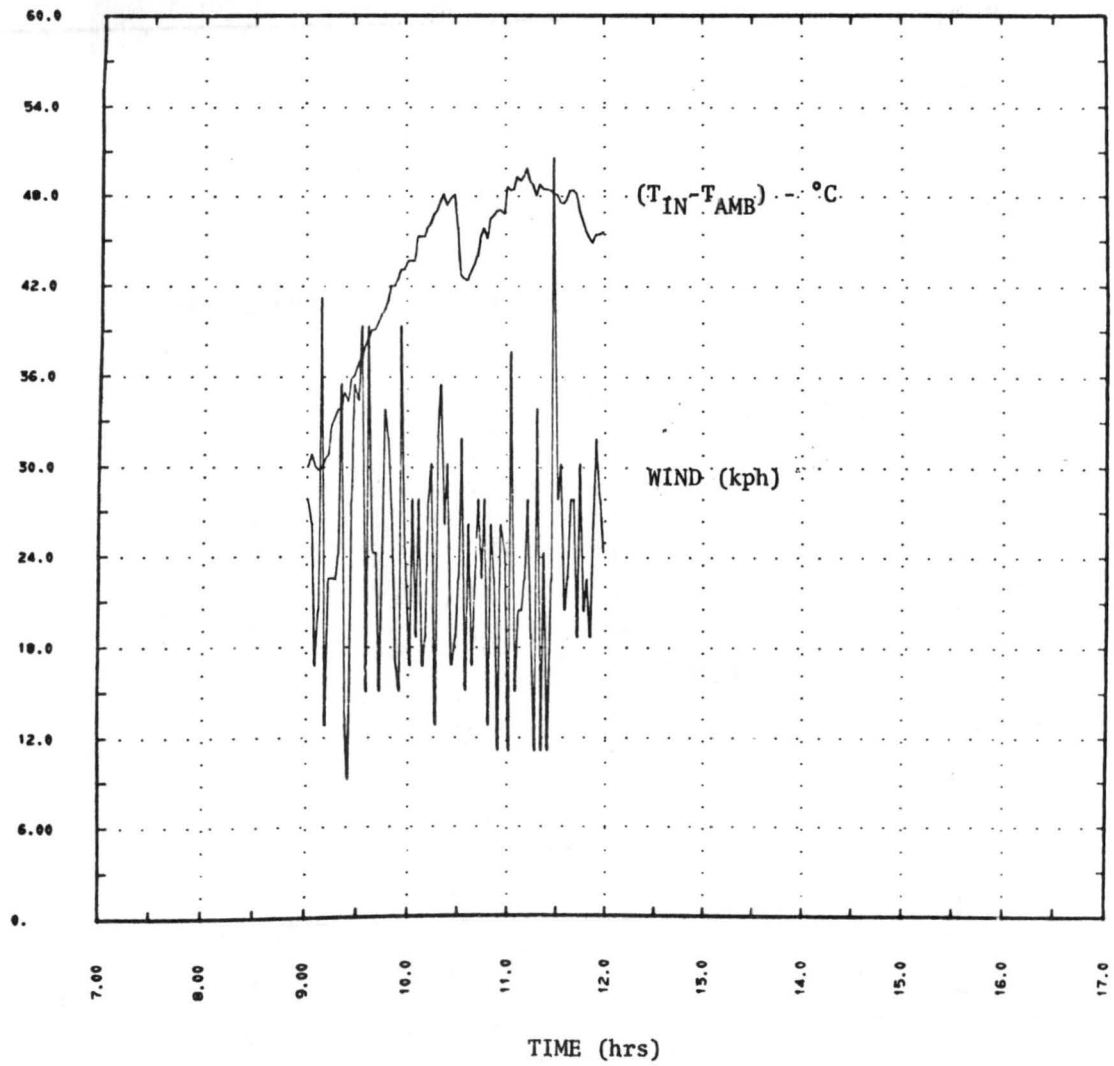


Figure A-III-1. Test Data Plot.

CORNING COLLECTOR JUNE 19, 1975

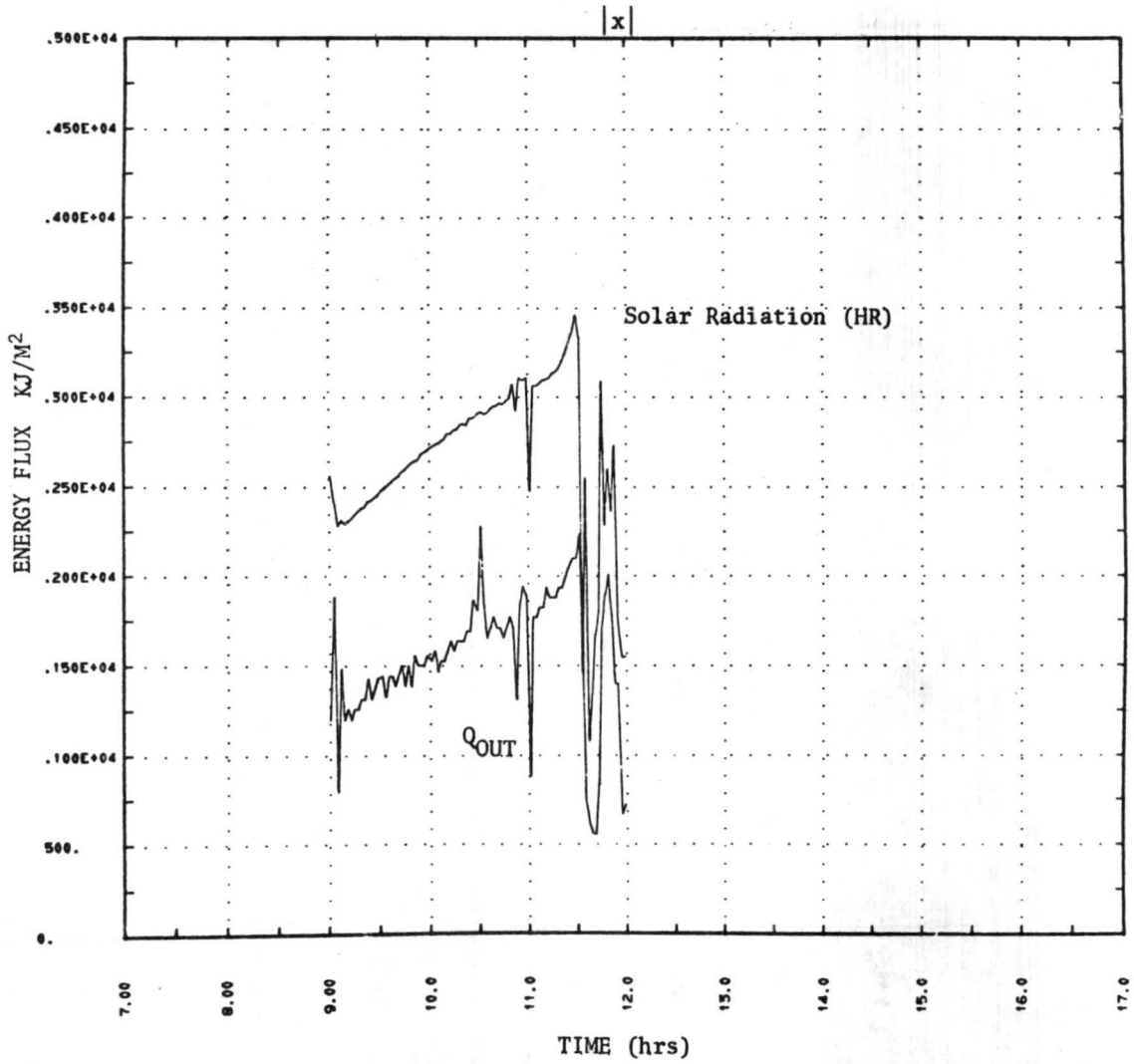


Figure A-III-2. Test Data Plot.

TABLE A-III-2 Summary of Test Data for June 20, 1975

| Test Period Ending Hr.-Min. | Average Inlet Fluid Temperature °C | Average Outlet Fluid Temperature °C | Fluid Flow Rate GPM | Average Ambient Temperature °C | Average Wind Speed KPH | Average Solar Radiation KJ Hr ⁻¹ m ⁻² | Average Energy Collected KJ Hr ⁻¹ m ⁻² | Test Period Efficiency | $\frac{T_{IN}-T_a}{(HR)}$ °Cm ² -MJ ⁻¹ |
|--------------------------------------|--|---|------------------------------|---|---------------------------------|--|---|------------------------------|---|
| 9 15 | 68.3 | 70.6 | .79 | 20.3 | 23.1 | 2245.5 | 1187.7 | 52.9 | 21.38 |
| 9 29 | 69.4 | 71.9 | .79 | 20.9 | 7.8 | 2376.5 | 1351.7 | 56.9 | 20.38 |
| 9 45 | 69.2 | 71.9 | .80 | 21.5 | 9.2 | 2513.4 | 1490.8 | 59.3 | 18.95 |
| 9 59 | 68.1 | 71.1 | .80 | 21.5 | 12.8 | 2636.0 | 1633.1 | 62.0 | 17.65 |
| 10 15 | 65.8 | 68.7 | .91 | 22.6 | 15.6 | 2751.7 | 1826.8 | 66.4 | 15.69 |
| 10 29 | 65.6 | 68.6 | .91 | 22.8 | 10.4 | 2846.7 | 1826.8 | 64.2 | 15.05 |
| 10 45 | 65.2 | 68.1 | .93 | 23.2 | 13.2 | 2932.0 | 1827.6 | 62.3 | 14.35 |
| 10 59 | 64.3 | 67.4 | .93 | 23.4 | 17.5 | 2989.1 | 1937.9 | 64.8 | 13.70 |
| 11 15 | 65.9 | 68.8 | .93 | 23.6 | 23.2 | 3049.5 | 1859.1 | 61.0 | 13.85 |
| 11 29 | 68.7 | 71.8 | .93 | 24.0 | 22.4 | 3084.1 | 1961.5 | 63.6 | 14.48 |
| 11 45 | 69.0 | 72.2 | .91 | 24.2 | 16.7 | 3100.5 | 1984.9 | 64.0 | 14.44 |
| 11 59 | 68.5 | 71.8 | .91 | 24.9 | 33.3 | 3124.0 | 2031.1 | 65.0 | 13.98 |
| 12 15 | 66.9 | 70.2 | .93 | 25.1 | 19.2 | 3139.9 | 2095.4 | 66.7 | 13.30 |
| 12 29 | 66.7 | 69.9 | .93 | 25.3 | 22.3 | 3170.8 | 2040.3 | 64.3 | 13.06 |
| 12 45 | 66.4 | 69.2 | .92 | 25.7 | 12.3 | 2978.5 | 1792.4 | 60.2 | 13.64 |
| 12 59 | 65.8 | 69.2 | .92 | 26.6 | 16.9 | 3096.5 | 2104.1 | 67.9 | 12.65 |
| 13 15 | 65.3 | 67.7 | .93 | 25.7 | 26.2 | 2299.0 | 1528.3 | 66.5 | 17.22 |
| 13 29 | 65.0 | 66.5 | .93 | 25.5 | 22.2 | 1696.0 | 929.6 | 54.8 | 23.28 |
| 13 45 | 67.1 | 70.1 | .91 | 26.9 | 20.1 | 2912.6 | 1834.5 | 63.0 | 13.79 |

TABLE A-III-2 Summary of Test Data for June 20, 1975

| Test Period Ending Hr.-Min. | Average Inlet Fluid Temperature °C | Average Outlet Fluid Temperature °C | Fluid Flow Rate GPM | Average Ambient Temperature °C | Average Wind Speed KPH | Average Solar Radiation KJ Hr ⁻¹ m ⁻² | Average Energy Collected KJ Hr ⁻¹ m ⁻² | Test Period Efficiency | $\frac{T_{IN}-T_a}{(HR)}$ °Cm ² -MJ ⁻¹ |
|--------------------------------------|--|---|------------------------------|---|---------------------------------|--|---|------------------------------|---|
| 13 59 | 69.2 | 72.1 | .91 | 27.5 | 24.2 | 2796.0 | 1842.3 | 65.9 | 14.88 |
| 14 15 | 69.0 | 72.0 | .97 | 27.4 | 27.8 | 2702.4 | 1955.5 | 72.4 | 15.39 |
| 14 29 | 68.2 | 71.1 | .97 | 27.7 | 21.9 | 2641.1 | 1947.3 | 73.7 | 15.32 |
| 14 45 | 66.9 | 69.5 | .96 | 27.8 | 16.2 | 2411.5 | 1707.7 | 70.8 | 16.22 |
| 14 59 | 66.6 | 66.7 | .96 | 27.2 | 18.7 | 908.6 | 105.7 | 11.6 | 43.32 |

CORNING COLLECTOR

JUNE 20, 1975

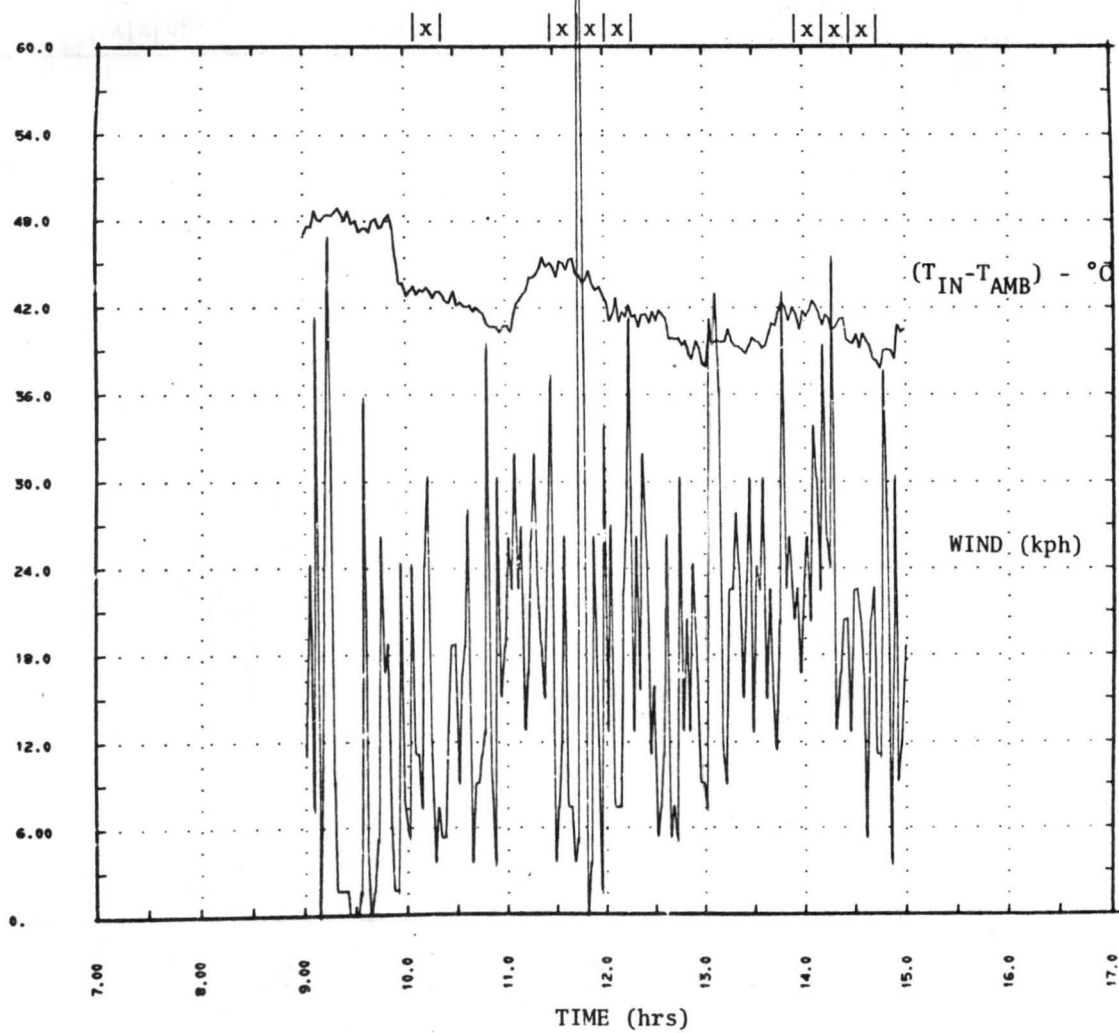


Figure A-III-3. Test Data Plot.

CORNING COLLECTOR JUNE 20, 1975

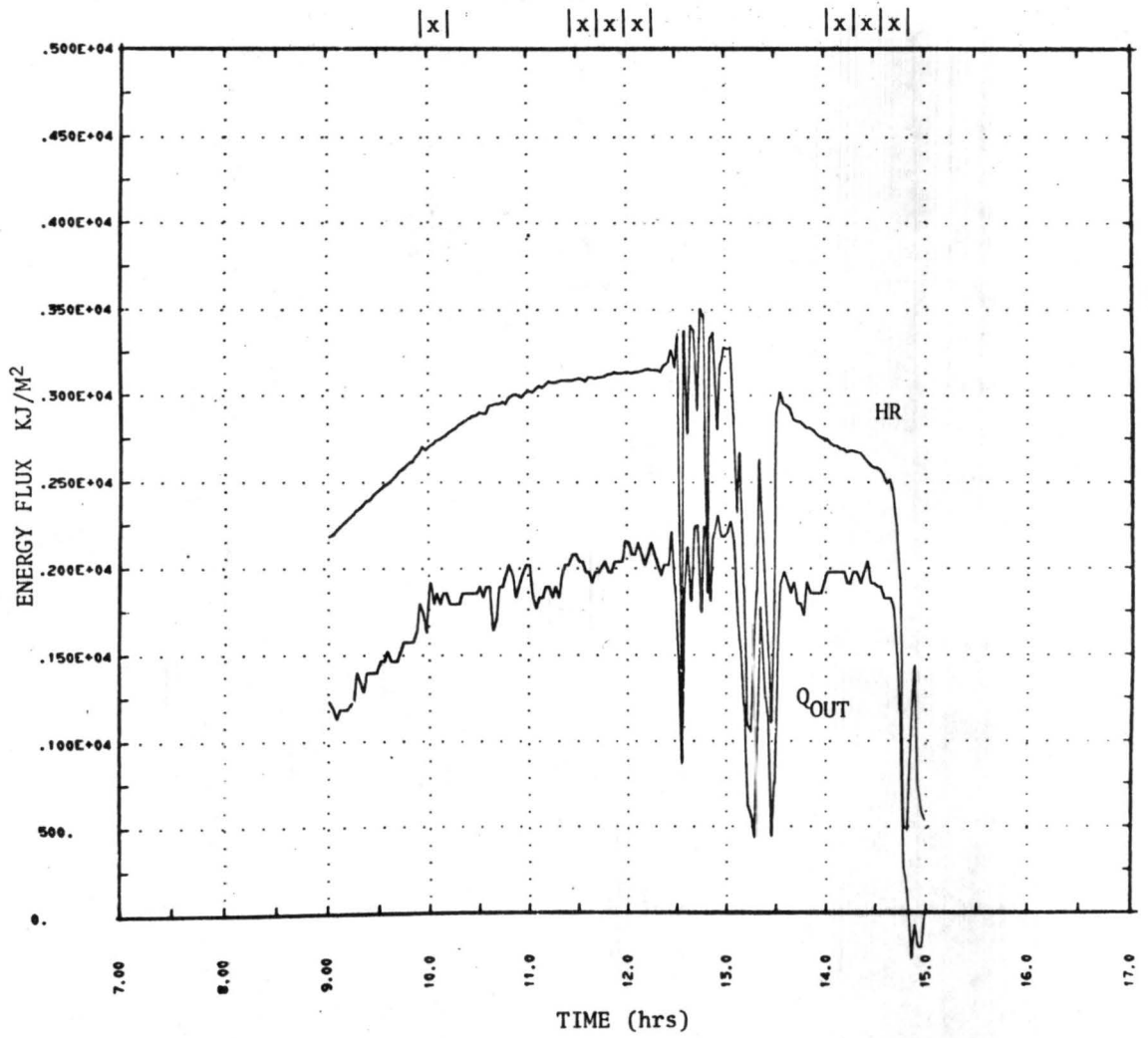


Figure A-III-4. Test Data Plot.

TABLE A-III-3 Summary of Test Data for June 23, 1975

| Test Period Ending Hr.-Min. | Average Inlet Fluid Temperature °C | Average Outlet Fluid Temperature °C | Fluid Flow Rate GPM | Average Ambient Temperature °C | Average Wind Speed KPH | Average Solar Radiation KJ Hr ⁻¹ m ⁻² | Average Energy Collected KJ Hr ⁻¹ m ⁻² | Test Period Efficiency | $\frac{T_{IN}-T_a}{(HR)}$ °Cm ² -MJ ⁻¹ |
|--------------------------------------|--|---|------------------------------|---|---------------------------------|--|---|------------------------------|---|
| 9 15 | 57.6 | 59.8 | 1.03 | 20.6 | 9.7 | 2206.3 | 1541.3 | 69.9 | 16.78 |
| 9 29 | 59.0 | 61.3 | 1.03 | 21.0 | 6.5 | 2351.1 | 1567.3 | 66.7 | 16.16 |
| 9 45 | 62.5 | 64.8 | 1.02 | 21.2 | 11.6 | 2499.5 | 1534.9 | 61.4 | 16.55 |
| 9 59 | 63.2 | 65.8 | 1.02 | 21.8 | 8.1 | 2611.6 | 1757.9 | 67.3 | 15.87 |
| 10 15 | 62.9 | 65.9 | 1.01 | 22.5 | 7.1 | 2723.1 | 2071.8 | 76.1 | 14.81 |
| 10 29 | 61.4 | 64.3 | 1.01 | 22.8 | 8.3 | 2819.5 | 1969.9 | 69.9 | 13.67 |
| 10 45 | 61.1 | 64.0 | 1.04 | 23.1 | 3.7 | 2910.8 | 2037.1 | 70.0 | 13.05 |
| 10 59 | 60.9 | 63.9 | 1.04 | 24.2 | 12.4 | 2975.3 | 2072.1 | 69.6 | 12.33 |
| 11 15 | 60.5 | 63.5 | 1.03 | 24.7 | 16.3 | 3033.8 | 2069.5 | 68.2 | 11.82 |
| 11 29 | 60.3 | 63.3 | 1.03 | 25.4 | 15.4 | 3081.3 | 2078.2 | 67.4 | 11.33 |
| 11 45 | 60.1 | 63.1 | 1.02 | 25.9 | 18.1 | 3108.5 | 2049.4 | 65.9 | 10.99 |
| 11 59 | 59.9 | 62.9 | 1.02 | 26.5 | 18.6 | 3122.4 | 2023.7 | 64.8 | 10.71 |
| 12 15 | 59.6 | 62.7 | 1.02 | 26.5 | 19.4 | 3160.2 | 2126.6 | 67.3 | 10.50 |
| 12 29 | 59.4 | 62.6 | 1.02 | 26.7 | 16.8 | 3012.6 | 2135.2 | 70.9 | 10.88 |
| 12 45 | 59.3 | 62.6 | 1.02 | 27.0 | 19.8 | 3168.9 | 2272.4 | 71.7 | 10.20 |
| 12 59 | 59.3 | 62.5 | 1.02 | 27.3 | 34.2 | 3145.9 | 2212.3 | 70.3 | 10.15 |
| 13 15 | 59.1 | 62.4 | 1.01 | 27.7 | 27.8 | 33742.0 | 2233.1 | 6.6 | .93 |
| 13 29 | 59.1 | 62.4 | 1.01 | 27.9 | 20.8 | 20130.5 | 2224.6 | 11.1 | 1.55 |

TABLE A-III-3 (Continued)

| Test Period Ending Hr.-Min. | Average Inlet Fluid Temperature °C | Average Outlet Fluid Temperature °C | Fluid Flow Rate GPM | Average Ambient Temperature °C | Average Wind Speed KPH | Average Solar Radiation KJ Hr ⁻¹ m ⁻² | Average Energy Collected KJ Hr ⁻¹ m ⁻² | Test Period Efficiency | $\frac{T_{IN}-T_a}{(HR)}$ °Cm ² -MJ ⁻¹ |
|--------------------------------------|--|---|------------------------------|---|---------------------------------|--|---|------------------------------|---|
| 13 45 | 59.2 | 62.7 | 1.01 | 28.4 | 17.8 | 3330.3 | 2402.9 | 72.2 | 9.24 |
| 13 59 | 59.3 | 62.6 | 1.01 | 28.8 | 24.8 | 3121.9 | 2275.6 | 72.9 | 9.76 |
| 14 15 | 57.4 | 57.8 | 1.01 | 28.7 | 41.7 | 2559.5 | 271.7 | 10.6 | 11.24 |
| 14 29 | 54.0 | 54.2 | 1.01 | 28.7 | 23.3 | 2346.0 | 127.4 | 5.4 | 10.78 |
| 14 45 | 50.3 | 50.8 | 1.03 | 28.6 | 20.6 | 2302.7 | 381.0 | 16.5 | 9.41 |
| 14 59 | 48.0 | 48.9 | 1.03 | 28.8 | 21.6 | 2072.7 | 640.8 | 30.9 | 9.23 |

CORNING COLLECTOR JUNE 23, 1975

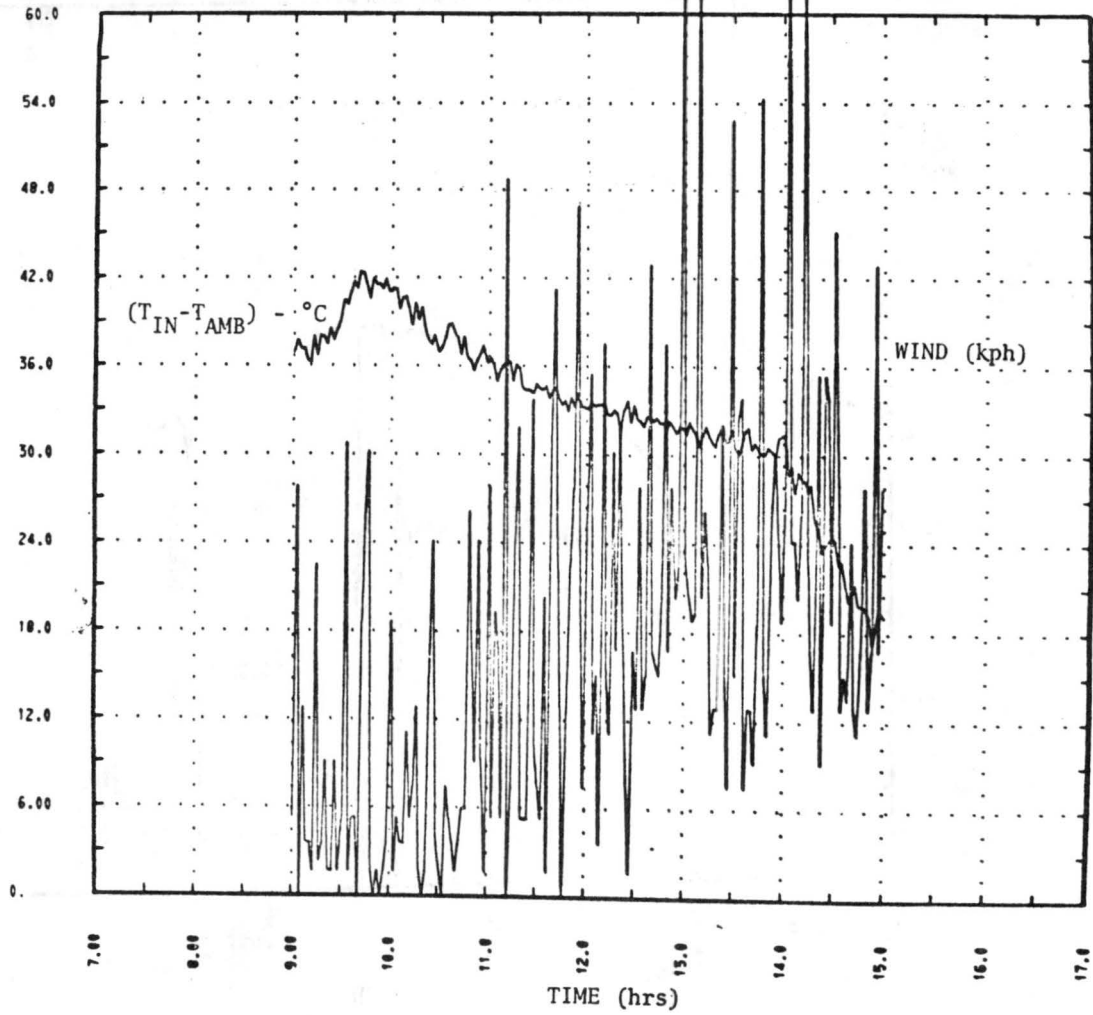


Figure A-III-5. Test Data Plot.

CORNING COLLECTOR JUNE 23, 1975

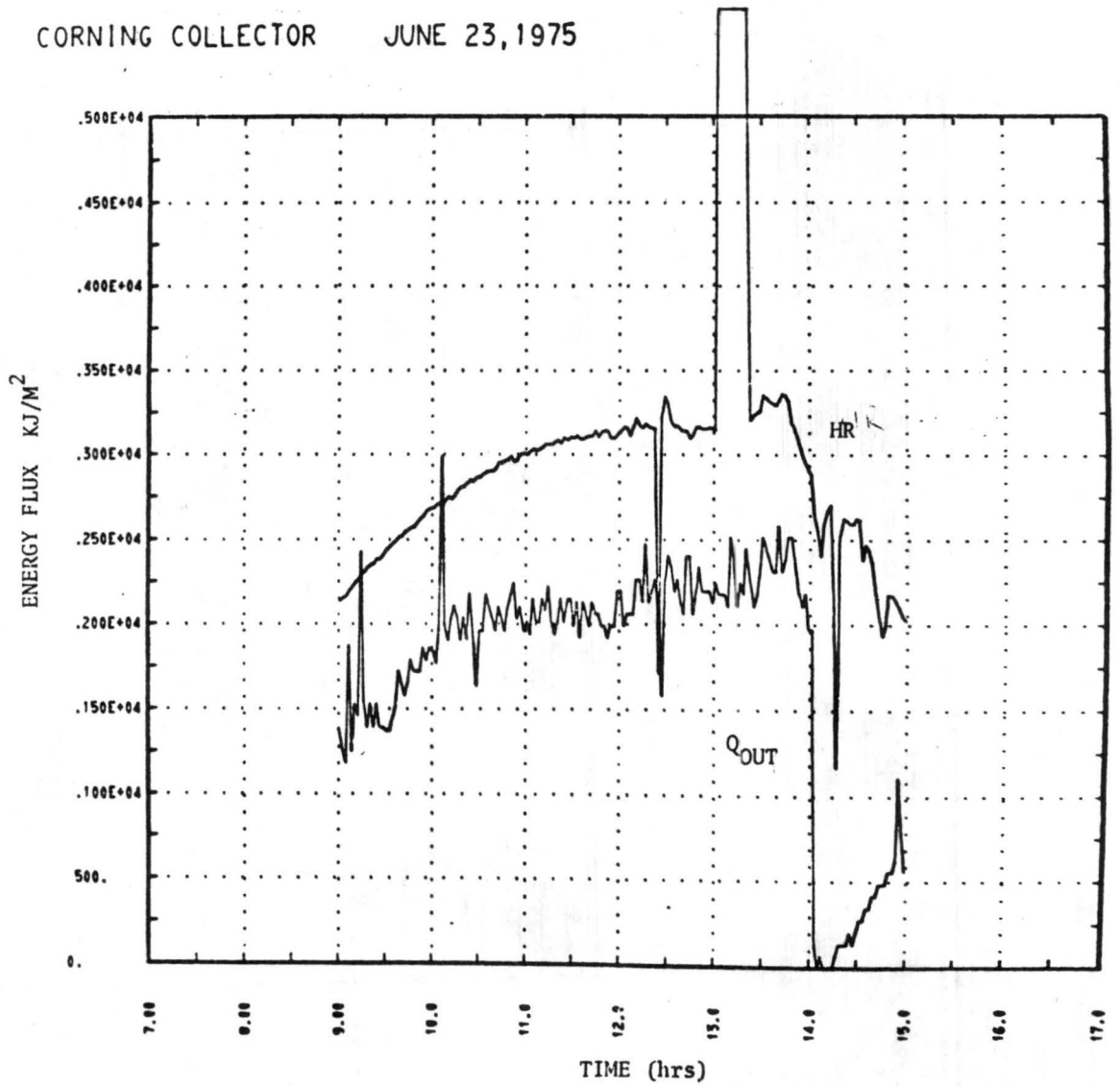


Figure A-III-6. Test Data Plot.

TABLE A-III-4 Summary of Test Data for June 25, 1975

| Test Period Ending Hr.-Min. | Average Inlet Fluid Temperature °C | Average Outlet Fluid Temperature °C | Fluid Flow Rate GPM | Average Ambient Temperature °C | Average Wind Speed KPH | Average Solar Radiation KJ Hr ⁻¹ m ⁻² | Average Energy Collected KJ Hr ⁻¹ m ⁻² | Test Period Efficiency | $\frac{T_{IN}-T_a}{(HR)}$ °Cm ² -MJ ⁻¹ |
|--------------------------------------|--|---|------------------------------|---|---------------------------------|--|---|------------------------------|---|
| 11 15 | 47.3 | 50.4 | 1.09 | 28.7 | 26.5 | 3081.3 | 2218.6 | 72.0 | 6.03 |
| 11 29 | 47.7 | 51.0 | 1.09 | 29.1 | 21.3 | 3122.8 | 2354.5 | 75.4 | 5.96 |
| 11 45 | 48.3 | 51.5 | 1.06 | 29.5 | 26.7 | 3162.0 | 2298.5 | 72.7 | 5.94 |
| 11 59 | 48.8 | 52.1 | 1.06 | 30.6 | 18.5 | 3187.4 | 2333.7 | 73.2 | 5.71 |
| 12 15 | 49.2 | 52.5 | 1.05 | 31.5 | 33.2 | 3201.6 | 2276.8 | 71.1 | 5.54 |
| 12 29 | 49.5 | 52.8 | 1.05 | 31.8 | 38.0 | 3215.0 | 2303.0 | 71.6 | 5.50 |
| 12 45 | 49.8 | 53.0 | 1.04 | 31.6 | 54.3 | 3169.8 | 2237.8 | 70.6 | 5.74 |
| 12 59 | 50.1 | 53.4 | 1.04 | 31.5 | 53.3 | 3240.4 | 2298.3 | 70.9 | 5.73 |
| 13 15 | 50.3 | 53.4 | 1.04 | 31.8 | 64.1 | 3171.2 | 2160.1 | 68.1 | 5.84 |
| 13 29 | 50.4 | 53.9 | 1.04 | 32.1 | 65.7 | 3207.6 | 2427.9 | 75.7 | 5.72 |
| 13 45 | 50.5 | 52.3 | 1.04 | 31.0 | 59.3 | 1478.9 | 1252.8 | 84.7 | 13.17 |
| 13 59 | 50.3 | 50.9 | 1.04 | 30.0 | 61.7 | 759.3 | 466.6 | 61.5 | 26.75 |

CORNING COLLECTOR JUNE 25, 1975

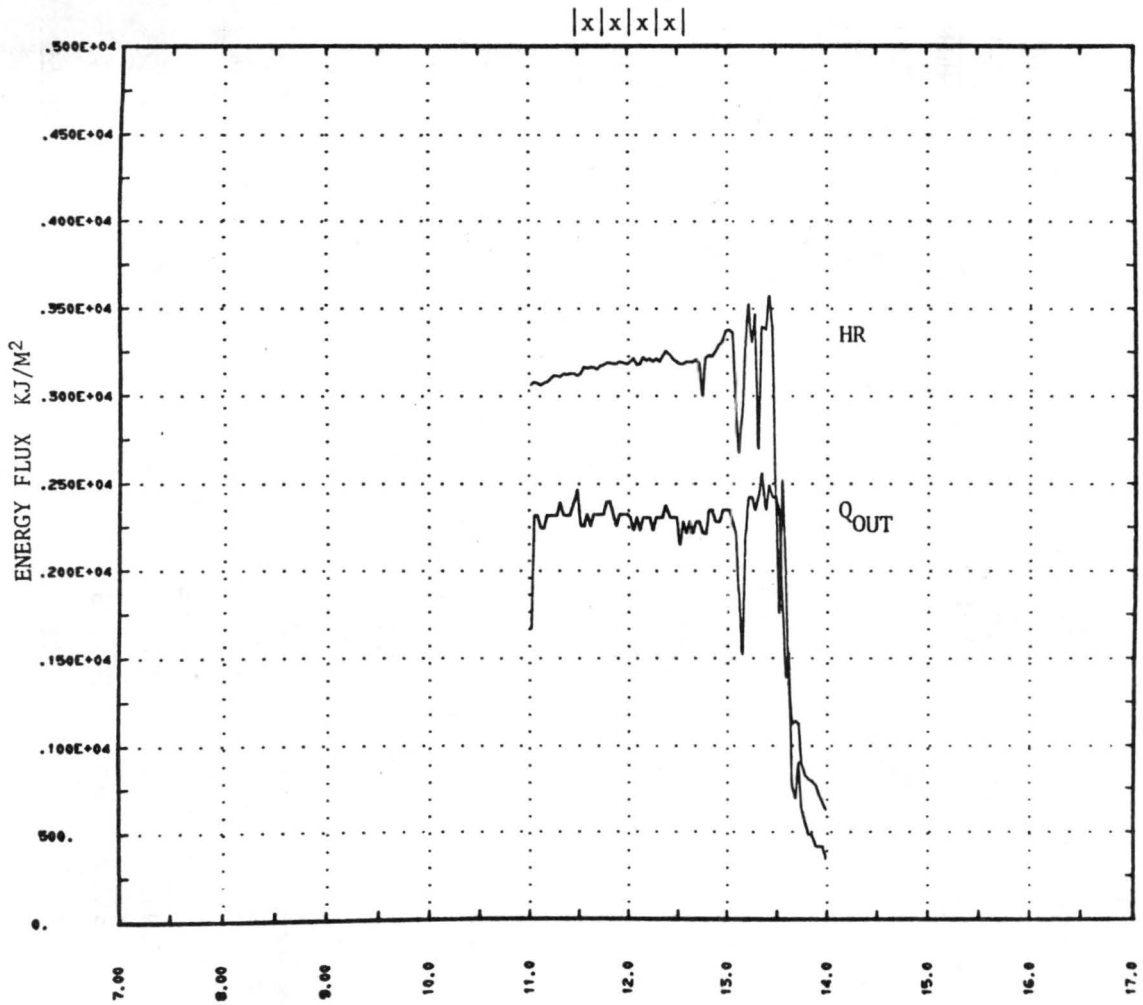


Figure A-III-8. Test Data Plot.

TABLE A-III-5 Summary of Test Data for June 27, 1975

| Test Period Ending Hr.-Min. | Average Inlet Fluid Temperature °C | Average Outlet Fluid Temperature °C | Fluid Flow Rate GPM | Average Ambient Temperature °C | Average Wind Speed KPH | Average Solar Radiation KJ Hr ⁻¹ m ⁻² | Average Energy Collected KJ Hr ⁻¹ n ⁻² | Test Period Efficiency | $\frac{T_{IN}-T_a}{(HR)}$ °Cm ² -MJ ⁻¹ |
|--------------------------------------|--|---|------------------------------|---|---------------------------------|--|---|------------------------------|---|
| 8 15 | 67.5 | 68.6 | 1.18 | 17.5 | 13.7 | 1669.7 | 903.7 | 54.1 | 29.95 |
| 8 29 | 70.0 | 71.3 | 1.18 | 18.3 | 12.5 | 1836.6 | 1045.8 | 56.9 | 28.18 |
| 8 45 | 72.9 | 74.3 | 1.17 | 19.2 | 14.9 | 1995.2 | 1157.8 | 58.0 | 26.91 |
| 8 59 | 75.3 | 77.0 | 1.17 | 20.0 | 8.6 | 2127.5 | 1328.9 | 62.5 | 25.99 |
| 9 15 | 78.1 | 80.0 | 1.15 | 21.2 | 33.4 | 2282.4 | 1454.6 | 63.7 | 24.96 |
| 9 29 | 80.3 | 82.3 | 1.15 | 21.9 | 5.2 | 2416.6 | 1563.5 | 64.7 | 24.20 |
| 9 45 | 83.1 | 85.2 | 1.11 | 22.1 | 8.3 | 2568.2 | 1595.0 | 62.1 | 23.72 |
| 9 59 | 85.6 | 87.8 | 1.11 | 23.1 | 11.9 | 2687.2 | 1728.8 | 64.3 | 23.23 |
| 10 15 | 84.2 | 86.9 | 1.07 | 24.3 | 13.2 | 2794.1 | 1970.3 | 70.5 | 21.47 |
| 10 29 | 84.8 | 87.2 | 1.07 | 24.9 | 19.8 | 2894.2 | 1767.7 | 61.1 | 20.71 |
| 10 45 | 87.4 | 90.0 | 1.01 | 24.7 | 22.2 | 3002.5 | 1755.5 | 58.5 | 20.89 |
| 10 59 | 89.6 | 92.3 | 1.01 | 26.0 | 17.7 | 3069.8 | 1851.1 | 60.3 | 20.73 |
| 11 15 | 92.2 | 95.0 | .91 | 26.2 | 16.2 | 3141.3 | 1754.0 | 55.8 | 21.00 |
| 11 29 | 92.7 | 95.7 | .91 | 27.1 | 28.3 | 3161.5 | 1863.6 | 58.9 | 20.77 |
| 11 45 | 91.6 | 94.5 | .92 | 27.0 | 18.9 | 3203.0 | 1892.0 | 59.1 | 20.16 |
| 11 59 | 91.5 | 94.3 | .92 | 27.5 | 16.7 | 3217.8 | 1773.2 | 55.1 | 19.88 |
| 12 15 | 94.4 | 97.2 | .93 | 28.0 | 30.1 | 3211.8 | 1808.5 | 56.3 | 20.65 |
| 12 29 | 96.1 | 99.0 | .93 | 28.2 | 37.4 | 3213.6 | 1880.5 | 58.5 | 21.13 |
| 12 45 | 95.5 | 98.1 | .92 | 29.0 | 37.3 | 3182.7 | 1638.7 | 51.5 | 20.91 |
| 12 59 | 89.3 | 84.9 | .92 | 29.8 | 32.9 | 3095.6 | 0.0 | 0.0 | 19.20 |

CORNING COLLECTOR JUNE 27, 1975

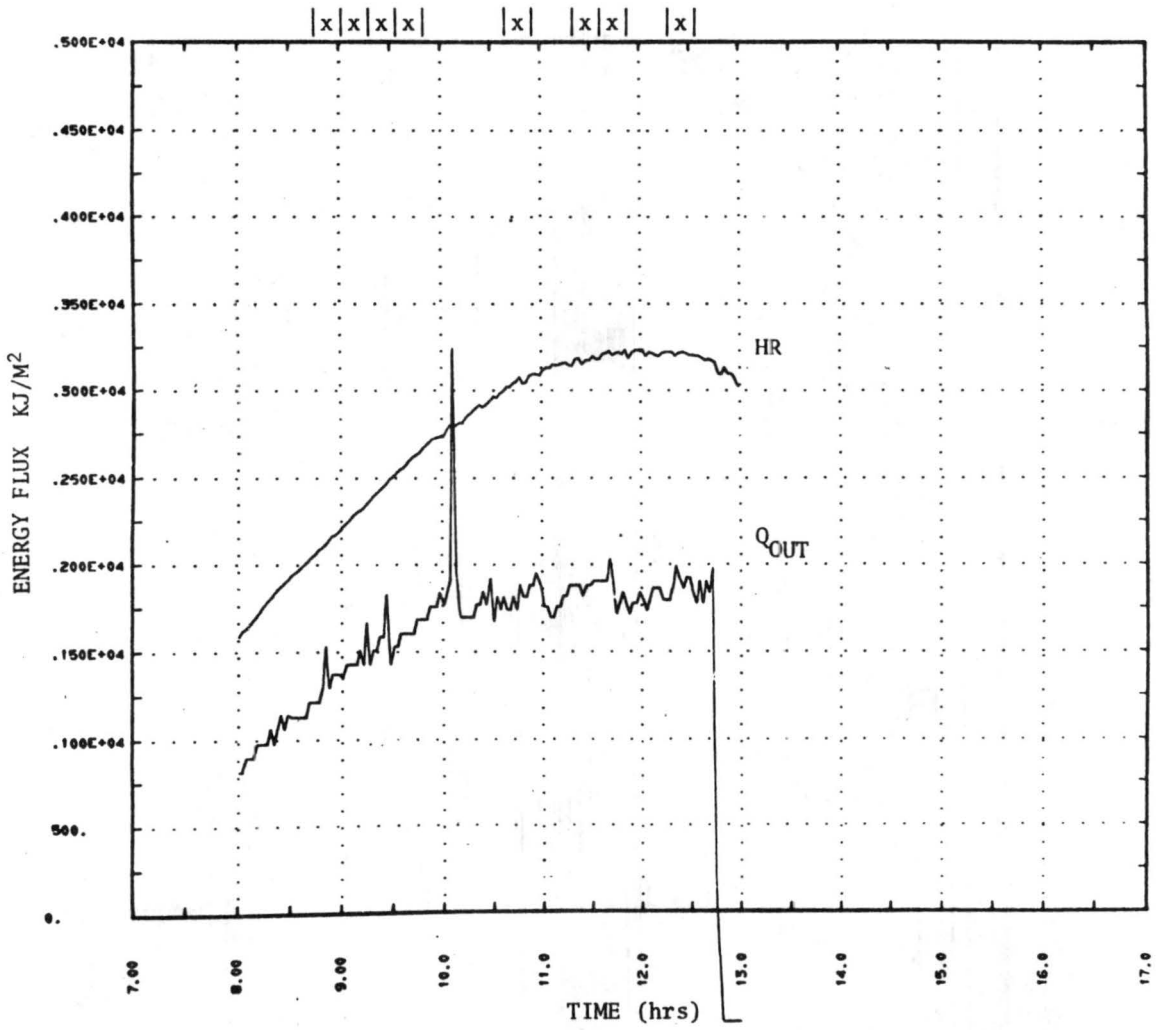


Figure A-III-10. Test Data Plot.

TABLE A-III-6 Summary of Test Data for July 8, 1975

| Test Period Ending Hr.-Min. | Average Inlet Fluid Temperature °C | Average Outlet Fluid Temperature °C | Fluid Flow Rate GPM | Average Ambient Temperature °C | Average Wind Speed KPH | Average Solar Radiation KJ Hr ⁻¹ m ⁻² | Average Energy Collected KJ Hr ⁻¹ m ⁻² | Test Period Efficiency | $\frac{T_{IN}-T_a}{(HR)}$ °Cm ² -MJ ⁻¹ |
|--------------------------------------|--|---|------------------------------|---|---------------------------------|--|---|------------------------------|---|
| 8 15 | 44.5 | 45.9 | 1.25 | 21.5 | 12.5 | 1622.7 | 1169.8 | 72.1 | 14.14 |
| 8 29 | 40.3 | 41.7 | 1.25 | 22.0 | 11.0 | 1763.8 | 1169.8 | 66.3 | 10.37 |
| 8 45 | 40.1 | 41.7 | 1.26 | 22.2 | 11.6 | 1927.0 | 1313.6 | 68.2 | 9.30 |
| 8 59 | 39.7 | 41.5 | 1.26 | 22.3 | 10.4 | 2043.2 | 1489.4 | 72.9 | 8.51 |
| 9 15 | 39.5 | 41.5 | 1.24 | 22.9 | 11.3 | 2196.7 | 1608.3 | 73.2 | 7.54 |
| 9 29 | 39.4 | 41.5 | 1.24 | 23.5 | 8.3 | 2339.1 | 1720.3 | 73.5 | 6.81 |
| 9 45 | 39.4 | 41.7 | 1.22 | 23.4 | 9.7 | 2481.6 | 1802.7 | 72.6 | 6.45 |
| 9 59 | 39.6 | 42.0 | 1.22 | 24.2 | 12.8 | 2595.4 | 1902.8 | 73.3 | 5.94 |
| 10 15 | 39.8 | 42.2 | 1.22 | 24.9 | 11.4 | 2701.0 | 1952.9 | 72.3 | 5.49 |
| 10 29 | 40.1 | 42.5 | 1.22 | 24.8 | 10.4 | 2793.7 | 1962.9 | 70.3 | 5.47 |
| 10 45 | 40.4 | 43.0 | 1.23 | 26.1 | 13.9 | 2887.2 | 2069.9 | 71.7 | 4.94 |
| 10 59 | 40.7 | 43.2 | 1.23 | 26.6 | 8.1 | 2953.2 | 2090.1 | 70.8 | 4.76 |
| 11 15 | 41.0 | 43.6 | 1.22 | 26.1 | 16.0 | 3011.3 | 2063.1 | 68.5 | 4.98 |
| 11 29 | 41.4 | 44.1 | 1.22 | 27.1 | 17.8 | 3048.6 | 2163.2 | 71.0 | 4.69 |
| 11 45 | 41.7 | 44.3 | 1.22 | 27.7 | 13.9 | 3089.2 | 2093.1 | 67.8 | 4.54 |
| 11 59 | 42.0 | 44.7 | 1.22 | 27.8 | 18.2 | 3102.1 | 2123.2 | 68.4 | 4.59 |
| 12 15 | 42.4 | 45.0 | 1.22 | 27.8 | 10.1 | 3132.0 | 2113.2 | 67.5 | 4.67 |
| 12 29 | 42.7 | 45.3 | 1.22 | 27.4 | 17.1 | 3159.2 | 2113.2 | 66.9 | 4.86 |
| 12 45 | 42.7 | 45.7 | 1.22 | 28.4 | 14.3 | 3137.6 | 2443.7 | 77.9 | 4.56 |

TABLE A-III-6 Summary of Test Data for July 8, 1975

| Test Period Ending Hr.-Min. | Average Inlet Fluid Temperature °C | Average Outlet Fluid Temperature °C | Fluid Flow Rate GPM | Average Ambient Temperature °C | Average Wind Speed KPH | Average Solar Radiation KJ Hr ⁻¹ m ⁻² | Average Energy Collected KJ Hr ⁻¹ m ⁻² | Test Period Efficiency | $\frac{T_{IN}-T_a}{(HR)}$ °Cm ² -MJ ⁻¹ |
|--------------------------------------|--|---|------------------------------|---|---------------------------------|--|---|------------------------------|---|
| 12 59 | 43.4 | 46.0 | 1.22 | 29.5 | 14.3 | 3130.2 | 2123.2 | 67.8 | 4.43 |
| 13 15 | 43.7 | 46.2 | 1.22 | 28.8 | 12.9 | 3095.2 | 2063.1 | 66.7 | 4.80 |
| 13 29 | 43.9 | 46.5 | 1.22 | 29.4 | 18.5 | 3064.7 | 2043.1 | 66.7 | 4.73 |
| 13 45 | 44.2 | 46.7 | 1.22 | 29.1 | 12.2 | 3000.6 | 2013.0 | 67.1 | 5.02 |
| 13 59 | 44.4 | 46.9 | 1.22 | 29.6 | 14.8 | 2947.6 | 1952.9 | 66.3 | 5.04 |
| 14 15 | 44.7 | 47.1 | 1.22 | 30.0 | 12.5 | 2902.0 | 1932.9 | 66.6 | 5.07 |
| 14 29 | 44.8 | 47.2 | 1.22 | 31.8 | 15.7 | 2909.8 | 1922.9 | 66.1 | 4.48 |
| 14 45 | 45.0 | 47.2 | 1.22 | 30.8 | 30.2 | 2772.9 | 1762.6 | 63.6 | 5.11 |
| 14 59 | 45.0 | 47.1 | 1.22 | 30.2 | 15.1 | 2642.0 | 1672.5 | 63.3 | 5.63 |
| 15 15 | 44.7 | 44.7 | 1.22 | 29.8 | 18.1 | 2004.0 | 60.1 | 3.0 | 7.42 |
| 15 29 | 43.5 | 43.3 | 1.22 | 28.9 | 17.7 | 1538.8 | 0.0 | 0.0 | 9.53 |
| 15 45 | 41.9 | 41.2 | 1.22 | 28.1 | 15.9 | 943.2 | 0.0 | 0.0 | 14.61 |
| 15 59 | 40.7 | 39.6 | 1.22 | 27.7 | 27.2 | 953.8 | 0.0 | 0.0 | 13.69 |

TABLE A-III-7 Summary of Test Data for July 14, 1975

| Test Period Ending Hr.-Min. | Average Inlet Fluid Temperature °C | Average Outlet Fluid Temperature °C | Fluid Flow Rate CPM | Average Ambient Temperature °C | Average Wind Speed KPH | Average Solar Radiation KJ Hr ⁻¹ m ⁻² | Average Energy Collected KJ Hr ⁻¹ m ⁻² | Test Period Efficiency | $\frac{T_{IN}-T_a}{(HR)}$ °Cm ² -MJ ⁻¹ |
|--------------------------------------|--|---|------------------------------|---|---------------------------------|--|---|------------------------------|---|
| 8 15 | 60.7 | 59.2 | .50 | 25.6 | 15.6 | 1536.1 | 0.0 | 0.0 | 22.84 |
| 8 29 | 66.9 | 69.4 | .50 | 26.5 | 13.2 | 1713.1 | 845.5 | 49.4 | 23.56 |
| 8 45 | 66.6 | 69.6 | .49 | 26.9 | 18.0 | 1883.6 | 992.1 | 52.7 | 21.07 |
| 8 59 | 67.3 | 70.7 | .49 | 27.5 | 21.5 | 2018.7 | 1136.8 | 56.3 | 19.70 |
| 9 15 | 67.1 | 71.0 | .48 | 28.0 | 20.6 | 2175.0 | 1253.7 | 57.6 | 17.98 |
| 9 29 | 66.9 | 71.1 | .48 | 29.0 | 20.6 | 2312.8 | 1375.4 | 59.5 | 16.39 |
| 9 45 | 66.5 | 71.0 | .48 | 29.9 | 23.9 | 2457.1 | 1487.1 | 60.5 | 14.86 |
| 9 59 | 64.6 | 69.6 | .48 | 30.0 | 19.0 | 2588.1 | 1625.6 | 62.8 | 13.39 |
| 10 15 | 63.9 | 68.9 | .49 | 30.7 | 18.0 | 2720.8 | 1687.2 | 62.0 | 12.21 |
| 10 29 | 63.7 | 69.1 | .49 | 31.0 | 21.3 | 2854.5 | 1774.9 | 62.2 | 11.48 |
| 10 45 | 63.7 | 69.3 | .49 | 31.7 | 17.3 | 3007.1 | 1874.8 | 62.3 | 10.64 |
| 10 59 | 63.6 | 69.4 | .49 | 32.7 | 19.5 | 3103.9 | 1933.4 | 62.3 | 9.96 |
| 11 15 | 63.5 | 69.4 | .49 | 33.4 | 21.1 | 3269.0 | 1991.8 | 60.9 | 9.20 |
| 11 29 | 63.5 | 68.8 | .49 | 33.7 | 16.1 | 2995.6 | 1786.4 | 59.6 | 9.95 |
| 11 45 | 63.4 | 67.2 | .50 | 33.7 | 17.1 | 2134.4 | 1269.9 | 59.5 | 13.90 |
| 11 59 | 63.1 | 64.8 | .50 | 32.5 | 18.4 | 1096.7 | 573.8 | 52.3 | 27.89 |
| 12 15 | 62.7 | 63.0 | .51 | 29.1 | 23.1 | 330.5 | 95.6 | 28.9 | 101.73 |
| 12 29 | 63.2 | 63.1 | .51 | 27.0 | 30.4 | 246.2 | 0.0 | 0.0 | 147.10 |
| 12 45 | 65.7 | 65.7 | .51 | 26.9 | 23.6 | 290.9 | 0.0 | 0.0 | 133.38 |
| 12 59 | 65.9 | 66.1 | .51 | 27.3 | 24.4 | 355.0 | 56.0 | 15.8 | 108.78 |

CORNING COLLECTOR JULY 14, 1975

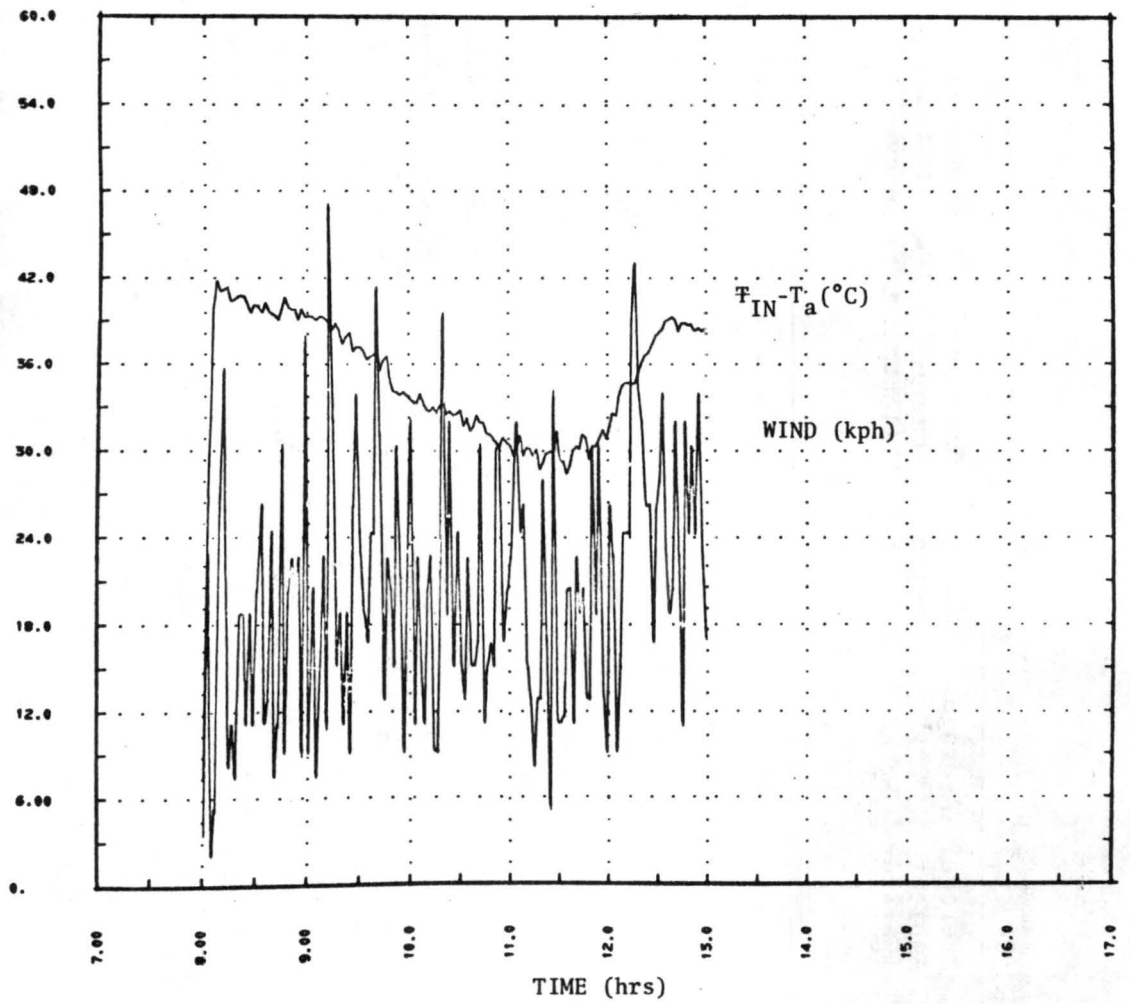


Figure A-III-13. Test Data Plot.

CORNING COLLECTOR JULY 14, 1975

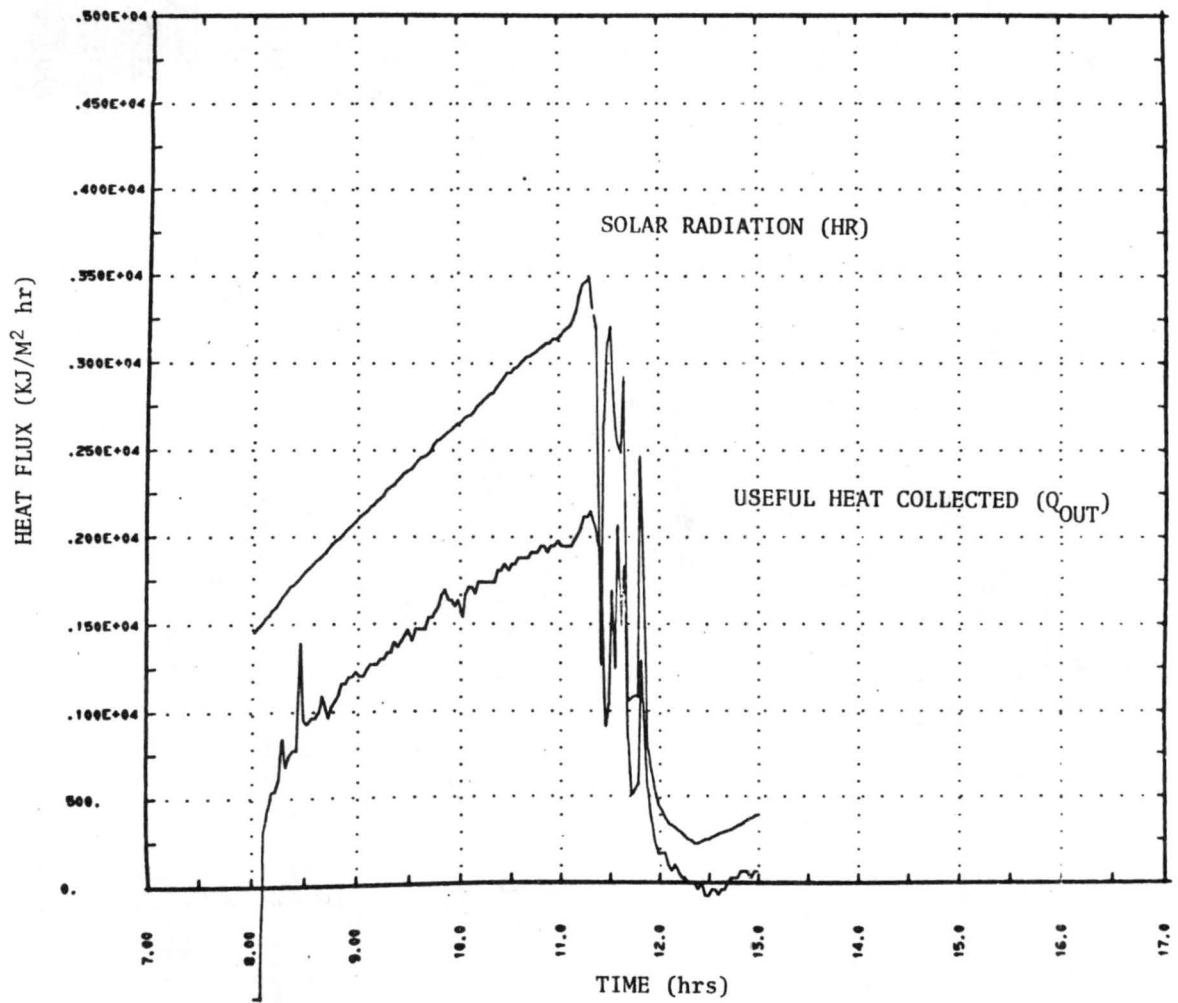


Figure A-III-14. Test Data Plot.

TABLE A-III-8 Summary of Test Data for July 16, 1975

| Test Period Ending Hr.-Min. | Average Inlet Fluid Temperature °C | Average Outlet Fluid Temperature °C | Fluid Flow Rate GPM | Average Ambient Temperature °C | Average Wind Speed KPH | Average Solar Radiation KJ Hr ⁻¹ m ⁻² | Average Energy Collected KJ Hr ⁻¹ m ⁻² | Test Period Efficiency | $\frac{T_{IN}-T_a}{(HR)}$ °Cm ² -MJ ⁻¹ |
|--------------------------------------|--|---|------------------------------|---|---------------------------------|--|---|------------------------------|---|
| 8 15 | 37.3 | 39.1 | .56 | 24.9 | 9.8 | 1545.3 | 676.0 | 43.7 | 7.98 |
| 8 29 | 37.6 | 40.6 | .56 | 25.4 | 9.5 | 1719.5 | 1101.9 | 64.1 | 7.13 |
| 8 45 | 37.7 | 40.8 | .55 | 26.2 | 18.5 | 1776.2 | 1151.0 | 64.8 | 6.47 |
| 8 59 | 37.6 | 41.2 | .55 | 26.6 | 11.6 | 2011.8 | 1300.5 | 64.6 | 5.49 |
| 9 15 | 37.5 | 41.6 | .56 | 27.5 | 13.3 | 2169.9 | 1508.9 | 69.5 | 4.60 |
| 9 29 | 37.8 | 42.3 | .56 | 28.1 | 14.7 | 2301.3 | 1627.8 | 70.7 | 4.20 |
| 9 45 | 38.2 | 44.1 | .55 | 28.8 | 18.6 | 2453.9 | 2113.0 | 86.1 | 3.85 |
| 9 59 | 38.4 | 51.0 | .55 | 29.1 | 13.3 | 2573.3 | 4578.2 | 177.9 | 3.59 |
| 10 15 | 38.9 | 45.6 | .55 | 29.6 | 10.0 | 2695.9 | 2433.6 | 90.3 | 3.45 |
| 10 29 | 39.6 | 44.9 | .55 | 30.8 | 16.7 | 2792.7 | 1918.9 | 68.7 | 3.16 |
| 10 45 | 40.2 | 45.6 | .56 | 30.7 | 8.2 | 2892.8 | 1984.4 | 68.6 | 3.27 |
| 10 59 | 40.7 | 46.3 | .56 | 31.3 | 11.1 | 2979.4 | 2034.7 | 68.3 | 3.14 |
| 11 15 | 41.3 | 47.0 | .56 | 32.1 | 11.8 | 3057.8 | 2075.9 | 67.9 | 3.00 |
| 11 29 | 41.8 | 47.5 | .56 | 32.8 | 16.7 | 3100.7 | 2098.7 | 67.7 | 2.89 |
| 11 45 | 42.3 | 48.1 | .55 | 32.3 | 17.7 | 3098.8 | 2094.2 | 67.6 | 3.23 |
| 11 59 | 42.8 | 48.6 | .55 | 32.8 | 14.5 | 3174.0 | 2094.2 | 66.0 | 3.14 |
| 12 15 | 43.3 | 49.1 | .56 | 33.1 | 16.8 | 3189.2 | 2149.9 | 67.4 | 3.19 |
| 12 29 | 43.8 | 49.6 | .56 | 33.9 | 19.0 | 3211.3 | 2149.9 | 66.9 | 3.06 |
| 12 45 | 44.3 | 50.2 | .56 | 34.2 | 14.3 | 3259.7 | 2186.8 | 67.1 | 3.09 |
| 12 59 | 44.7 | 50.5 | .56 | 33.9 | 14.2 | 3293.8 | 2131.4 | 64.7 | 3.30 |

CORNING-COLLECTOR

JULY 16, 1975

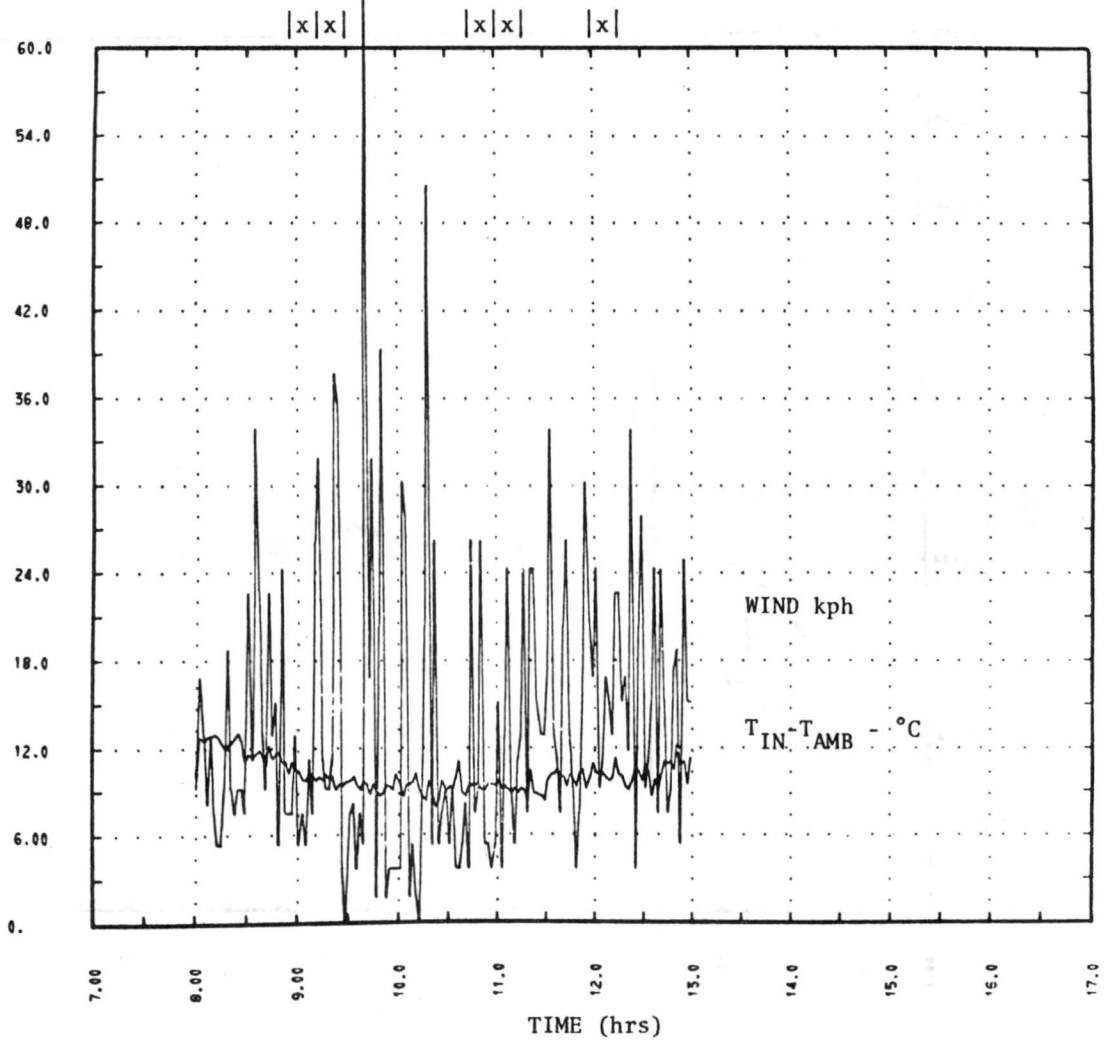


Figure A-III-15. Test Data Plot.

CORNING COLLECTOR JULY 16, 1975

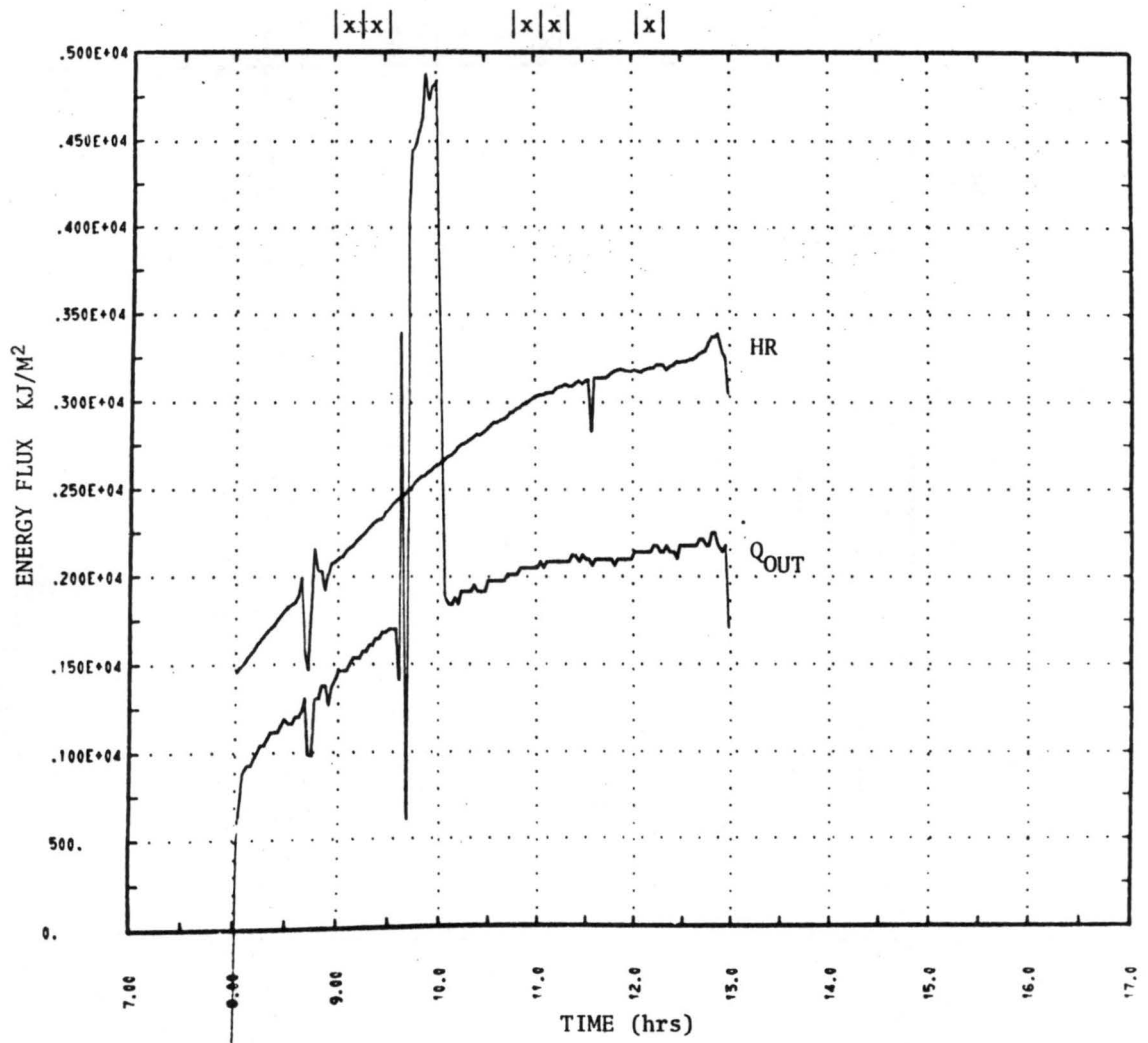


Figure A-III-16. Test Data Plot.

TABLE A-III-9 Summary of Test Data for July 25, 1975

| Test Period Ending Hr.-Min. | Average Inlet Fluid Temperature °C | Average Outlet Fluid Temperature °C | Fluid Flow Rate GPM | Average Ambient Temperature °C | Average Wind Speed KPH | Average Solar Radiation KJ Hr ⁻¹ m ⁻² | Average Energy Collected KJ Hr ⁻¹ m ⁻² | Test Period Efficiency | $\frac{T_{IN}-T_a}{(HR)}$ °Cm ² -MJ ⁻¹ |
|--------------------------------------|--|---|------------------------------|---|---------------------------------|--|---|------------------------------|---|
| 8 15 | 73.6 | 74.4 | 1.59 | 23.4 | 7.7 | 1570.6 | 875.6 | 55.7 | 31.95 |
| 8 29 | 75.9 | 76.8 | 1.59 | 24.0 | 18.3 | 1748.6 | 998.7 | 57.1 | 29.67 |
| 8 45 | 78.7 | 79.7 | 1.58 | 25.0 | 15.1 | 1913.6 | 1155.6 | 60.4 | 28.04 |
| 8 59 | 81.2 | 82.3 | 1.58 | 25.5 | 13.5 | 2057.9 | 1182.8 | 57.5 | 27.04 |
| 9 15 | 83.8 | 85.1 | 1.57 | 26.4 | 21.7 | 2225.2 | 1350.9 | 60.7 | 25.80 |
| 9 29 | 84.7 | 86.1 | 1.57 | 27.0 | 36.2 | 2359.9 | 1567.1 | 66.4 | 24.45 |
| 9 45 | 84.6 | 86.1 | 1.57 | 27.8 | 15.1 | 2510.6 | 1567.1 | 62.4 | 22.66 |
| 9 59 | 85.8 | 87.5 | 1.57 | 28.3 | 12.5 | 2630.0 | 1756.2 | 66.8 | 21.87 |
| 10 15 | 84.4 | 86.1 | 1.57 | 29.1 | 14.9 | 2755.9 | 1850.8 | 67.2 | 20.08 |
| 10 29 | 83.4 | 85.1 | 1.57 | 29.6 | 9.2 | 2861.9 | 1918.3 | 67.0 | 18.79 |
| 10 45 | 82.1 | 83.9 | 1.58 | 29.8 | 13.5 | 2975.3 | 1984.9 | 66.7 | 17.59 |
| 10 59 | 81.3 | 83.1 | 1.58 | 29.7 | 11.4 | 3043.1 | 1984.9 | 65.2 | 16.94 |
| 11 15 | 81.6 | 83.4 | 1.52 | 30.3 | 12.6 | 3102.1 | 1818.0 | 58.6 | 16.56 |
| 11 29 | 86.3 | 88.1 | 1.52 | 31.4 | 15.8 | 3133.4 | 1857.2 | 59.3 | 17.53 |
| 11 45 | 89.4 | 91.2 | 1.52 | 32.0 | 12.5 | 3142.6 | 1896.5 | 60.3 | 18.24 |
| 11 59 | 91.8 | 93.6 | 1.52 | 31.3 | 7.7 | 3208.6 | 1896.5 | 59.1 | 18.83 |
| 12 15 | 92.5 | 94.4 | 1.48 | 32.3 | 11.5 | 3218.7 | 1986.6 | 61.7 | 18.68 |
| 12 29 | 88.9 | 90.7 | 1.48 | 32.3 | 11.4 | 3208.6 | 1884.8 | 58.7 | 17.62 |

TABLE A-III-9 (Continued)

| Test Period Ending Hr.-Min. | Average Inlet Fluid Temperature °C | Average Outlet Fluid Temperature °C | Fluid Flow Rate GPM | Average Ambient Temperature °C | Average Wind Speed KPH | Average Solar Radiation KJ Hr ⁻¹ m ⁻² | Average Energy Collected KJ Hr ⁻¹ m ⁻² | Test Period Efficiency | $\frac{T_{IN}-T_a}{(HR)}$ °Cm ² -MJ ⁻¹ |
|--------------------------------------|--|---|------------------------------|---|---------------------------------|--|---|------------------------------|---|
| 12 45 | 88.0 | 89.9 | 1.56 | 32.2 | 8.6 | 3190.1 | 2026.9 | 63.5 | 17.49 |
| 12 59 | 86.8 | 88.7 | 1.56 | 32.8 | 14.5 | 3157.8 | 1986.6 | 62.9 | 17.10 |
| 13 15 | 85.7 | 87.5 | 1.55 | 32.4 | 13.2 | 3129.7 | 1933.9 | 61.8 | 17.05 |
| 13 29 | 84.8 | 86.5 | 1.55 | 32.9 | 16.8 | 3075.8 | 1867.2 | 60.7 | 16.87 |
| 13 45 | 83.8 | 85.5 | 1.55 | 33.1 | 17.9 | 2997.9 | 1813.9 | 60.5 | 16.90 |
| 13 59 | 82.9 | 84.6 | 1.55 | 32.9 | 16.2 | 2918.6 | 1813.9 | 62.1 | 17.14 |
| 14 15 | 81.9 | 83.6 | 1.54 | 32.7 | 11.4 | 2808.4 | 1722.6 | 61.3 | 17.52 |
| 14 29 | 81.2 | 82.7 | 1.54 | 33.7 | 10.0 | 2698.7 | 1603.4 | 59.4 | 17.61 |
| 14 45 | 80.3 | 81.7 | 1.56 | 33.4 | 19.4 | 2557.2 | 1503.4 | 58.8 | 18.34 |
| 14 59 | 79.4 | 80.8 | 1.56 | 33.6 | 21.3 | 2432.2 | 1463.1 | 60.2 | 18.83 |
| 15 15 | 78.5 | 79.7 | 1.58 | 33.1 | 18.3 | 2289.3 | 1400.3 | 61.2 | 19.80 |
| 15 29 | 77.8 | 78.9 | 1.58 | 32.9 | 16.7 | 2144.6 | 1182.8 | 55.2 | 20.91 |
| 15 45 | 82.6 | 83.5 | 1.59 | 32.2 | 16.4 | 1955.6 | 916.7 | 46.9 | 25.79 |
| 15 59 | 85.2 | 86.0 | 1.59 | 32.0 | 14.7 | 1796.1 | 820.9 | 45.7 | 29.61 |

CORNING COLLECTOR

JULY 25, 1975

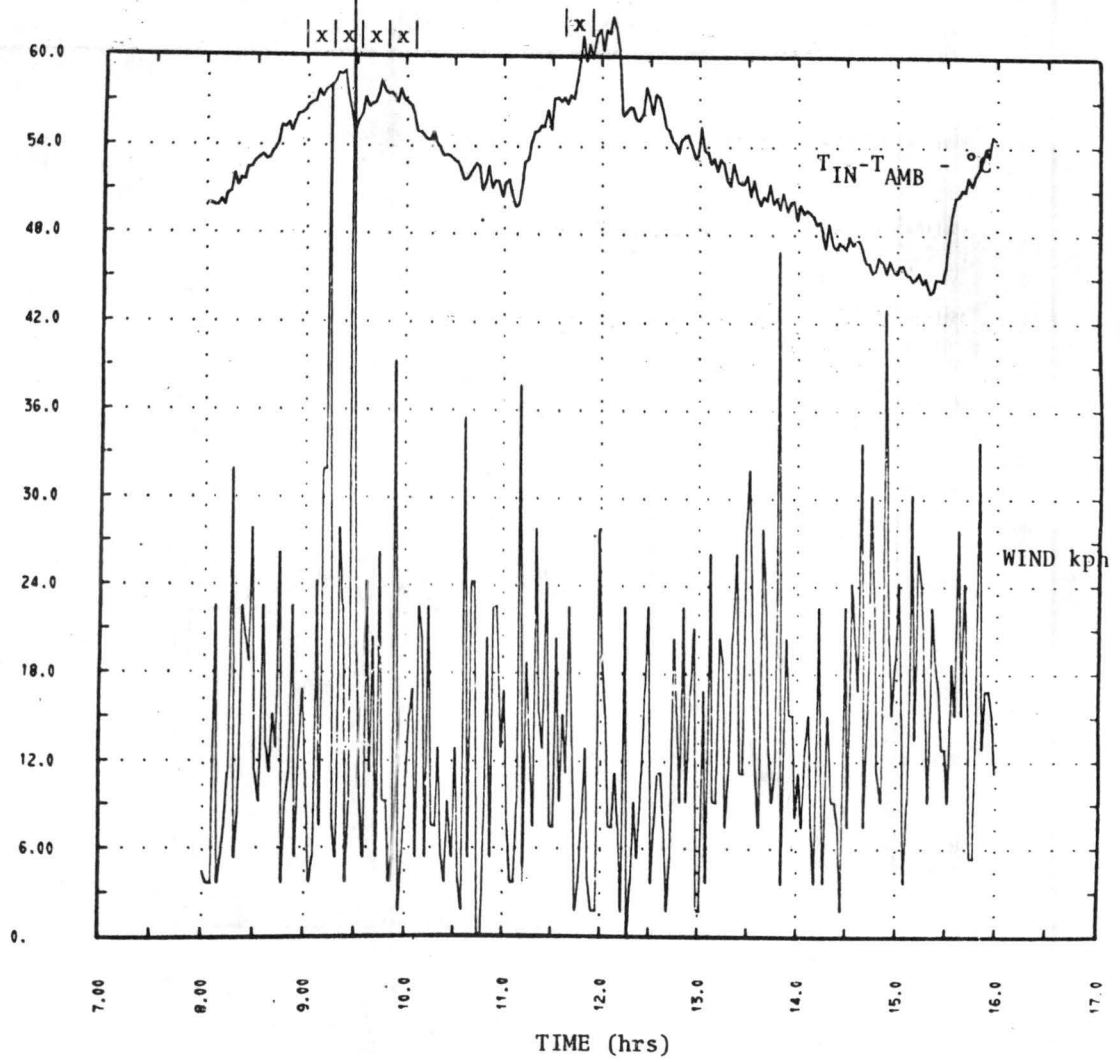


Figure A-III-17. Test Data Plot.

CORNING COLLECTOR JULY 25, 1975

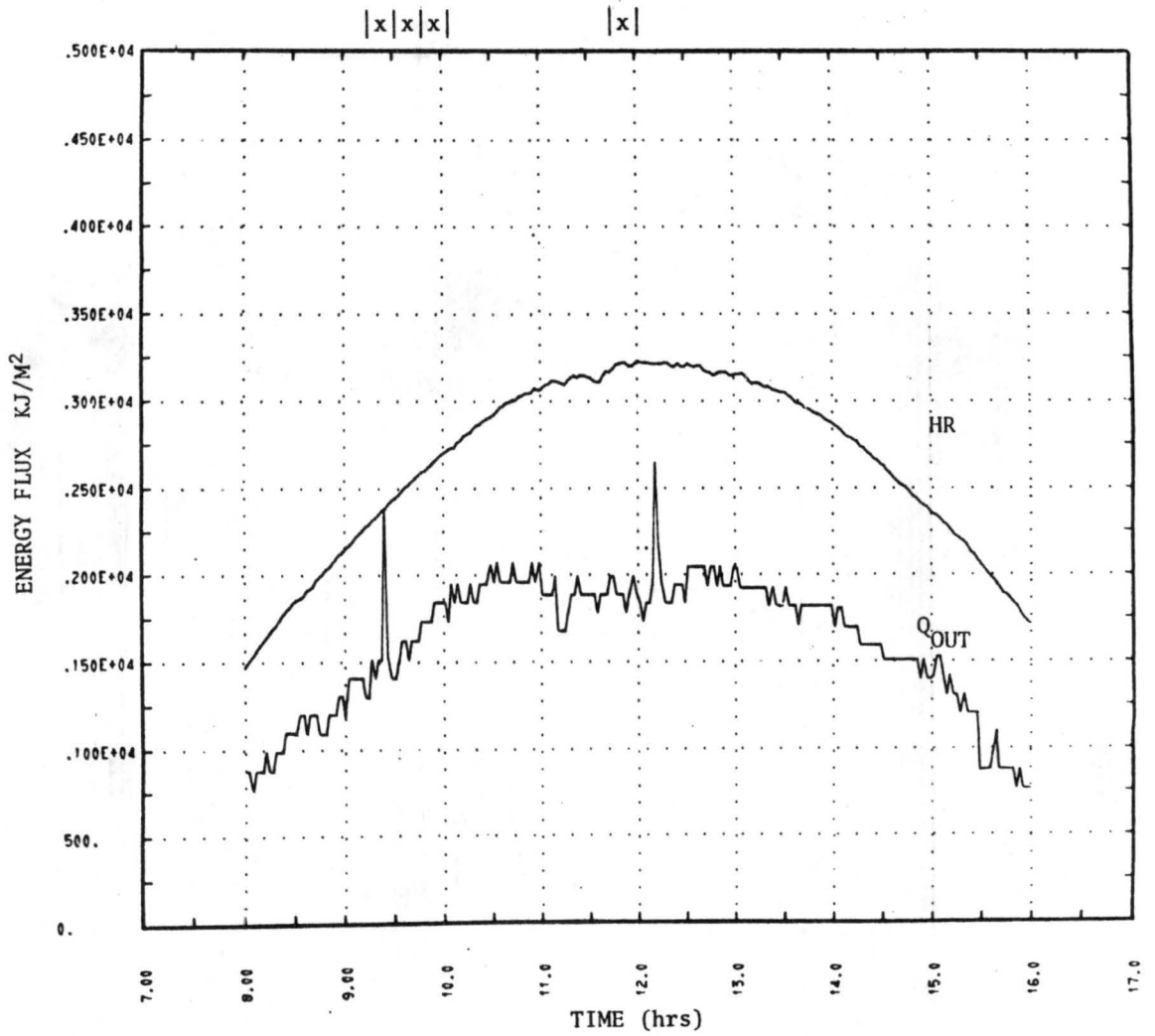


Figure A-III-18. Test Data Plot.

TABLE A-III-10 Summary of Test Data for August 4, 1975

| Test Period Ending Hr.-Min. | Average Inlet Fluid Temperature °C | Average Outlet Fluid Temperature °C | Fluid Flow Rate GPM | Average Ambient Temperature °C | Average Wind Speed KPH | Average Solar Radiation KJ Hr ⁻¹ m ⁻² | Average Energy Collected KJ Hr ⁻¹ m ⁻² | Test Period Efficiency | $\frac{T_{IN}-T_a}{(HR)}$ °Cm ² -MJ ⁻¹ |
|--------------------------------------|--|---|------------------------------|---|---------------------------------|--|---|------------------------------|---|
| 9 15 | 28.1 | 29.6 | 1.69 | 27.6 | 5.5 | 2305.9 | 1609.3 | 69.8 | .21 |
| 9 29 | 29.0 | 30.6 | 1.69 | 28.1 | 10.3 | 2450.2 | 1817.4 | 74.2 | .36 |
| 9 45 | 30.1 | 31.8 | 1.69 | 29.0 | 16.5 | 2587.6 | 1900.6 | 73.5 | .41 |
| 9 59 | 31.0 | 32.8 | 1.69 | 29.5 | 17.9 | 2711.1 | 2011.6 | 74.2 | .55 |
| 10 15 | 32.2 | 34.1 | 1.68 | 30.3 | 12.3 | 2836.5 | 2110.0 | 74.4 | .67 |
| 10 29 | 33.2 | 35.2 | 1.68 | 30.4 | 17.5 | 2955.0 | 2192.8 | 74.2 | .97 |
| 10 45 | 34.4 | 36.4 | 1.66 | 31.2 | 21.5 | 3069.8 | 2207.6 | 71.9 | 1.03 |
| 10 59 | 35.5 | 37.5 | 1.66 | 31.5 | 20.2 | 3145.9 | 2207.6 | 70.2 | 1.26 |
| 11 15 | 36.5 | 38.6 | 1.65 | 31.4 | 69.0 | 3202.1 | 2302.6 | 71.9 | 1.58 |
| 11 29 | 37.4 | 39.6 | 1.65 | 31.9 | 154.6 | 3248.2 | 2356.8 | 72.6 | 1.71 |
| 11 45 | 38.5 | 40.6 | 1.65 | 32.9 | 16.8 | 3270.8 | 2289.1 | 70.0 | 1.71 |
| 11 59 | 39.4 | 41.5 | 1.65 | 33.0 | 19.0 | 3303.5 | 2248.4 | 68.1 | 1.94 |
| 12 15 | 40.4 | 42.4 | 1.64 | 33.0 | 26.0 | 3324.3 | 2194.4 | 66.0 | 2.22 |
| 12 29 | 41.2 | 43.2 | 1.64 | 33.4 | 20.1 | 3316.4 | 2167.5 | 65.4 | 2.35 |
| 12 45 | 42.0 | 44.1 | 1.64 | 33.8 | 19.5 | 3289.2 | 2221.4 | 67.5 | 2.51 |
| 12 59 | 42.7 | 44.7 | 1.64 | 33.7 | 25.8 | 3281.4 | 2181.0 | 66.5 | 2.73 |
| 13 15 | 43.4 | 45.4 | 1.63 | 34.1 | 29.0 | 3242.7 | 2114.1 | 65.2 | 2.89 |
| 13 29 | 44.0 | 46.0 | 1.63 | 34.1 | 23.7 | 3204.9 | 2154.3 | 67.2 | 3.08 |

TABLE A-III-10 (Continued)

| Test Period Ending Hr.-Min. | Average Inlet Fluid Temperature °C | Average Outlet Fluid Temperature °C | Fluid Flow Rate GPM | Average Ambient Temperature °C | Average Wind Speed KPH | Average Solar Radiation KJ Hr ⁻¹ m ⁻² | Average Energy Collected KJ Hr ⁻¹ m ⁻² | Test Period Efficiency | $\frac{T_{IN}-T_a}{(HR)}$ °Cm ² -MJ ⁻¹ |
|--------------------------------------|--|---|------------------------------|---|---------------------------------|--|---|------------------------------|---|
| 13 45 | 44.7 | 46.6 | 1.63 | 35.0 | 24.4 | 2982.7 | 2020.5 | 67.7 | 3.24 |
| 13 59 | 45.2 | 47.1 | 1.63 | 34.7 | 18.8 | 3112.7 | 2033.9 | 65.3 | 3.36 |
| 14 15 | 45.8 | 47.5 | 1.62 | 35.1 | 17.3 | 2959.2 | 1861.8 | 62.9 | 3.62 |
| 14 29 | 46.1 | 47.5 | 1.62 | 34.8 | 17.4 | 2332.2 | 1489.4 | 63.9 | 4.87 |
| 14 45 | 46.3 | 47.9 | 1.62 | 34.8 | 19.1 | 2608.8 | 1702.2 | 65.2 | 4.41 |
| 14 59 | 46.6 | 47.9 | 1.62 | 34.9 | 19.2 | 2449.8 | 1462.8 | 59.7 | 4.77 |

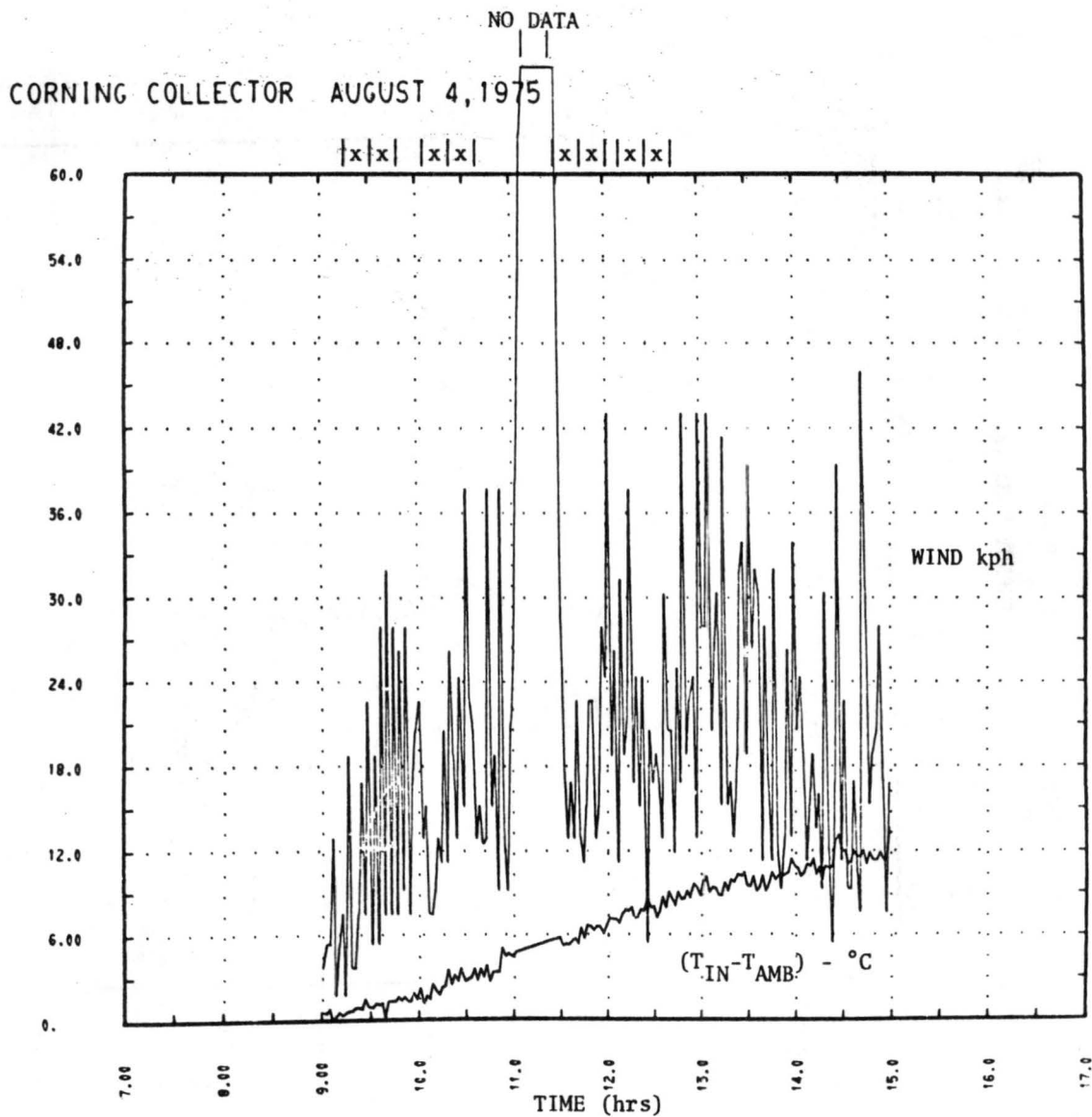


Figure A-III-19. Test Data Plot.

CORNING COLLECTOR AUGUST 4, 1975

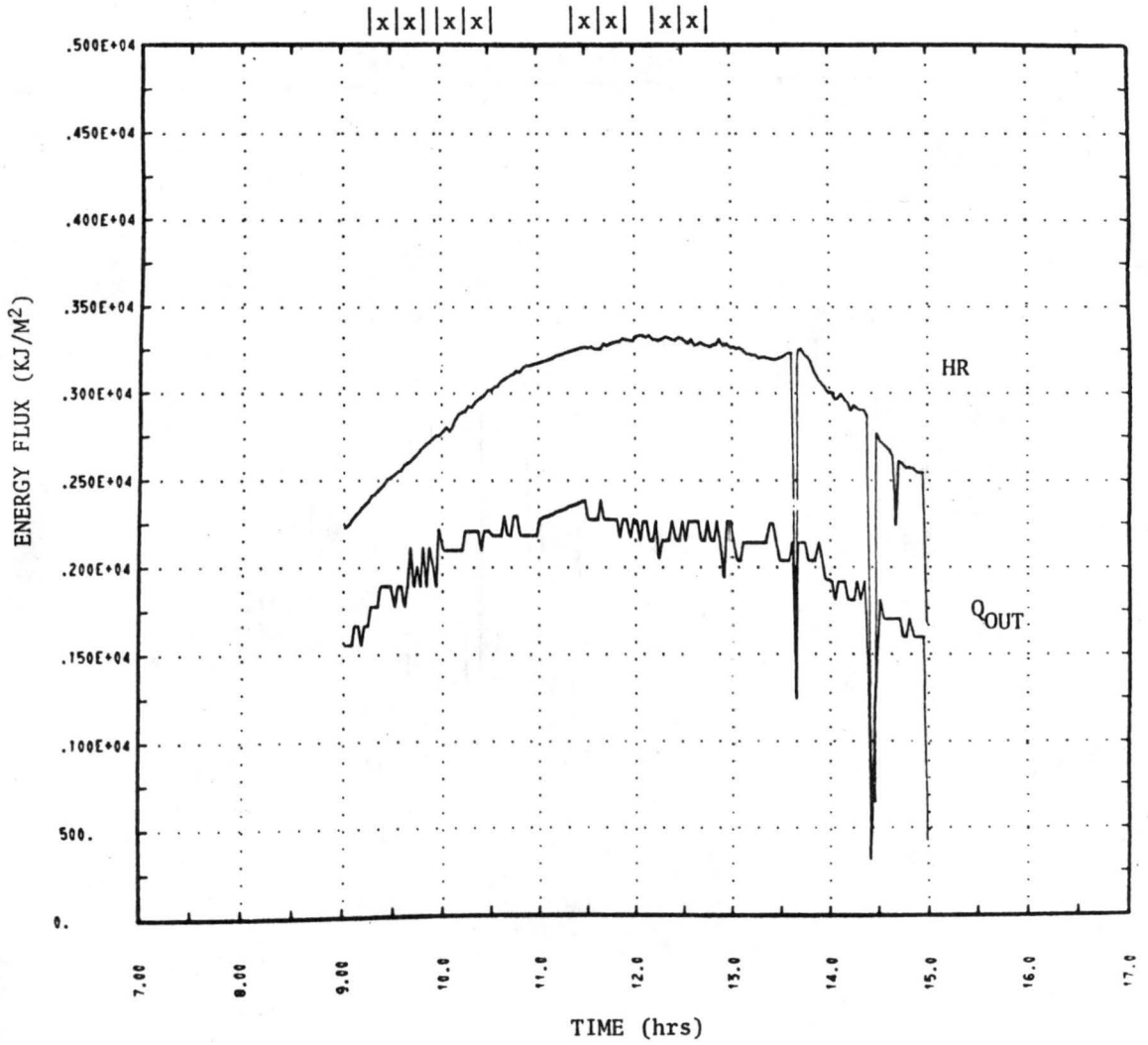


Figure A-III-20. Test Data Plot.

437948